

**Statistical Models for Characterizing and Reducing Uncertainty in Seasonal
Rainfall Pattern Forecasts to inform Decision Making**

Submitted in partial fulfillment of the requirements for the degree of

Doctor of Philosophy

in

Civil and Environmental Engineering

Bandar Saud AlMutairi

B.S., Civil Engineering, Kuwait University

M.S., Civil Engineering, North Carolina State University

M.S., Civil and Environmental Engineering, Carnegie Mellon University

Carnegie Mellon University
Pittsburgh, PA

July, 2017

ACKNOWLEDGEMENTS

I would like to acknowledge and express my thanks to my advisors Professor Mitchell J. Small and Professor Iris Grossmann who both provided me with invaluable guidance and support. They shared their knowledge and expertise with me throughout my work on this research. It is also a pleasure to express my gratitude to the other committee members, Professor Peter Adams and Professor Constantine Samaras for serving on the committee and for their comments and suggestions.

I would also like to thank Professor Kelvin Gregory for his encouragement and support and to all the CEE staffs, especially Ms. Maxine Leffard for their great assistance. Special thanks to Professor Douw Steyn from the University of British Columbia, who shared the research idea and motivation.

I am deeply indebted to express my heartfelt gratitude to my parent and wife for their support during this season of life. My sincere appreciation is also extended to Kuwait University for sponsoring my PhD study at Carnegie Mellon University.

Committee Members

Mitchell Small

H. John Heinz III Professor, Civil and Environmental Engineering & Engineering and Public Policy
Carnegie Mellon University, Pittsburgh, PA, USA

Peter Adams

Professor, Civil and Environmental Engineering & Engineering and Public Policy
Carnegie Mellon University, Pittsburgh, PA, USA

Constantine Samaras

Assistant Professor, Civil and Environmental Engineering
Carnegie Mellon University, Pittsburgh, PA, USA

Iris Grossmann

Assistant Professor of Sustainable Technology
Chatham University, Pittsburgh, PA, USA

Abstract

Uncertainty in rainfall forecasts affects the level of quality and assurance for decisions made to manage water resource-based systems. However, eliminating uncertainty in a complete manner could be difficult, decision-makers thus are challenged to make decisions in the light of uncertainty. This study provides statistical models as an approach to cope with uncertainty, including: a) a statistical method relying on a Gaussian mixture (GM) model to assist in better characterize uncertainty in climate model projections and evaluate their performance in matching observations; b) a stochastic model that incorporates the El Niño–Southern Oscillation (ENSO) cycle to narrow uncertainty in seasonal rainfall forecasts; and c) a statistical approach to determine to what extent drought events forecasted using ENSO information could be utilized in the water resources decision-making process. This study also investigates the relationship between calibration and lead time on the ability to narrow the interannual uncertainty of forecasts and the associated usefulness for decision making. These objectives are demonstrated for the northwest region of Costa Rica as a case study of a developing country in Central America. This region of Costa Rica is under an increasing risk of future water shortages due to climate change, increased demand, and high variability in the bimodal cycle of seasonal rainfall. First, the GM model is shown to be a suitable approach to compare and characterize long-term projections of climate models. The GM representation of seasonal cycles is then employed to construct detailed comparison tests for climate models with respect to observed rainfall data. Three verification metrics demonstrate that an acceptable degree of predictability can be obtained by incorporating ENSO information in reducing error and interannual variability in the forecast of seasonal rainfall. The predictability of multicategory rainfall forecasts in the late portion of the wet season surpasses

that in the early portion of the wet season. Later, the value of drought forecast information for coping with uncertainty in making decisions on water management is determined by quantifying the reduction in expected losses relative to a perfect forecast. Both the discrimination ability and the relative economic value of drought-event forecasts are improved by the proposed forecast method, especially after calibration. Positive relative economic value is found only for a range of scenarios of the cost-loss ratio, which indicates that the proposed forecast could be used for specific cases. Otherwise, taking actions (no-actions) is preferred as the cost-loss ratio approaches zero (one). Overall, the approach of incorporating ENSO information into seasonal rainfall forecasts would provide useful value to the decision-making process - in particular at lead times of one year ahead.

Table of Contents

Abstract	iii
Chapter 1: Introduction	1
1.1 Overview.....	1
1.2 Case Study	6
1.2.1 Seasonal Cycle of Precipitation	6
1.2.2 Large scale variability	7
References.....	8
Chapter 2: Bimodal Seasonal Rainfall Model for Evaluating of Long-term Climate Model Projections	10
Abstract.....	10
2.1 Introduction.....	11
2.2 Data and model inputs	15
2.2.1 Precipitation data	15
2.2.2 CMIP5 models and simulations.....	15
2.3 Materials and Methods.....	17
2.3.1 Gaussian mixture model and fitting.....	17
2.3.2 The nine features of the bimodal seasonal cycle of precipitation.....	20
2.4 Results.....	22
2.4.1 Model evaluation	22
2.4.2 Future climate projections	29
2.5 Conclusions.....	35
Acknowledgments.....	36
References.....	37

Chapter 3: Predictability of Multicategory Seasonal Probabilistic Forecast of Precipitation Conditioned on ENSO Phase	42
Abstract	42
3.1 Introduction	43
3.2 Data and climate models inputs	47
3.3 Materials and Methods	48
3.3.1 Model training, validation, and testing	48
3.3.2 ENSO occurrence model	50
3.3.3 Rainfall intensity model	51
3.3.4 Bias correction method	53
3.3.5 Stochastic weather generation model	53
3.3.6 Verification metrics	57
3.4 Results and discussion	59
3.4.1 Modeling ENSO occurrence	59
3.4.2 Seasonal precipitation modeling	61
3.4.3 Predictability and calibration	64
3.4.4 Predictability and lead times	69
3.4.5 Predictability for climate model simulations	72
3.5 Conclusions	74
Acknowledgments	76
References	76
Chapter 4: The Relative Value of Seasonal Drought-event Forecasts Conditioned on ENSO Phase for Water Management Decisions	83
Abstract	83
4.1 Introduction	84

4.2 Data used.....	89
4.3 Materials and Methods.....	90
4.3.1 Model construction.....	90
4.3.2 Relative operating characteristic (ROC).....	93
4.3.3 Relative (Economic) value	95
4.4 Results and discussion	100
4.4.1 Effect of calibration	100
4.4.2 Effect of lead times.....	108
4.5 Conclusions.....	109
References.....	111
Chapter 5: Conclusion.....	116
Appendix 1: Detailed information about the methods used to construct the multicategory seasonal probabilistic forecast model of precipitation	120
Appendix 2: Supporting Materials for Chapter 3: Predictability of Multicategory Seasonal Probabilistic Forecast of Precipitation Conditioned on ENSO Phase	127
Appendix 3: Supporting Materials for Chapter 4: The Relative Value of Seasonal Drought-event Forecasts Conditioned on ENSO Phase for Water Management Decisions.....	135

List of Figures

Figure 1. Map of the case study in Costa Rica in green (the northwest region) -----	7
Figure 2. Single Gaussian distribution curve -----	19
Figure 3. The nine features of the seasonal cycle: maximum/minimum rainfall rates ($H1, Hd, H2$), seasonal period durations ($L1, Ld, L2$), and seasonal transition times (ts, td, te). (Note: Lw denotes the wet season duration) -----	21
Figure 4. Boxplot of the GPCP observed seasonal cycle of precipitation (9-15 N and 90-84 W) over the (1979-2005) period and the solid line represents its average seasonal cycle. (The box represents maximum ($Q3 + 1.5 \times IQR$), third quartile ($Q3$), median, first quartile ($Q1$), and minimum ($Q1 - 1.5 \times IQR$)).-----	22
Figure 5. The interannual variability index (IAV) (horizontal axis) and the test statistic (D_{max}) of the seasonal pattern KS test (vertical axis). Models in the lower left quadrant exhibit acceptable performance for simulating both features of the annual and monthly rainfall (1979-2005)-----	26
Figure 6. Distribution of average simulated (by CGCMs) and observed monthly precipitation (mm/d) over the baseline (1979-2005) period-----	28
Figure 7. Change in average monthly precipitation (BCSD) for the (2074-2100) period relative to the baseline (1979-2005) period for the selected models and the MEM -----	30
Figure 8. Percentage change in the seasonal mean precipitation over the (2074-2100) period relative to the (1979-2005) period under RCP8.5 -----	33
Figure 9. Percentage change in the standard deviation of (2074-2100) period relative to that of the (1979-2005) period under RCP8.5-----	34
Figure 10. Flowchart of the process taken by the WG to forecast seasonal precipitation with different lead time ($N=1000$; $T=20$ years; $L=1, 2, \text{ or } 3$ years)-----	56
Figure 11. Joint probability density function of the bivariate model conditioned on each of the three ENSO phases -----	63
Figure 12. RPSS values of the raw and calibrated rainfall forecasts in the early and late wet seasons -----	66
Figure 13. RMSE computed between the raw, calibrated, and climatological rainfall forecasts and observations -----	66

Figure 14. Reliability diagram of the raw, calibrated, and climatology rainfall forecasts in the a) early wet season, and b) late wet season. Note that the error bars on the reliability curves are not shown for readability (see Appendix 2). -----68

Figure 15. Multicategory reliability diagram for the calibrated rainfall forecast in the a) early wet season and b) late wet season computed with respect to different lead times (year) -----71

Figure 16. Decision tree demonstrating strategies associated with the use of a forecast scenario F. Decision: Action or Inaction; Dry-event occurrence: Y (yes) or N (no); Expense: C (cost), L (loss), or 0 (nothing).-----99

Figure 17. ROC curve generated based on the raw calibrated, climatology dry-event forecast in the a) early, and b) late wet season over the 1996-2015 period ----- 101

Figure 18. Relative value of the raw, calibrated and climatological dry-event forecasts in the a) early and b) late wet season according to the use of optimal cutoff points (Table 13)----- 105

Figure 19. Expected expense generated by forecasting dry events in both the a) early, and b) late wet season based on the raw, calibrated, climatology, perfect (dash gray), and no-forecast (dark black) scenarios. ----- 107

Figure 20. Cumulative distribution functions (CDF) for both the observations and fitted lognormal distributions ----- 130

Figure 21. Difference between error bars in the MCRD generated by the raw, calibrated, climatological forecast for dry events in the a) early and b) late portion of the wet season. ---- 131

Figure 22. Multicategory reliability diagram for the calibrated rainfall forecast in the early wet season driven by the output of six climate models (separated into two plots for readability)--- 132

Figure 23. Multicategory reliability diagram for the calibrated rainfall forecast in the late wet season driven by the output of six climate models (separated into two plots for readability)--- 133

Figure 24. Difference between error bars in the MCRD generated by the calibrated forecast- based ENSO information obtained from climate model in the a) early and b) late portion of the wet season. ----- 134

Figure 25. ROC curves of the calibrated forecast of dry events in both the a) early and b) late wet season with respect to three different lead times----- 135

Figure 26. Relative value obtained by optimal cutoff points of the calibrated forecast of dry events in both the a) early and b) late wet season with respect to different lead times ----- 136

List of Tables

Table 1. CMIP5 models used in this study.....	18
Table 2. Indicators of statistical agreement between CGCMS (and their MEM) predicted and observed GPCP precipitation over the period 1979-2005.	26
Table 3. Percentage changes in the maximum/minimum rainfall rates, seasonal period duration and seasonal transition times of early, middle, and late wet season	30
Table 4. The selected CMIP5 CGCMs used in the study.....	49
Table 5. The log-likelihood, number of parameters, AIC and BIC for the two orders of the NHMC that are proposed in this study. A lower value of the AIC and BIC indicates a perfect model; the number of parameters is computed (with each order) for two Markov Chains: from early to late wet season and vice versa	60
Table 6. The likelihood ratios and associated p-values based on the 1 st order NHMC for the validation and testing periods	61
Table 7. The p-values for χ^2 test for the lognormal distribution goodness of fit.....	62
Table 8. RPSS and RMSE (mm/d) for the calibrated forecasts of both early and late wet season performed with different lead times (year)	70
Table 9. RPSS values for the raw and calibrated forecasts computed based on ENSO information from climate models	73
Table 10. RMSE (mm/d) computed between both raw and calibrated forecasts and observations	74
Table 11. Contingency table of an adverse event forecast performance over a set of cases during a range of time frames.....	93
Table 12. Expense matrix for the four combinations of decisions and dry-event occurrence	96
Table 13. Optimal cutoff points and associated Hit and false-alarm rates for the raw, calibrated, and climatology forecasts of dry events in the early and late wet season.....	104
Table 14. The 1 st order Nonhomogeneous Markov Chain for training period 1916-1975	127

Table 15. The 2nd order Nonhomogeneous Markov Chain for training period 1916-1975 128

Table 16. The 1st order Non-homogeneous Markov Chain for the testing (1996-2015) period 129

Chapter 1: Introduction

1.1 Overview

Water regulation and planning decisions are mainly made for maintaining a sustainable water, food, and energy nexus, as well as for achieving some economic and environmental purposes. The sustainability of water resource-based systems including hydropower generation, farming, and water supply, relies on making well-informed, reliable decisions toward more resilient systems that can cope with potential extreme conditions. These decisions are limited in their efficacy by constraints imposed by the accuracy of weather and climate information. Due to the difficulty of completely eliminating uncertainty in this kind of information, decision-makers must make decisions in the light of uncertainty. Hence, interest in narrowing uncertainty associated with weather and climate information (e.g. rainfall, surface temperature) has grown, particularly in many developing nations (e.g., Conway et al., 2015) where there is increasing water stress arising from climate change and variability, population growth, and the expansion in agricultural and industrial sectors. Reducing uncertainty through better information and forecasts can improve the decision-making process by avoiding undesirable environmental and socioeconomic losses including: blackouts and interruptions in the hydropower supply, deterioration of water supply for drinking and sanitation, and crop failure.

Future changes in the amount, timing and seasonal cycle of precipitation provide useful information to the process of making short and long-time scale planning and regulating decisions. This information in turn has critical implications for the effectiveness of some decisions made in

many water-based sectors. For example, decisions related to the selection of appropriate crop cultivars and varieties, the timing of agricultural operations, fertilizer implementation, and livestock management strategies are all critical to agricultural revenues. Recent advances in the parameterization of Coupled General Circulation Models (CGCMs), together with their cross-comparison in the Coupled Model Intercomparison Project (CMIP), now provide the potential for improved future precipitation projections. However, global climate model projections remain uncertain on the regional scale, in particular for precipitation (Lobell and Burke, 2008). Methods are needed to better characterize the uncertainty in future precipitation outcomes. This study provides a statistical approach (Chapter 2) for characterizing and evaluating uncertainty associated with climate model projections for the long-term change in seasonal rainfall pattern.

Narrowing uncertainty in seasonal precipitation predictions to reduce the complexity in a decision-making process could help inform the development of more efficient strategies and regulations. The failure of most prediction models in fully addressing the interannual variability of seasonal precipitation might be due to a failure to incorporate the effect of large-scale climate variables (Woolhiser, 1992; Katz and Parlange 1998), such as the El Niño–Southern Oscillation (ENSO). ENSO is the main natural source of interannual climate variability in the tropical Pacific region (Vecchi and Wittenberg, 2010). This phenomenon is recognized by an interchangeable cycle that consists of three phases including a warm phase known as El Niño, a cold phase known as La Niña, and a neither warm nor cold phase called neutral. The ENSO cycle has been related to the drying and wetting of rainfall at annual and interannual time-scales across Central America (Karmalkar et al., 2011). Therefore, incorporating the influence of interannual variability could be a possible approach to narrow uncertainty in seasonal precipitation forecasts. In this study, a

statistical method (Chapter 3) is developed to determine the degree of predictability of multicategory probabilistic seasonal precipitation forecasts through incorporating ENSO information. The multicategory forecasts serve to quantify the uncertainty associated with a prediction by providing the likelihood of having dry, wet, and normal rainfall amounts during the forecast period.

The level of quality in a forecast system does not ensure ultimate benefit to the decision-making process (Palmer et al., 2000; Hartmann et al. 2002). This poses the question of how to distinguish between beneficial and non-beneficial forecast systems in the context of making decisions. Tradeoffs among decisions often involve economic factors in terms of gains or losses, which emphasizes that forecast value could be deduced by the resultant expenses/returns associated with decisions (including action or inaction). Therefore, the approach to quantify the level of usefulness of a forecast system could be described by a relative economic value (Murphy 1977) that provides an indication of the achieved amount of savings relative to the perfect forecast system. This study assesses (Chapter 4) the relative value of seasonal drought-event forecasts that are predicted by incorporating ENSO information. It also analyzes to what extent this kind of forecast system could be utilized in the decision-making process.

The study is demonstrated for the northwest region of Costa Rica as a case study of many developing nations. The objectives of this dissertation are: a) characterizing uncertainty associated with regional climate model projections of future changes in seasonal cycle of precipitation, b) demonstrating the potential for reducing uncertainty in seasonal precipitation forecasts by

incorporating ENSO information, and c) assessing the relative (economic) value of an ENSO-based forecast of drought events in the context of decision-making.

In Chapter 2, a statistical method is developed to characterize possible changes in the bimodal cycle of seasonal precipitation based on the outcomes of 19 Coupled General Circulation Models (CGCMs). The proposed method relies on a Gaussian Mixture (GM) model that is applied to both current observations and climate projections. The study develops a new metric to measure and compare the degree of bimodality in the seasonal precipitation cycle. Three other metrics are also used to evaluate the performance of these CGCMs over an area centered on the northwest region of Costa Rica (9-15 N and 90-84 W) with respect to observed precipitation during the period 1979-2005. Then monthly bias-corrected and spatially disaggregated (BCSD) rainfall projections of the best performing models as well as the multi-ensemble mean (MEM) for a high emissions climate scenario, the representative concentration pathway RCP8.5, are used to quantify future changes in the seasonal cycle over the region (9.5-11 N and 85-86 W) surrounding northwest Costa Rica. The projected future changes are characterized in terms of nine features of the bimodal cycle, as a further step towards model comparison and uncertainty characterization.

In Chapter 3, a stochastic weather generation (WG) model is developed to examine the predictability of seasonal precipitation forecast models conditioned on ENSO cycle. The proposed WG model consists of: a) a bivariate normal (BVN) model that is fitted to the early and late wet season precipitation over the period 1916-1975 conditioned on ENSO phase, and b) an ENSO occurrence model that is formulated as 1st order Nonhomogeneous Markov Chain. The predictability of the raw and calibrated probabilistic forecasts of three precipitation categories (dry,

normal, and wet) are measured through three verification metrics over the period 1996-2015. The verification metrics include the ranked probability score skill (RPSS), root mean square error (RMSE), and multicategory reliability diagram (MCRD). The relationship between the calibration and verification of the forecast is discussed and the effect of different lead times on the verification is demonstrated. Furthermore, six climate model outputs for the Nino3.4 SSTs are employed to test the degree of predictability and reliability conditioned on the generated ENSO pattern.

Chapter 4 presents an analysis of the relative (economic) value of water management decisions that can be made based on a probabilistic dry-event forecast in the early and late wet season conditioned on ENSO phase. A Relative Operating Characteristic (ROC) curve is drawn to measure the ability of the raw and calibrated forecast to discriminate between the two alternative outcomes. Then, a decision-analytic model (or cost-loss decision model) is constructed for each possible cutoff point with respect to the cost/loss ratio, which is ranging from 0 to 1. Furthermore, the analysis aims to determine to what extent the raw, calibrated, and climatological forecasts can be reliable through studying the relationship between expected expense and cost/loss ratios. The effect of different lead times on the gained relative value is also investigated. The objective of this chapter is to provide a statistical tool that copes with the uncertainty associated with the dry-event forecast in the two portions of the wet season in order to make water-related decisions.

Chapter 5 summarizes the major conclusions of this research, highlights contributions to the state-of-the science.

1.2 Case Study

1.2.1 Seasonal Cycle of Precipitation

Northwest Costa Rica (9.5-11.0 N and 85-86 W) (Figure 1) experiences a tropical Savanna climate, where the wet season lasts from May through October (Hastenrath, 1967). The seasonal cycle of precipitation has a bimodal pattern in which the wet season can be divided into three portions: a) early wet season, b) midsummer drought (MSD), and c) late wet season. The bimodality in the seasonal cycle of precipitation is related to the topography of Costa Rica, in which a chain of mountains divide the country into two different slopes each with different climate (Maldonado et al., 2013). The northeasterly trade winds drive moisture and rains to the Caribbean slope, while rain shadows occur on the Pacific slope (Waylen et al., 1996). However, early wet season rains take place by the northward migration of the Intertropical Convergence Zone (ITCZ), which brings Pacific moisture embedded in a southwesterly flow to the Pacific slope (Waylen et al., 1996; Maldonado et al., 2013).

Recent studies point out that the evolution of the midsummer drought is related to a westward extension and intensification of the North Atlantic Subtropical High (NASH) and a strengthening of the Pacific-Atlantic sea surface temperature (SST) gradient, which result in an intensification of the easterly winds and the Caribbean Low-Level Jet (CLLJ) (Curtis and Gamble, 2008; Rauscher et al., 2008; Ryu and Hayhoe, 2014; Hidalgo et al., 2015). An alternative hypothesis reported by Magaña et al (1999) proposes that the MSD evolution can be explained by feedbacks between solar radiation, sea surface temperature (SST), and convection. Specifically, the enhanced convection due to the northward migration of the ITCZ during the early wet season reduces the

solar insolation which in turn increases cloud cover and cools SST. The cooler SSTs reduce convection and initiate the MSD.

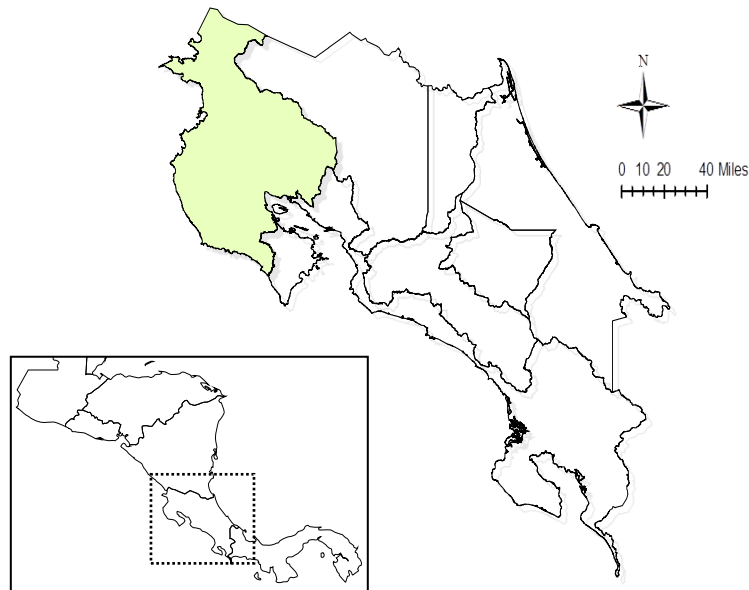


Figure 1. Map of the case study in Costa Rica in green (the northwest region)

1.2.2 Large scale variability

The influence of ENSO phenomenon over Costa Rica has been related to flooding (Waylen et al., 1996; Waylen and Laporte, 1999) and to fluctuations in monthly and interannual precipitation (George et al., 1998). Waylen et al. (1994) found that annual and seasonal precipitation at San Jose

in Costa Rica appears to be conditioned on ENSO. There is a tendency of having dry (wet) events during El Niño (La Niña) years (Waylen et al., 1996). Babcock et al., (2016) conducted semi-structured interviews across groups of stakeholders in the northwest Costa Rica to study their level of perceptions towards a number of water-related issues. The authors found that climate change and ENSO are the major concerned drivers of rainfall and groundwater resources. Tropical cyclones in the Caribbean Sea are also found to play a role in strengthening the southwesterly flow during the summer (Vargas and Trejos, 1994; Harrison and Waylen, 2000).

References

- Babcock, M., Wong-Parodi, G., Small, M. J., & Grossmann, I. (2016). Stakeholder perceptions of water systems and hydro-climate information in Guanacaste, Costa Rica. *Earth Perspectives*, 3(1), 1-13.
- Conway, D., van Garderen, E.A., Deryng, D., Dorling, S., Krueger, T., Landman, W., Lankford, B., Lebek, K., Osborn, T., Ringler, C. and Thurlow, J., 2015. Climate and southern Africa's water-energy-food nexus. *Nature Climate Change*, 5: 837-846.
- Curtis, S. and Gamble, D.W., (2008). Regional variations of the Caribbean mid-summer drought. *Theoretical and Applied Climatology*, 94: 25-34.
- George, R. K., Waylen, P., & Laporte, S. (1998). Interannual variability of annual streamflow and the Southern Oscillation in Costa Rica. *Hydrological Sciences Journal*, 43(3), 409-424.
- Harrison, M., & Waylen, P. (2000). A note concerning the proper choice for Markov model order for daily precipitation in the humid tropics: A case study in Costa Rica. *International Journal of Climatology*, 20(14), 1861-1872.
- Hartmann, H. C., Pagano, T. C., Sorooshian, S., & Bales, R. (2002). Confidence builders: Evaluating seasonal climate forecasts from user perspectives. *Bulletin of the American Meteorological Society*, 83(5), 683-698.
- Hastenrath, S.L., (1967). Rainfall distribution and regime in Central America. *Archiv für Meteorologie, Geophysik und Bioklimatologie, Serie B*, 15: 201-241.
- Hidalgo, H. G., Durán-Quesada, A. M., Amador, J. A., & Alfaro, E. J. (2015). The Caribbean Low-Level Jet, the Inter-Tropical Convergence Zone and Precipitation Patterns in the Intra-Americas Sea: A Proposed Dynamical Mechanism. *Geografiska Annaler: Series A, Physical Geography*, 97(1), 41-59.

- Karmalkar, A. V., Bradley, R. S., & Diaz, H. F. (2011). Climate change in Central America and Mexico: regional climate model validation and climate change projections. *Climate dynamics*, 37(3-4), 605-629.
- Katz, R. W., & Parlange, M. B. (1998). Overdispersion phenomenon in stochastic modeling of precipitation. *Journal of Climate*, 11(4), 591-601.
- Lobell, D.B. and Burke, M.B., (2008). Why are agricultural impacts of climate change so uncertain? The importance of temperature relative to precipitation. *Environmental Research Letters*, 3: 034007.
- Magaña, V., Amador, J.A. and Medina, S., (1999). The midsummer drought over Mexico and Central America. *Journal of Climate*, 12: 1577-1588.
- Maldonado, T., Alfaro, E., Fallas-López, B. and Alvarado, L., (2013). Seasonal prediction of extreme precipitation events and frequency of rainy days over Costa Rica, Central America, using Canonical Correlation Analysis. *Advances in Geosciences*, 33: 41-52.
- Murphy, A. H. (1977). The value of climatological, categorical and probabilistic forecasts in the cost-loss ratio situation. *Monthly Weather Review*, 105(7), 803-816.
- Palmer, T. N., Branković, Č., & Richardson, D. S. (2000). A probability and decision-model analysis of PROVOST seasonal multi-model ensemble integrations. *Quarterly Journal of the Royal Meteorological Society*, 126(567), 2013-2033.
- Rauscher, S.A., Giorgi, F., Diffenbaugh, N.S. and Seth, A., (2008). Extension and intensification of the Meso-American mid-summer drought in the twenty-first century. *Climate Dynamics*, 31: 551-571.
- Ryu, J.H. and Hayhoe, K., (2014). Understanding the sources of Caribbean precipitation biases in CMIP3 and CMIP5 simulations. *Climate dynamics*, 42: 3233-3252.
- Vargas, A.B. and Trejos, V.F.S., (1994). Changes in the general circulation and its influence on precipitation trends in Central America: Costa Rica. *Ambio*.
- Vecchi, G. A., & Wittenberg, A. T. (2010). El Niño and our future climate: where do we stand?. *Wiley Interdisciplinary Reviews: Climate Change*, 1(2), 260-270.
- Waylen, P. R., Caviedes, C. N., & Quesada, M. E. (1996). Interannual variability of monthly precipitation in Costa Rica. *Journal of Climate*, 9(10), 2606-2613.
- Waylen, P. R., Quesada, M. E., & Caviedes, C. N. (1994). The effects of EL Niño-southern oscillation on precipitation in san José, costa rica. *international Journal of Climatology*, 14(5), 559-568.
- Waylen, P., & Laporte, M. S. (1999). Flooding and the El Niño-Southern Oscillation phenomenon along the Pacific coast of Costa Rica. *Hydrological processes*, 13, 2623-2638.
- Woolhiser, D. A. (1992). Modeling daily precipitation—progress and problems. *Statistics in the environmental and Earth sciences*, 5, 71-89.

Chapter 2: Bimodal Seasonal Rainfall Model for Evaluating of Long-term Climate Model Projections

This chapter is the basis of an article that is under-review by the International Journal of Climatology (IJC)

Abstract

Increasing water scarcity due to rising demand and changes in climate and land use are expected to exert significant stress on water resources in many parts of the world. In many areas, distinctive patterns of seasonal precipitation play an important role in regional ecosystems, economies, and food and energy supplies. This study assesses the potential impact of climate change on the bimodal seasonal pattern of precipitation in northwest Costa Rica. A Gaussian mixture model is employed to describe the bimodal pattern and quantify changes in the seasonal precipitation cycle projected by 19 Coupled General Circulation Models (CGCMs). The model simulations for the current period (1979-2005) are compared to observed monthly precipitation data based on four goodness-of-fit metrics. The monthly bias-corrected and spatially disaggregated (BCSD) climate projections of the best performing models are employed to investigate the projected change in the bimodal seasonal pattern, seasonal mean precipitation and interannual variability at the late twenty-first century. Under a high emissions climate scenario, the representative concentration pathway RCP8.5, all but one of the selected BCSD CGCMs and the multi-ensemble mean (MEM) indicate intensification of the midsummer drought (MSD) and with some degree of uncertainty in the MSD-onset. The models project three alternative responses in the seasonal pattern: a) lower and shorter early season (ES) peak with a higher and longer late season (LS) peak, b) higher and

longer ES peak with higher and shorter LS peak; or c) reductions in both the ES and LS peaks, associated with the greatest reductions in wet season precipitation.

2.1 Introduction

Future changes in the amount, timing and seasonal distribution of precipitation have the potential to cause major impacts on ecosystems, water management decisions, and economic activities dependent upon these decisions (Bates et al., 2008; Jacobs and Snow, 2015; Watts et al., 2015; Arnell et al., 2016). However, projections of changes in precipitation that might result from future climate change, in particular on the regional level, remain highly uncertain (Lobell and Burke, 2008; Knutti and Sedláček, 2013; Zhao and Dai, 2016). Methods are needed to better characterize the uncertainty in future precipitation outcomes, the potential for reducing this uncertainty, and the implications for water management decisions. Recent advances in the parameterization of Coupled General Circulation Models (CGCMs), together with their cross-comparison in the Climate Model Intercomparison Project (CMIP), now provide the potential for improved characterization of the uncertainty in future precipitation projections. In this paper we discuss a method for multi-model selection and application to predict changes in specific features of seasonal regional precipitation patterns under future climate change. The method is demonstrated for a region in northwest Costa Rica, where distinctive patterns of dry and wet seasons exert a strong influence on water management decisions and economic behavior.

Like many portions of developing nations (e.g., Conway et al., 2015; Frumhoff et al., 2015; Whitehead et al., 2015; Porkka et al., 2016), Costa Rica has experienced growing water demand in the agricultural, municipal, electric power, and tourist sectors, exerting considerable stress upon

surface and groundwater supplies. Forecasts and planning based on the seasonal precipitation pattern have critical implications for community development as well as energy and food security. Changes in these patterns are likely to be especially important in the context of an expected overall regional drying under future climate change (Rauscher et al., 2008).

Northwest Costa Rica experiences a tropical Savanna climate, where the wet season lasts from May through October (Hastenrath, 1967) and accumulates approximately 84% of the annual total precipitation. The wet season is interrupted by a relative midsummer drought (MSD) which forms the trough of the bimodal distribution of the seasonal cycle (Waylen et al., 1996b; Magaña et al., 1999). The wet season thus consists of three recognizable periods: (a) early season (ES), (b) midsummer drought (MSD), and (c) late season (LS). The onset and end of the wet season affects the success and failure of most local agricultural practices (Magaña et al., 1999, Alfaro, 2002). Anticipation of the start of the early wet season and the MSD is of great value to farmers, as it helps them decide when to plant and start investing in land and seedbed preparation. As such, it is reported that farmers pay particular attention to the MSD-onset, even more than its duration and severity (Allen et al., 2010; Gamble et al., 2010), as this occurs at a critical time for young crops. In addition, the region's climate is strongly influenced by large-scale climate variability, in particular the El Niño Southern Oscillation (ENSO) phenomenon (Waylen et al., 1996b; Rauscher et al., 2011). El Niño (La Niña) years are characterized by below (above) average precipitation (Waylen et al., 1996b).

The Fifth Assessment Report of the Intergovernmental Panel on Climate Change (IPCC-AR5) emphasizes that climate models can be used as a tool to investigate future projections over the

coming century and beyond (Flato et al., 2013). The skill and accuracy of climate models within the third and fifth phase of the Coupled Model Intercomparison Project (CMIP3 and CMIP5) in simulating precipitation have been evaluated over Central America and larger subdivisions of Central America (Rauscher et al., 2008; Karmalkar et al., 2013; Hidalgo and Alfaro, 2014; Ryu and Hayhoe, 2014). Hidalgo and Alfaro (2014) ranked 107 runs from 48 CMIP5 models according to their performance in reproducing the mean and standard deviation of both precipitation and surface temperature over Central America, as well as the ENSO-precipitation teleconnection of the observation and reanalysis dataset. Ryu and Hayhoe (2014) assessed the ability of 18 CMIP3 and 26 CMIP5 models to simulate the seasonal cycle of precipitation over three Caribbean regions (Central America, Greater Antilles, Lesser Antilles), and the role of the models' ability to simulate the CLLJ, NASH and SST patterns. They suggested grouping climate models into three categories, those that (1) simulate a bimodal distribution, (2) reproduce the MSD and the late season maximum, and (3) simulate only one precipitation maximum. They reported that most of the models in group 1 and 2 tend to underestimate the early wet season precipitation and overestimate that of the late wet season. Rauscher et al. (2008) assessed the ability of 17 CMIP3 general circulation models (GCMs) to capture the pattern of the seasonal cycle, the summer season precipitation (JJA), and the evolution of the MSD over Central America and the Inter-America Seas. They also discussed the role of large-scale dynamics in the evolution of the MSD.

A number of studies have projected future changes in precipitation over Central America for different time scales (e.g. seasonal, annual); such studies have pointed out the likelihood of decreasing precipitation, and increasing incidences of extreme weather conditions (Rauscher et al., 2008; Anderson et al., 2008; Neelin et al., 2006; Maldonado et al., 2013; Karmalkar et al., 2013).

Recent studies predict that the number of dry days over the tropical savanna regions will increase in the twenty-first century (Polade et al., 2014; Pascale et al., 2015). Pascale et al. (2015) estimated an increase in the annual number of dry days over South and Central America of up to 1 month by the end of the twenty-first century. Rauscher et al. (2008) projected a reduction in summer precipitation over Central America by 25% in the twenty-first century, with the greatest reduction experienced in June and July, as well as a longer MSD with an earlier onset. Hidalgo et al. (2013) identified a reduction in the runoff over Central America of 10 to 30% through employing downscaled runs from 30 GCMs.

In this paper, a Gaussian mixture model is used to describe and quantify the timing, duration, and intensity of the seasonal precipitation cycle both in observed data and in CMIP5 model projections. The model parameters are determined by fitting to monthly precipitation. The outputs of 19 CGCMs are evaluated over a box centered on the northwest region of Costa Rica (9-15 N and 90-84 W) with respect to observed precipitation during the period 1979-2005 according to four proposed metrics. Then, the RCP8.5 monthly bias-corrected and spatially disaggregated (BCSD) projections (0.5° resolution) of the best performing models, including the MEM are used to project future changes in the seasonal cycle over the region (9.5-11 N and 85-86 W) surrounding northwest Costa Rica. The average seasonal cycles of BCSD simulations in the period (2074-2100) are compared to the historical BCSD simulations in the baseline (1979-2005) period.

The paper is divided into the following sections: section 2.2 introduces the data sets and coupled GCM simulations; section 2.3 presents information on the study area and the used statistical

methods used for model evaluation; section 2.4 discusses the results of the model evaluation and presents future projections in the seasonal precipitation cycle; and section 2.5 presents conclusions.

2.2 Data and model inputs

2.2.1 Precipitation data

This study uses version 2.2 of the Global Precipitation Climatology Project (GPCP) monthly precipitation from 1979 to 2005 as the reference data (Huffman et al., 2012). The GPCP combines observations from over 6,000 rain gauge stations, satellite precipitation data, and sounding data. This combination provides the most complete analysis of rainfall to date over global oceans, as well as providing spatial detail over land. Adjusting the bias of satellite precipitation using data from land gauges provides a better land product (Adler et al., 2003). It was previously noted that GPCP underestimated precipitation over land in some regions due to the relative lack of rain gauges, especially in mountainous areas (Adler et al., 2003). However, Ryu and Hayhoe (2014) compared the GPCP version 2.0 with station-based precipitation over Central America, including Guanacaste, and found that GPCP agrees with station data, with the exception of the late wet season peak precipitation, which was thought to be due to the limited number of stations. The latest version (2.2) has reduced or eliminated a number of these sources of bias (Huffman et al., 2012).

2.2.2 CMIP5 models and simulations

CMIP5 simulations provide higher resolution models and new forcing scenarios that include new socioeconomic, technological, and environmental data (Moss et al. 2010); the simulations can be

used to identify a broad range of climate change expectations and adaptation strategies (Brekke et al., 2013). The treatment of atmospheric chemistry and response to aerosols has also been improved with CMIP5 (Yeh et al., 2012). Knutti and Sedláček (2013) identified large improvements in the robustness of precipitation projections of CMIP5 in the tropics, including Central America, compared to CMIP3.

This study employs the ‘raw’ outputs of 19 CMIP5 models (Taylor et al., 2012) (Table 1) in simulating the observed seasonal cycle of precipitation and in evaluating their performance. Possible changes in the seasonal precipitation cycle of the smaller subregion of Guanacaste (9.5-11 N and 85-86 W) in the late 21st century are derived by comparing the future and historical outputs of the best performing models according to the selected criteria. Since the spatial resolution of CMIP5 GCMs is still too coarse to support characterizing long-term changes in the seasonal precipitation cycle over such a small subregion, the monthly bias-corrected and spatially disaggregated (BCSD) projections (0.5° resolution) are used rather than the raw outputs of the GCMs. BCSD projections are obtained from the “Downscaled CMIP3 and CMIP5 Climate and Hydrology Projections” archive, a collaboration of the United States Bureau of Reclamation, the Climate Analytics Group, Climate Central, Lawrence Livermore National Laboratory, Santa Clara University, Scripps Institution of Oceanography, U.S. Army Corps of Engineers, and the U.S. Geological Survey. BCSD has been applied to CMIP3 and CMIP5 model outputs to assess climate change impacts (Cayan et al., 2008, Barnett et al., 2008, Girvetz et al., 2009, Cavazos et al., 2012, Demirel and Moradkhani, 2015). The procedure used in applying the bias correction and spatial disaggregation to GCM data is introduced in Wood et al. (2004), and Maurer (2007). Future climate change projections are based on the RCP8.5 scenario, which is considered a high radiative

forcing scenario leading to 8.5 W/m² in 2100 (Moss et al., 2010). Table 1 lists general information (modeling groups, atmospheric resolution, and number of ensembles) for the 19 models used in the study.

Due to random internal variability within models the multi-ensemble mean (MEM) can yield better agreement with observations than individual models (Phillips and Gleckler, 2006; Knutti et al., 2010; Miao et al., 2013). While the use of the MEM does reduce the error variance of the estimate of the mean, it also smoothes and underestimates the extent of interannual variability in model predictions and fails to adequately consider the implications of occasional extreme outcomes (e.g., very wet or very dry months). For an individual model, the mean of its ensembles is expected to lower the error by mutual cancelation. Therefore, the multi-ensemble mean (MEM) (mean of 37 ensembles) is included in the analysis and individual models are represented by the mean of their respective ensembles.

2.3 Materials and Methods

2.3.1 Gaussian mixture model and fitting

The Gaussian mixture model has been utilized for data processing and pattern recognition in areas including nuclear spectroscopy, electrokinetic capillary chromatography, speech recognition and pharmacokinetics (e.g., Reynolds, 1995; Abdel-Aal, 1998; Godfrey et al., 2010). Recently, Steyn et al. (2016) applied the Gaussian mixture model to the seasonal rainfall pattern of Costa Rica. Here, we apply and compare a single and double Gaussian model in fitting the seasonal cycle of

precipitation both in the current and in projected future climate regimes. Equation 1 is the general Gaussian function for a mixture of multiple Gaussians ($i = 1, np$).

Table 1. CMIP5 models used in this study

Model Name	Model Groups (Country)	Horizontal spatial Resolution (°lon × °lat)	Number Ensembles
ACCESS 1.0	Commonwealth Scientific and Industrial Research Organization) and Bureau of Meteorology (Australia)	1.875 × 1.25	1
ACCESS 1.3		1.875 × 1.25	1
BNU-ESM	Beijing Normal University (China)	2.81 × 2.81	1
CanESM2	Canadian Center for Climate Modeling and Analysis (Canada)	2.8 × 2.8	5
CESM1-CAM5	NSF-DOE-NCAR (USA)	1.4 × 1.4	3
CNRM-CM5	Centre National de Recherches Meteorologiques and Centre Européen de Recherche et Formation Avancées en Calcul Scientifique (France)	1.4 × 1.4	5
FIO-ESM	The First Institute of Oceanography, State Oceanic Administration (China)	2.8 × 2.8	3
FGOALS-g2	Flexible Global Ocean-Atmosphere-Land System	2.8 × 2.8	1
FGOALS-s2		1.6 × 2.8	2
HADGEM2-AO	National Institute of Meteorological Research and Korea Meteorological Administration (Korea)	1.8 × 1.25	1
HADGEM2-ES	UK Met Office Hadley Centre (UK)	1.8 × 1.25	4
HADGEM2-CC		1.8 × 1.25	1
MIROC5	University of Tokyo, National Institute for Environmental Studies, and Japan Agency for Marine-Earth Science and Technology (Japan)	1.4 × 1.4	1
MIROC-ESM- CHEM		2.8 × 2.8	1
MPI-ESM-LR	Max Planck Institute for Meteorology (Germany)	1.9 × 1.9	3
MPI-ESM-MR		1.9 × 1.9	1
MRI-CGCM3	Meteorological Research Institute (Japan)	1.1 × 1.1	1
NorESM1-M	Norwegian Climate Centre (Norway)	2.5 × 1.9	1
Inmcm4	Russian Institute for Numerical Mathematics (Russia)	2 × 1.5	1

$$f(t) = y_o + \sum_{i=1}^{np} \frac{A_i}{\sigma_i \sqrt{2\pi}} \exp\left(-\frac{(t-t_{ci})^2}{2\sigma_i^2}\right) \quad (1)$$

The Gaussian components are assumed to be superimposed upon a baseline rainfall rate y_o . The parameters for each component i are shown in Figure 2: the area under the curve A_i , the peak location t_{ci} , and the temporal standard deviation σ_i . np denotes the number of the simulated peaks, so a single and double peak can be fitted with four and seven parameters, respectively. If a CGCM reproduces a single peak with an MSD, the simulation profile is fitted as a single peak only.

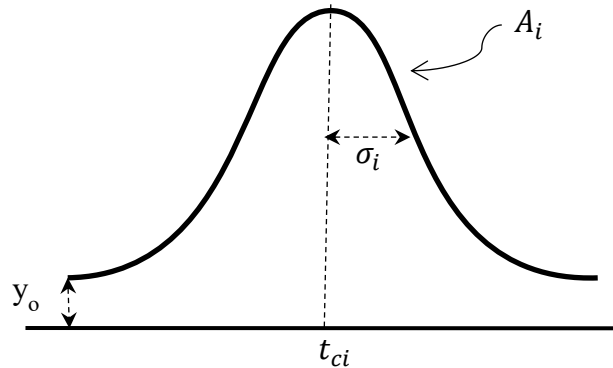


Figure 2. Single Gaussian distribution curve

To estimate the parameters for the model the least squares method is applied by minimizing the square difference between the climate models simulated monthly precipitation y_j for month j ($j =$

1, N) and the Gaussian mixture model prediction f_j . The nonlinear function requires the use of a search and optimization method in which a large number of initial guesses are made for the function parameters in order to be reasonably certain that the global minimum is reached.

The fit is deemed acceptable when the root mean squared error (RMSE) is less than 1 mm/d. In cases when the seasonal cycle produces a single peak with an MSD, the RMSE is found to be higher relative to double and single peaks.

2.3.2 The nine features of the bimodal seasonal cycle of precipitation

After obtaining the best estimate for the Gaussian mixture model parameters, we can quantify the changes in nine proposed features of the bimodal distribution. These features (Figure 3) can be categorized into three general groups: (a) maximum/minimum rainfall rates (mm/d), (b) seasonal period durations (days), and (c) seasonal transition times (days). The maximum/minimum rainfall rate group consists of three rainfall rates: H_1 denotes the maximum (peak) rainfall rate of the early wet season precipitation (ES), H_2 the maximum rainfall rate of the late wet season precipitation (LS), and H_d the minimum rainfall rate of the MSD (Equation 3). The rainfall rate of early (first) and late (second) wet season peaks can be approximated using Equation 2, whereas the MSD-rainfall rate is computed by finding the minimum between the two peaks.

$$H_i = \frac{A_i}{\sigma_i \sqrt{2\pi}} \quad (2)$$

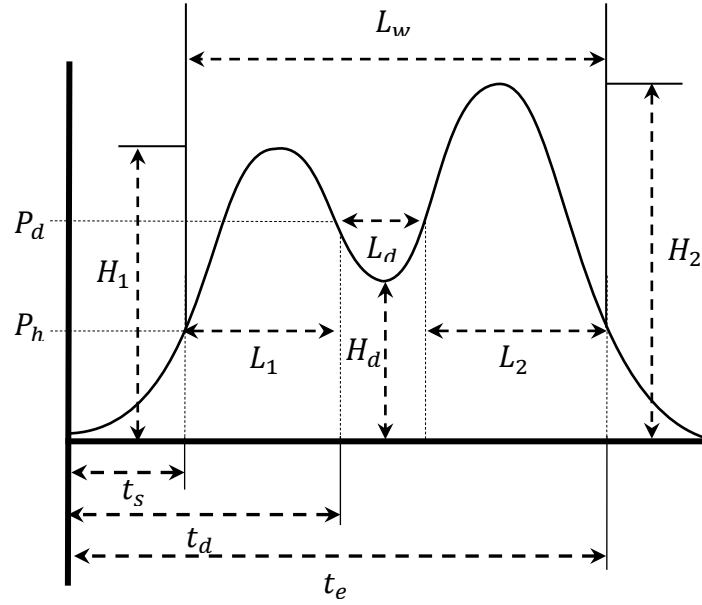


Figure 3. The nine features of the seasonal cycle: maximum/minimum rainfall rates (H_1, H_d, H_2), seasonal period durations (L_1, L_d, L_2), and seasonal transition times (t_s, t_d, t_e). (Note: L_w denotes the wet season duration)

The seasonal transition time parameters consist of the onset t_s and ending t_e times of the wet season, and the MSD onset t_d . We assume the wet season starts (ends) when monthly precipitation is above (below) a threshold value P_h . Since the wet season typically begins in May, we set the threshold P_h to be 4 mm/d, which is the first quartile of May precipitation (Figure 4). Therefore, both t_s and t_e can be determined when the fitted bimodal curve (double Gaussian) is intersected with a straight line drawn from the threshold precipitation (4 mm/d). The first (last) intersection point is the start t_s (end t_e) of the wet season. The MSD onset is determined as the second intersection point between the fitted bimodal curve and a horizontal straight line P_d , representing a 33% $(H_1 - H_d) + H_d$.

It is assumed that at that level the onset of the drought is apparent. After finding these transition times, the seasonal period durations (early wet season duration L_1 , late wet season duration L_2 , and MSD duration L_d) can be determined as the differences in the time line.

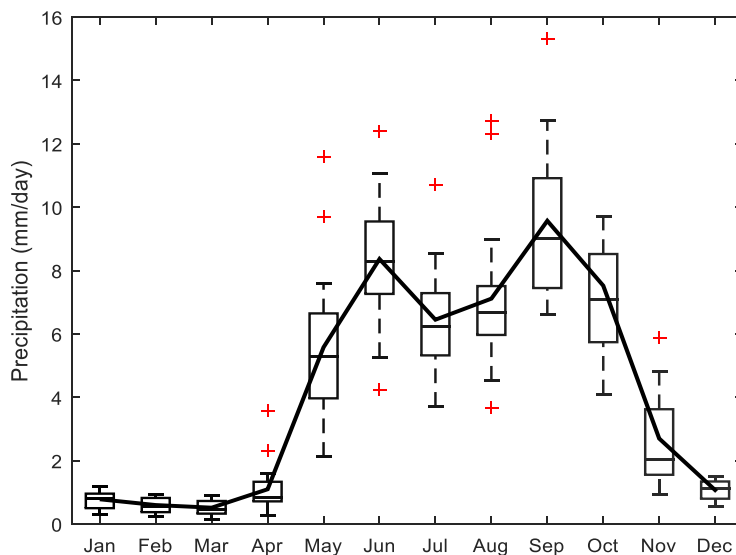


Figure 4. Boxplot of the GPCP observed seasonal cycle of precipitation (9-15 N and 90-84 W) over the (1979-2005) period and the solid line represents its average seasonal cycle. (The box represents maximum ($Q3 + 1.5 \times IQR$), third quartile ($Q3$), median, first quartile ($Q1$), and minimum ($Q1 - 1.5 \times IQR$)).

2.4 Results

2.4.1 Model evaluation

Four measures are proposed to compare climate model simulations with observations over the baseline (1979-2005) period: (1) annual mean precipitation, (2) interannual variability of

precipitation, (3) mean length of the dry season, and (4) the degree of bimodality in the seasonal pattern of precipitation.

We use the relative bias to measure the ability of a given model to simulate the observed annual mean precipitation (Su et al., 2013) and an interannual variability index *I**AV* to judge agreement between the modeled and observed interannual variability (Gleckler et al., 2008; Scherrer, 2011) for the period 1979-2005. The relative bias *RB* in the annual precipitation is computed by Equation 3, where P_m and P_o are the annual mean precipitation for a given model *m* and the observation respectively. A negative (positive) RB_m indicates underestimation (overestimation) relative to the GPCP annual mean. Table 2 shows the simulated annual mean and the relative bias of the 19 CMIP5 models and the MEM.

$$RB_m = \frac{P_m - P_o}{P_o} \quad (3)$$

The bias of the CMIP5 models relative to the observed annual mean precipitation (51 mm/day) ranges from -0.64 to 0.54. Eleven models underestimate the observed mean, while the other eight models overestimate the mean. NorESM1-M exhibits the most negative bias ($RB = -0.64$); MPI-ESM-MR exhibits the most positive bias ($RB = 0.54$); and CNRM-CM5 and CESM1-CAM5 produce the least ($RB = 0.02$ and 0.03 , respectively). The underestimation of the annual mean precipitation by CGCMs is due to the underestimation of local SSTs (Dai 2006; Martin and Schumacher 2011) and the associated early onset of the Atlantic warm pool (Wang 2007).

The simulated and observed interannual variations in yearly precipitation are compared using the *I**AV* (the observed interannual standard deviation is 6.4 mm/day). Table 2 also shows the predicted

standard deviation and coefficient of variation (standard deviation divided by the mean, as a percent) for each model.

Models with higher relative bias (overestimating the mean) also tend to overestimate the standard deviation (except MPI-ESM-MR and MPI-ESM-LR), so that the predicted coefficients of variation of the annual precipitation are more stable across models than is the case for the standard deviations. For the interannual variability evaluation, the *I*AV index is computed between observation and model *i* output from the ratio of the standard deviation of the model divided by that of the observation (Equation 5).

$$I\text{AV}_i = \left(\frac{\sigma_i}{\sigma_o} - \frac{1}{\frac{\sigma_i}{\sigma_o}} \right)^2 \quad (4)$$

The IAV ranges from Zero (when $\sigma_i = \sigma_o$) to infinity (when σ_i is either much larger than, or much smaller than, σ_o). Scherrer, (2011) proposed an accurate representation of observed interannual variability by model *i* with a IAV less than 0.5. Six models (HadGem2-AO, ACCESS1.0, ACCESS1.3, NorESM1-M, inmcm4, Fgoals-g2) obtain an IAV below 0.5. The lowest IAV indexes are determined for the CNRM-CM and CanESM2 models (IAV=0.0003 and IAV=0.0015, respectively). Other models that simulate a good representation for the observed interannual variability of the annual precipitation record include MRI-CGCM3 (IAV = 0.01) and MPI-ESM-LR (IAV = 0.02), as well as the MEM (IAV = 0.05). The high spatial resolution models (MRI-CGCM3, CESM1-CAM5, CNRM-CM5 and MIROC5) perform well in capturing the annual mean and interannual variability. However, some of the low spatial resolution models (e.g. HadGem2-

ES and HadGem2-CC) produce better performance than MRI-CGM3 (MIROC5) in matching the observed annual mean (interannual variability). This suggests some difficulty in determining whether there is a link between a model’s regional performance and horizontal spatial resolution.

A change in the length of the dry season could significantly influence agriculture and tourism in northwest Costa Rica. We evaluated the models’ performance in simulating the observed mean length of the dry season over the period 1979-2005. We define the length of the dry season as the remainder of a year after subtracting the length of the wet season L_w (see section 2.3). Table 2 shows the mean length of the simulated dry season and the bias in the simulated versus observed dry season length. MPI-ESM-LR and MPI-ESM-MR underestimate the mean length of the dry season by 33 and 31 days respectively, whereas all other models and the MEM overestimate the dry season length by 3-79 days. It can be noted that low performance in simulating mean dry season length is associated with low performance in capturing the annual mean precipitation. This may be due to the tendency of GCMs to underestimate the intensity of heavy precipitation (>10 mm/d) and overestimate the frequency of light precipitation (1-10 mm/d) (Sun et al., 2006).

To quantify models’ ability to capture the observed bimodal pattern of the seasonal precipitation cycle, a yearly pattern coefficient α_{pk} is defined as follows:

$$\alpha_{pk} = \frac{A_{1k}}{A_{1k}+A_{2k}} \quad (5)$$

A_{1k} and A_{2k} denote the area under the early and late wet season’s peaks, respectively, for a given year k . Hence, a model producing a single peak with or without an MSD over the seasonal cycle

for a year k would have $\alpha_{pk}=1$, since A_{2k} is zero (see section 2.3). In the case of a bimodal cycle, α_{pk} ranges from near 0 (most of the rain during the late wet season, $A_{2k} \gg A_{1k}$) to near 1 (most of the rain during the early wet season, $A_{1k} \gg A_{2k}$). A two-sided Kolmogorov-Smirnov (KS) test (Smirnov, 1939) is used to compare the cumulative distribution of the yearly pattern coefficient α_{pk} of the observed data to that of the simulations for the period 1979-2005. Its test statistic represents the maximum distance D_{max} between the two cumulative distributions. In this study, we note that (for the period 1979-2005) D_{max} below 0.4 is approximately associated with p-value at the 0.01 significance level. Figure 5 displays the two-sample KS test statistic for the 19 models and the MEM, along with the corresponding value of the interannual variability index.

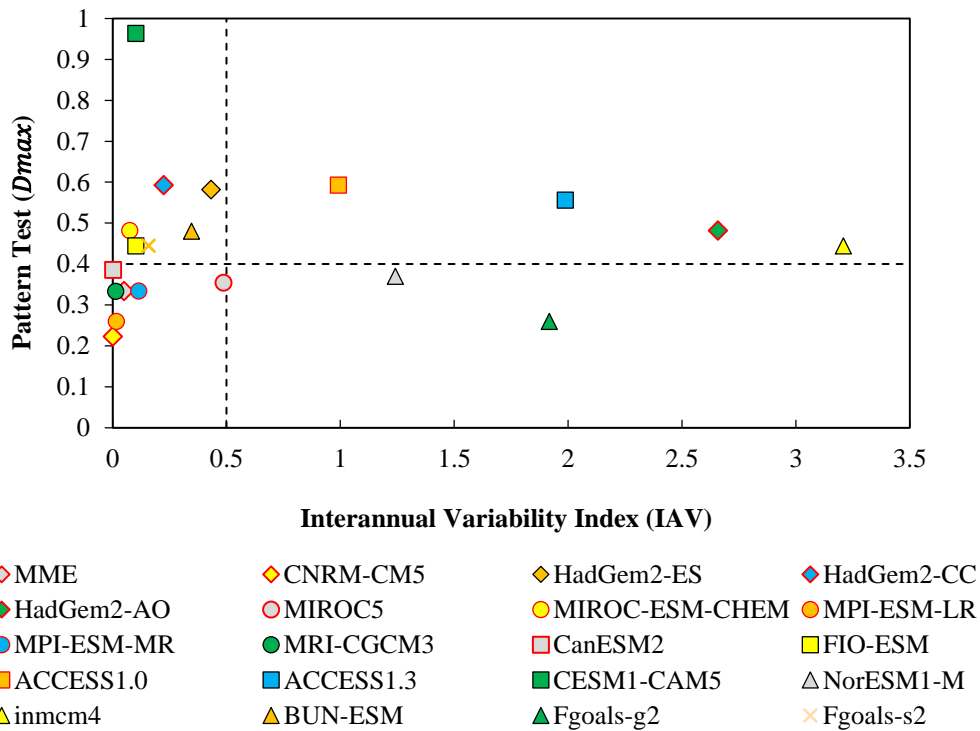


Figure 5. The interannual variability index (IAV) (horizontal axis) and the test statistic (D_{max}) of the seasonal pattern KS test (vertical axis). Models in the lower left quadrant exhibit acceptable performance for simulating both features of the annual and monthly rainfall (1979-2005)

Table 2. Indicators of statistical agreement between CGCMS (and their MEM) predicted and observed GPCP precipitation over the period 1979-2005.

Observation/ Climate model	Annual precipitation					Dry season	
	Mean precipitation (mm/d)	Relative bias	Interannual standard deviation (mm/d)	Coefficient of variation	IAV	Mean length (days)	Relative bias
GPCP	50.8	0	6.2	12.3	0	187	0
CNRM-CM5	51.8	0.02	6.3	12.2	0.0003	216	0.13
HadGem2-ES	57.9	0.14	8.6	14.9	0.43	243	0.3
HadGem2-CC	54.4	0.07	7.9	14.5	0.22	177	0.02
HadGem2-AO	46.4	-0.09	13.2	28.4	2.65	204	0.09
MIROC5	45.7	-0.1	8.8	19.2	0.48	189	0.02
MIROC-ESM-CHEM	25.9	-0.49	5.5	21.0	0.07	255	0.37
MPI-ESM-LR	73.7	0.45	5.9	8.0	0.01	153	-0.18
MPI-ESM-MR	78.0	0.54	5.3	6.8	0.11	156	-0.16
MRI-CGCM3	36.9	-0.27	6.6	17.9	0.01	228	0.21
CanESM2	31.1	-0.39	6.1	19.7	0.001	228	0.23
FIO-ESM	31.1	-0.39	5.3	17.1	0.10	228	0.24
ACCESS1.0	61.5	0.21	10.1	16.4	0.99	192	0.03
ACCESS1.3	62.8	0.24	12.1	19.2	1.98	213	0.14
CESM1-CAM5	52.5	0.03	7.3	14.0	0.10	192	0.03
NorESM1-M	18.4	-0.64	3.7	20.0	1.24	276	0.39
inmcm4	28.7	-0.43	2.8	9.7	3.2	255	0.38
BUN-ESM	21.2	-0.58	4.7	22.1	0.35	273	0.42
Fgoals-g2	27.8	-0.45	3.3	11.8	1.91	249	0.35
Fgoals-s2	19.9	-0.61	5.1	25.7	0.16	264	0.41
MEM	44.4	-0.13	7.0	15.7	0.05	188	0.01

Six models (CNRM-CM5, MIROC5, MPI-ESM-LR, MPI-ESM-LR, MRI-CGCM3 and CanESM2), as well as the MEM, show a good ability to reproduce the distribution of the observed coefficient α_{pk} over the 27 years, as their KS test statistics D_{max} are below 0.4. Thus, the null hypothesis that the observed α_{pk} and their distributions are sampled from the same population cannot be rejected. The agreement between the predicted and observed bimodal distributions is

most pronounced for the CNRM-CM5, while four models (CESM1-CAM5, ACCESS1.0, and HadGem2-CC) exhibit poor agreement with the observed seasonal pattern distribution. Figure 5 also indicates that both Fgoals-g2 and NorESM1-M have the capability to simulate the observed pattern of the seasonal cycle, but with low skill to match the observed interannual variability. All selected models and the MEM generate a bimodal distribution over the averaged seasonal cycle for the baseline (1979-2005) period as shown in Figure 6, though even among these, MPI-ESM models systematically overestimate the monthly precipitation, while other models systematically underestimate it.

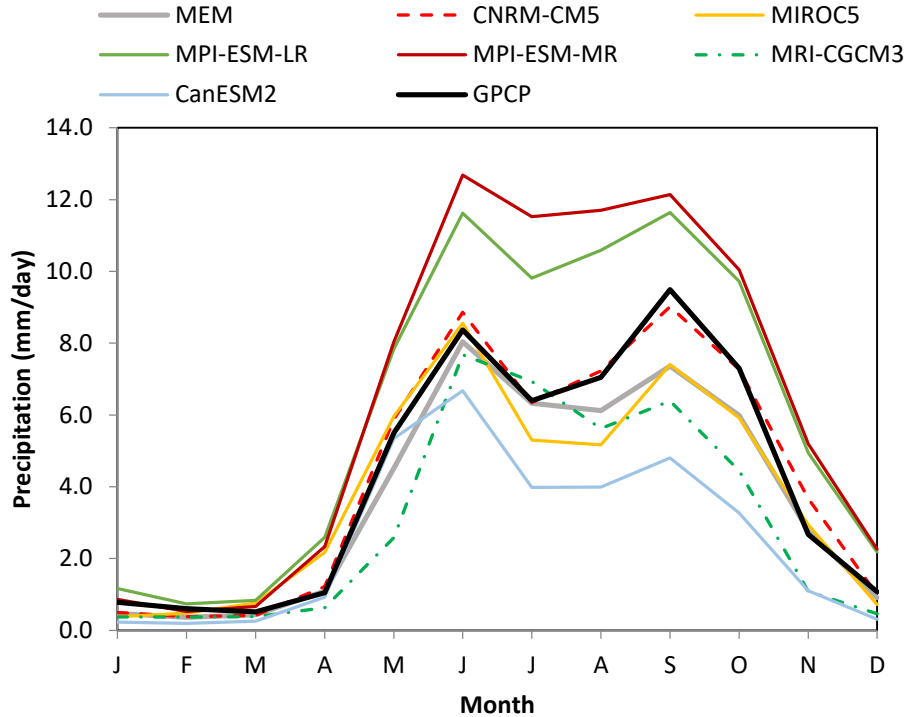


Figure 6. Distribution of average simulated (by CGCMs) and observed monthly precipitation (mm/d) over the baseline (1979-2005) period

Based on the four metrics compared, we are able to determine that six models (CNRM-CM5, MIROC5, MPI-ESM-MR, MPI-ESM-LR, MRI-CGCM3 and CanESM2) and the MEM show a

good overall agreement with the tested characteristics of the GPCP observations over the period 1979-2005.

2.4.2 Future climate projections

This sub-section analyzes the projected future changes in the seasonal cycle of precipitation according to the BCSD of the selected CGCMs and the MEM over the (9.5-11 N and 85-86 W) region. In addition, it determines the contribution of these predicted changes to the seasonal (mm/d) mean precipitation and the interannual variability. The projected long-term changes in the seasonal cycle under RCP8.5 can be quantified by comparing the average of the baseline test period (1979-2005) with the future projection period (2074-2100).

Long-term changes in the distribution of the ES precipitation are quantified by changes in the peak ES rainfall rate H_1 , ES duration L_1 , and ES onset time t_s . Changes in the distribution of precipitation during the MSD and LS are similarly quantified. Figure 7 shows the change in monthly precipitation projected to occur from the baseline (1979-2005) to the future (2074-2100) based on the selected BCSD CGCMs and the MEM. The MPI-ESM-MR is found to be the only model that is sensitive to the selected region, so by shifting longitude toward the mountains (0.5° to the right) this model predicts a one peak seasonal cycle. As shown in figure 7, the changes in predicted precipitation vary considerably across models and time of year, through a relatively even reduction is predicted across the wet season by the MEM.

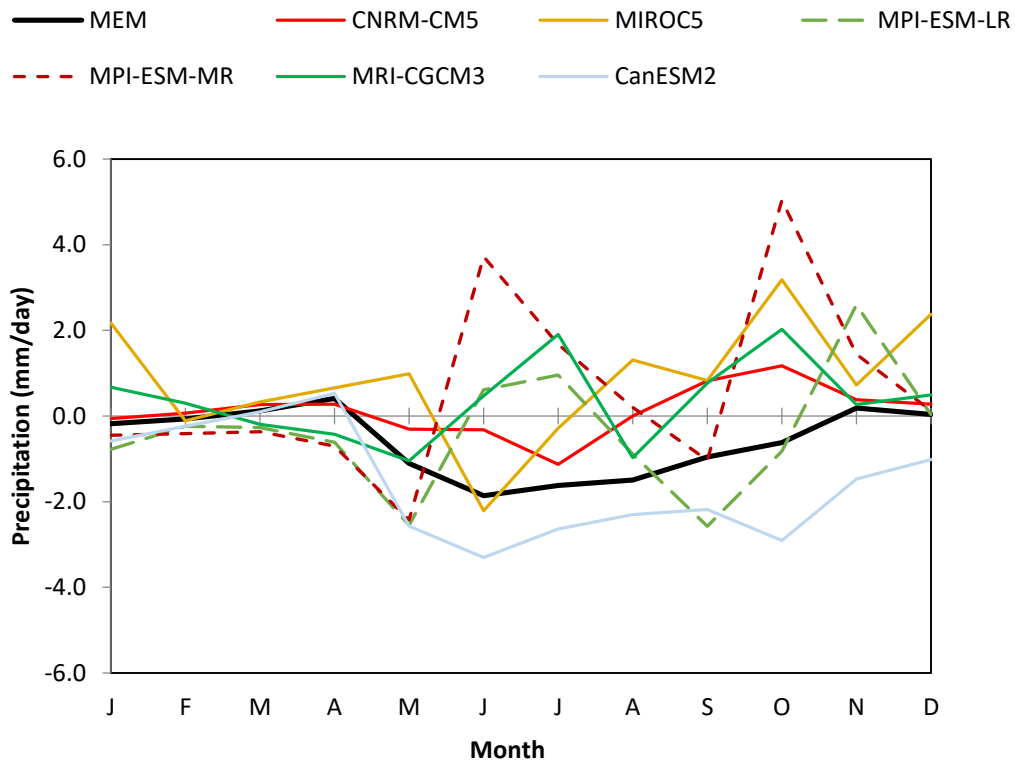


Figure 7. Change in average monthly precipitation (BCSD) for the (2074-2100) period relative to the baseline (1979-2005) period for the selected models and the MEM

Table 3 shows the projected changes in the nine features of the bimodal seasonal cycle of precipitation in the future (2074-2100) period with respect to the baseline (1979-2005) period. Four of the selected BCSD CGCMs and the MEM predict a reduction in the peak ES rainfall rate H_1 and a shortening in the duration L_1 of the ES ranging from 2 to 42 % and 4 to 14 days, respectively. MIROC5 is the only model that predicts an earlier ES onset, while the other models project a late onset, from 1 to 13 days.

Table 3. Percentage changes in the maximum/minimum rainfall rates, seasonal period duration and seasonal transition times of early, middle, and late wet season (actual changes in parentheses)

Early Wet Season			
Model/Feature	Maximum rainfall rate, H_1 % (mm/d)	Duration, L_1 % (days)	Starting time, t_s % (days)
MEM	-23 (2)	-7 (4)	2.5 (4)
CNRM-CM5	-6 (0.5)	-4 (3)	0.2 (1)
MIROC5	-15 (1.5)	-22 (14)	-2 (4)
MPI-ESM-LR	-2 (0.2)	19 (13)	8 (10)
MPI-ESM-MR	21 (2)	31 (15)	5 (8)
MRI-CGCM3	3 (0.2)	25 (12)	4 (7)
CanESM2	-42 (3.6)	-23 (14)	9 (13)
Midsummer drought			
Model/Feature	Minimum rainfall rate, H_d % (mm/d)	Duration, L_d % (days)	Starting time, t_d % (days)
MEM	-26 (1.8)	-5 (3)	-0.3 (1)
CNRM-CM5	-15 (1)	-9 (4)	-1 (2)
MIROC5	-15 (1.0)	-15 (8)	-9 (18)
MPI-ESM-LR	-18 (1.1)	-10 (5)	11 (22)
MPI-ESM-MR	-5 (0.3)	-2 (1)	13 (25)
MRI-CGCM3	-10 (0.6)	-27 (14)	11 (22)
CanESM2	-40 (2.5)	-15 (7)	-0.2 (1)
Late Wet Season			
Model/Feature	Maximum rainfall rate, H_2 % (mm/d)	Duration, L_2 % (days)	Ending time, t_e % (days)
MEM	-10 (1)	3 (4)	0.1 (1)
CNRM-CM5	8 (0.9)	8 (8)	0.6 (3)
MIROC5	14 (1.5)	30 (28)	6 (19)
MPI-ESM-LR	-3 (0.3)	-9 (9)	3 (10)
MPI-ESM-MR	30 (3.3)	-23 (24)	0.8 (3)
MRI-CGCM3	24 (2.5)	-12 (11)	-0.8 (3)
CanESM2	-24 (2.5)	-8 (10)	-4 (15)

For the MSD, the selected BCSD CGCMs plus the MEM predict a decrease in the minimum rainfall rate H_d and a reduction in the duration L_d of the MSD. In contrast, they disagree on the change in its onset with three models (CNRM-CM5, MIROC5, and CanESM2; and the MEM) projecting an earlier onset and the other three models (MRI-CGCM3, MPI-ESM-MR and MPI-ESM-LR) project a later onset. Low agreement is also found in the projected change of both the maximum rainfall rate H_2 and the duration L_2 of the LS. MRI-CGCM3 and CanESM2 project a late end of the wet season t_e , while the other models and the MEM project an early end.

The changes in the seasonal mean precipitation (mm/d) for the ES, MSD, and LS are shown in Figure 8. Note the predominant decrease in the seasonal mean precipitation is pronounced in the MSD, which implies a more severe relative drought. The projected changes in the MSD agree with Rauscher et al. (2008), who found an intensification for the MSD based on the analysis of CMIP3 models and the A1B emissions scenario. Figure 8 shows that the selected BCSD CGCMs and the MEM predict a reduction in the MSD precipitation ranging from -11% to -51% except for MPI-ESM-MR, which predicts an increase in the MSD precipitation of about 8.5%. There is less agreement on the projections for both ES and LS precipitation, with three models (MRI-CGCM3, MPI-ESM-MR, and MPI-ESM-LR) projecting an increase in the ES, and the other three models (MIROC5, CNRM-CM5 and MPI-ESM-MR) predicting an increase in the LS precipitation.

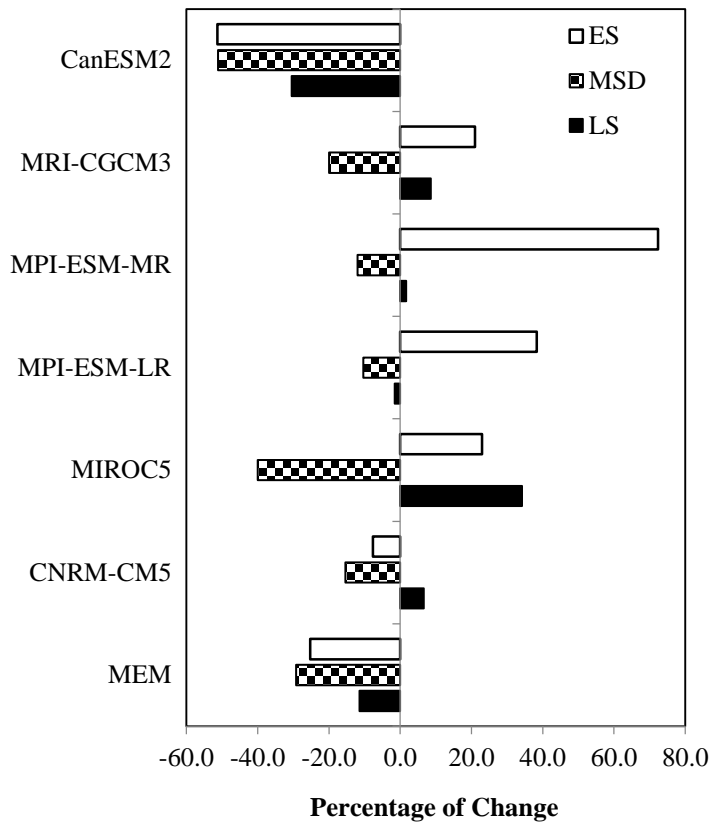


Figure 8. Percentage change in the seasonal mean precipitation over the (2074-2100) period relative to the (1979-2005) period under RCP8.5

The full representation of the change in the seasonal precipitation under global climate change cannot be determined only by relying on the climatology, but must also consider interannual variability (Fu, 2012; Menon et al., 2013). In fact, the complexity of northwest Costa Rica's climate places particular importance on interannual variability (Alfaro, 2002). Figure 9 presents the percentage changes in the interannual variability of the three seasonal (ES, MSD, and LS) precipitation periods based on the selected BCSD CGCMs and the MEM. The change in the interannual variability is determined by the percentage change in the standard deviation of the

(integrated) mean precipitation for the period 2074-2100, with respect to that of the period 1979-2005. The percentage change is given as $\left(\left(\frac{\sigma_{(2074-2100)}}{\sigma_{(1979-2005)}} * 100 \right) - 100 \right)$.

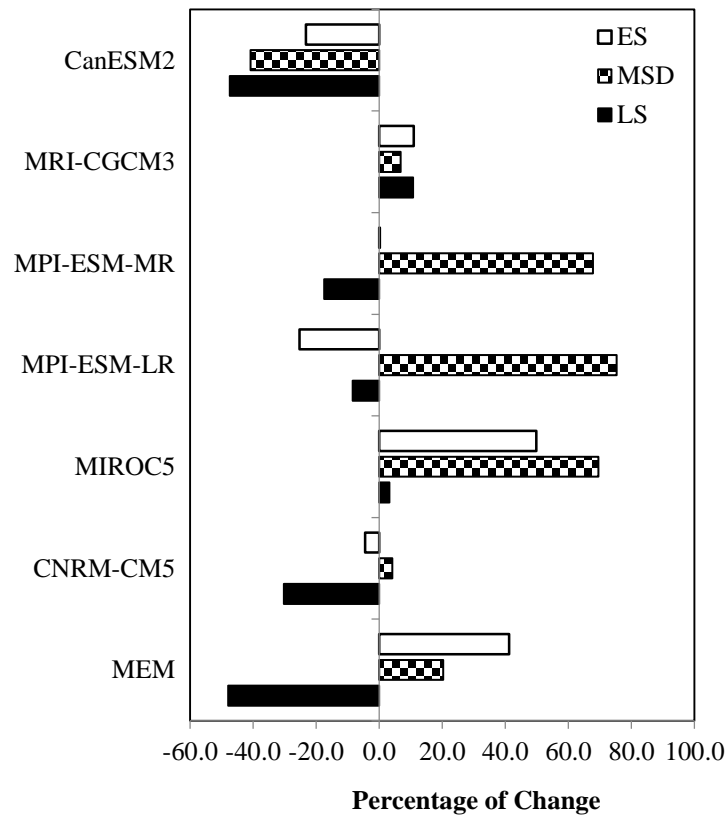


Figure 9. Percentage change in the standard deviation of (2074-2100) period relative to that of the (1979-2005) period under RCP8.5

CanESM2 projects a consistent increase in the interannual variability of seasonal precipitation, while MRI-CGCM3 predicts a consistent decrease. The other models exhibit less agreement on the change in the interannual variability for the ES and LS precipitation, through considerable agreement on more interannual variability for the MSD precipitation.

2.5 Conclusions

Changes in the seasonal cycle of precipitation over northwest Costa Rica are expected to have a significant impact on the region's water budget, agricultural production, and energy security. This paper presents a method to better characterize the uncertainty in the future seasonal precipitation cycle in northwest Costa Rica projected by climate models. The performance of 19 CMIP5 CGCMs is evaluated with regard to their capacity to simulate four characteristics of the observed precipitation (GPCP) over the region 9-15 N and 90-84 W during the 1979-2005 period. The considered characteristics of the seasonal cycle are: (1) the annual mean precipitation, (2) the interannual variability, (3) the mean length of the dry season, and (4) the degree of bimodality in the seasonal cycle. Six CGCMs (CNRM-CM5, MIROC5, MPI-ESM-MR, MPI-ESM-LR, MRI-CGCM3 and CanESM2) and the multi-ensemble mean (MEM) show the closest agreement to the observed characteristics. The role of the horizontal spatial resolution in the model performance is not yet clear, since the high resolution models do not always perform better than low resolution models. Thus, determining the optimum resolution is not possible because it is difficult to distinguish between the level of interaction between resolution, physical parameterizations and the models' convergence (IPCC, 2013).

The study finds that all the selected BCSD CGCMs and the MEM (except MPI-ESM-MR) agree on an intensification of the MSD associated with a reduction in its duration. A degree of uncertainty in the MSD-onset projection has been noted as three (four) models predict a later (earlier) MSD-onset ranging from 22 to 25 (1 to 18) days. The future projections for ES and LS precipitation can be summarized in three possible scenarios as follows: a) lower and shorter ES

peak with higher and longer LS peak associated with an increase (decrease) in the LS (ES) precipitation, b) higher and longer ES peak with higher and shorter LS peak associated with an increase (decrease) in ES (LS) precipitation, and c) reduced ES and LS peaks with a reduction in the ES and LS precipitation.

With the exception of CanESm2, the MEM and the selected BCSD CGCMs all project an increase in the interannual variability of the MSD precipitation. The ES (LS) precipitation interannual variability is projected to be reduced (increased) according to MPI-ESM-LR and CNRM-CM5 and CanESM2 (MRI-CGCM3 and MIROC5), while the other models project the opposite.

Acknowledgments

We acknowledge the World Climate Research Programme's Working Group on Coupled Modelling, which is responsible for CMIP, and we thank the climate modeling groups (listed in Table 1 of this paper) for producing and making available their model output. For CMIP, the U.S. Department of Energy's Program for Climate Model Diagnosis and Intercomparison provides coordinating support and led development of software infrastructure in partnership with the Global Organization for Earth System Science Portals. The first author work's was supported by Kuwait University. The second and third author received support from the Belmont Forum / NSF, G8MUREFU3FP-2200-139, through the international project 'FuturAgua: Enhancing adaptation and resilience to drought in dry tropical social-ecological systems'. We acknowledge also the idea and motivation shared with our colleagues in the FuturAgua project, especially Professor Douw Steyn (University of British Columbia). The authors also declare that there is no conflict of interest.

References

- Abdel-Aal, R.E., 1998. Automatic fitting of Gaussian peaks using abductive machine learning. *IEEE Transactions on Nuclear Science*, 45:1-16.
- Adler, R.F., Huffman, G.J., Chang, A., Ferraro, R., Xie, P.P., Janowiak, J., Rudolf, B., Schneider, U., Curtis, S., Bolvin, D. and Gruber, A., 2003. The version-2 global precipitation climatology project (GPCP) monthly precipitation analysis (1979-present). *Journal of hydrometeorology*, 4:1147-1167.
- Alfaro, E.J., 2002. Some characteristics of the annual precipitation cycle in Central America and their relationships with its surrounding tropical oceans. *Tópicos Meteorológicos y Oceanográficos*, 9: 88-103.
- Allen, T.L., Curtis, S. and Gamble, D.W., 2010. The midsummer dry spell's impact on vegetation in Jamaica. *Journal of Applied Meteorology and Climatology*, 49:1590-1595.
- Anderson, E.R., Cherrington, E.A., Tremblay-Boyer, L., Flores, A.I. and Sempris, E., 2008. Identifying critical areas for conservation: Biodiversity and climate change in Central America, Mexico, and the Dominican Republic. *Biodiversity*, 9: 89-99.
- Arnell, N.W., Brown, S., Gosling, S.N., Gottschalk, P., Hinkel, J., Huntingford, C., Lloyd-Hughes, B., Lowe, J.A., Nicholls, R.J., Osborn, T.J. and Osborne, T.M., 2016. The impacts of climate change across the globe: A multi-sectoral assessment. *Climatic Change*, 134: 457-474.
- Barnett, T.P., Pierce, D.W., Hidalgo, H.G., Bonfils, C., Santer, B.D., Das, T., Bala, G., Wood, A.W., Nozawa, T., Mirin, A.A. and Cayan, D.R., 2008. Human-induced changes in the hydrology of the western United States. *science*, 319: 1080-1083.
- Bates, B., Kundzewicz, Z.W., Wu, S. and Palutikof, J., 2015. Climate change and water: technical paper VI. Intergovernmental Panel on Climate Change (IPCC).
- Brekke, L.D., Maurer, E.P., Anderson, J.D., Dettinger, M.D., Townsley, E.S., Harrison, A. and Pruitt, T., 2009. Assessing reservoir operations risk under climate change. *Water Resources Research*, 45.
- Cavazos, T., Torres, A. and Arriaga-Ramirez, S., 2012, December. Climate change scenarios for the North American monsoon using CMIP3 and CMIP5 models. In *AGU Fall Meeting Abstracts (Vol. 1, p. 06)*.
- Cayan, D.R., Maurer, E.P., Dettinger, M.D., Tyree, M. and Hayhoe, K., 2008. Climate change scenarios for the California region. *Climatic change*, 87: 21-42.
- Conway, D., van Garderen, E.A., Deryng, D., Dorling, S., Krueger, T., Landman, W., Lankford, B., Lebek, K., Osborn, T., Ringler, C. and Thurlow, J., 2015. Climate and southern Africa's water-energy-food nexus. *Nature Climate Change*, 5: 837-846.

- Curtis, S. and Gamble, D.W., 2008. Regional variations of the Caribbean mid-summer drought. *Theoretical and Applied Climatology*, 94: 25-34.
- Dai, A., 2006. Recent climatology, variability, and trends in global surface humidity. *Journal of Climate*, 19: 3589-3606.
- Demirel, M.C. and Moradkhani, H., 2016. Assessing the impact of CMIP5 climate multi-modeling on estimating the precipitation seasonality and timing. *Climatic Change*, 135: 357-372.
- Flato, G., Marotzke, J., Abiodun, B., Braconnot, P., Chou, S.C., Collins, W.J., Cox, P., Driouech, F., Emori, S., Eyring, V. and Forest, C., 2013. Evaluation of Climate Models. In: *Climate Change 2013: The Physical Science Basis. Contribution of Working Group I to the Fifth Assessment Report of the Intergovernmental Panel on Climate Change. Climate Change 2013*, 5: 741-866.
- Frumhoff, P.C., Burkett, V., Jackson, R.B., Newmark, R., Overpeck, J. and Webber, M., 2015. Vulnerabilities and opportunities at the nexus of electricity, water and climate. *Environmental Research Letters*, 10: 080201.
- Fu, Y., 2013. The projected temporal evolution in the interannual variability of East Asian summer rainfall by CMIP3 coupled models. *Science China Earth Sciences*, 56: 1434-1446.
- Gamble, D.W., Campbell, D., Allen, T.L., Barker, D., Curtis, S., McGregor, D. and Popke, J., 2010. Climate change, drought, and Jamaican agriculture: local knowledge and the climate record. *Annals of the Association of American Geographers*, 100: 880-893.
- Giannini, A., Kushnir, Y. and Cane, M.A., 2000. Interannual variability of Caribbean rainfall, ENSO, and the Atlantic Ocean*. *Journal of Climate*, 13: 297-311.
- Girvetz, E.H., Zganjar, C., Raber, G.T., Maurer, E.P., Kareiva, P. and Lawler, J.J., 2009. Applied climate-change analysis: the climate wizard tool. *PLoS One*, 4: e8320.
- Gleckler, P. J., Taylor, K. E., & Doutriaux, C., 2008. Performance metrics for climate models. *Journal of Geophysical Research: Atmospheres*, 113.
- Godfrey, K.R., Arundel, P.A., Zhu, W., Dong, Z. and Bryant, R., 2012. Modelling the double peak phenomenon. *Journal of Bioequivalence & Bioavailability*, 2011.
- Harrison, M. and Waylen, P., 2000. A note concerning the proper choice for Markov model order for daily precipitation in the humid tropics: A case study in Costa Rica. *International Journal of Climatology*, 20: 1861-1872.
- Hastenrath, S., 1976. Variations in low-latitude circulation and extreme climatic events in the tropical Americas. *Journal of the Atmospheric Sciences*, 33: 202-215.
- Hastenrath, S.L., 1967. Rainfall distribution and regime in Central America. *Archiv für Meteorologie, Geophysik und Bioklimatologie, Serie B*, 15: 201-241.
- Hidalgo, H.G. and Alfaro, E.J., 2015. Skill of CMIP5 climate models in reproducing 20th century basic climate features in Central America. *International Journal of Climatology*, 35: 3397-3421.
- Hidalgo, H.G., Amador, J.A., Alfaro, E.J. and Quesada, B., 2013. Hydrological climate change projections for Central America. *Journal of Hydrology*, 495: 94-112.

- Huffman, G.J., Bolvin, D.T. and Adler, R.F., 2012. GPCP version 2.2 SG Combined Precipitation Data Set (last updated 2012). World Data Center for Meteorology (Asheville), NCDC.[Available online at <https://www.ncdc.noaa.gov/wdc/wdcamet-ncdc.html>.].
- Jacobs, K.L. and Snow, L., 2015. Adaptation in the Water Sector: Science & Institutions. *Dædalus*, 144: 59-71.
- Karmalkar, A.V., Taylor, M.A., Campbell, J., Stephenson, T., New, M., Centella, A., Benzanilla, A. and Charlery, J., 2013. A review of observed and projected changes in climate for the islands in the Caribbean. *Atmósfera*, 26: 283-309.
- Knutti, R. and Sedláček, J., 2013. Robustness and uncertainties in the new CMIP5 climate model projections. *Nature Climate Change*, 3: 369-373.
- Knutti, R., Furrer, R., Tebaldi, C., Cermak, J. and Meehl, G.A., 2010. Challenges in combining projections from multiple climate models. *Journal of Climate*, 23: 2739-2758.
- Lobell, D.B. and Burke, M.B., 2008. Why are agricultural impacts of climate change so uncertain? The importance of temperature relative to precipitation. *Environmental Research Letters*, 3: 034007.
- Magaña, V., Amador, J.A. and Medina, S., 1999. The midsummer drought over Mexico and Central America. *Journal of Climate*, 12: 1577-1588.
- Maldonado, T., Alfaro, E., Fallas-López, B. and Alvarado, L., 2013. Seasonal prediction of extreme precipitation events and frequency of rainy days over Costa Rica, Central America, using Canonical Correlation Analysis. *Advances in Geosciences*, 33: 41-52.
- Mapes, B.E., Liu, P. and Buening, N., 2005. Indian monsoon onset and the Americas midsummer drought: Out-of-equilibrium responses to smooth seasonal forcing. *Journal of climate*, 18: 1109-1115.
- Martin, E.R. and Schumacher, C., 2011. The Caribbean low-level jet and its relationship with precipitation in IPCC AR4 models. *Journal of Climate*, 24: 5935-5950.
- Maurer, E.P., 2007. Uncertainty in hydrologic impacts of climate change in the Sierra Nevada, California, under two emissions scenarios. *Climatic Change*, 82: 309-325.
- Menon, A., Levermann, A., Schewe, J., Lehmann, J. and Frieler, K., 2013. Consistent increase in Indian monsoon rainfall and its variability across CMIP-5 models. *Earth System Dynamics*, 4: 287-300.
- Miao, C., Duan, Q., Sun, Q. and Li, J., 2013. Evaluation and application of Bayesian multi-model estimation in temperature simulations. *Progress in physical geography* 37: 727-44.
- Moss, R.H., Edmonds, J.A., Hibbard, K.A., Manning, M.R., Rose, S.K., Van Vuuren, D.P., Carter, T.R., Emori, S., Kainuma, M., Kram, T. and Meehl, G.A., 2010. The next generation of scenarios for climate change research and assessment. *Nature*, 463: 747-756.
- Neelin, J.D., Münnich, M., Su, H., Meyerson, J.E. and Holloway, C.E., 2006. Tropical drying trends in global warming models and observations. *Proceedings of the National Academy of Sciences*, 103: 6110-6115.

- Pascale, S., Lucarini, V., Feng, X., Porporato, A. and ul Hasson, S., 2016. Projected changes of rainfall seasonality and dry spells in a high greenhouse gas emissions scenario. *Climate Dynamics*, 46: 1331-1350.
- Phillips, T.J. and Gleckler, P.J., 2006. Evaluation of continental precipitation in 20th century climate simulations: The utility of multimodel statistics. *Water Resources Research*, 42.
- Polade, S.D., Pierce, D.W., Cayan, D.R., Gershunov, A. and Dettinger, M.D., 2014. The key role of dry days in changing regional climate and precipitation regimes. *Scientific reports*, 4.
- Porkka, M., Gerten, D., Schaphoff, S., Siebert, S. and Kummu, M., 2016. Causes and trends of water scarcity in food production. *Environmental Research Letters*, 11.
- Rauscher, S.A., Giorgi, F., Diffenbaugh, N.S. and Seth, A., 2008. Extension and intensification of the Meso-American mid-summer drought in the twenty-first century. *Climate Dynamics*, 31: 551-571.
- Rauscher, S.A., Kucharski, F. and Enfield, D.B., 2011. The role of regional sst warming variations in the drying of meso-america in future climate projections*. *Journal of Climate*, 24: 2003-2016.
- Reclamation, 2013. Downscaled CMIP3 and CMIP5 climate and hydrology projections: Release of downscaled CMIP5 climate projections, comparison with preceding information, and summary of user needs, US Dept. of the Interior, Bureau of Reclamation, Technical Services Center, Denver. (Archive, http://gdodcp.ucllnl.org/downscaled_cmip_projections)
- Reynolds, D. A., 1995. Speaker identification and verification using Gaussian mixture speaker models. *Speech communication*, 17: 91-108.
- Ryu, J.H. and Hayhoe, K., 2014. Understanding the sources of Caribbean precipitation biases in CMIP3 and CMIP5 simulations. *Climate dynamics*, 42: 3233-3252.
- Scherrer, S. C., 2011. Present-day interannual variability of surface climate in CMIP3 models and its relation to future warming. *International Journal of Climatology*, 31:1518-1529.
- Small, R.J.O., De Szoek, S.P. and Xie, S.P., 2007. The Central American Midsummer Drought: regional aspects and large-scale forcing. *Journal of Climate*, 20:4853-4873.
- Smirnov, N.V., 1939. On the estimation of the discrepancy between empirical curves of distribution for two independent samples. *Bull. Math. Univ. Moscou*, 2.
- Steyn, D., Moisseeva, N., Harari, O., and Welch, W.J., 2016. Temporal and Spatial Variability of Annual Rainfall Patterns in Guanacaste, Costa Rica. *FuturAgua internal project report*. 17 p.
- Su, F., Duan, X., Chen, D., Hao, Z. and Cuo, L., 2013. Evaluation of the global climate models in the CMIP5 over the Tibetan Plateau. *Journal of Climate*, 26: 3187-3208.
- Sun, Y., Solomon, S., Dai, A. and Portmann, R.W., 2006. How often does it rain?. *Journal of Climate*, 19: 916-934.
- Taylor, K.E., Stouffer, R.J. and Meehl, G.A., 2012. An overview of CMIP5 and the experiment design. *Bulletin of the American Meteorological Society*, 93.

- Vargas, A.B. and Trejos, V.F.S., 1994. Changes in the general circulation and its influence on precipitation trends in Central America: Costa Rica. *Ambio*.
- Wang, C., 2007. Variability of the Caribbean Low-Level Jet and its relations to climate. *Climate Dynamics*, 4: 411-422.
- Watts, G., Battarbee, R.W., Bloomfield, J.P., Crossman, J., Daccache, A., Durance, I., Elliott, J.A., Garner, G., Hannaford, J., Hannah, D.M. and Hess, T., 2015. Climate change and water in the UK—past changes and future prospects. *Progress in Physical Geography*, 39: 6-28.
- Waylen, P.R., Caviedes, C.N. and Quesada, M.E., 1996a. Interannual variability of monthly precipitation in Costa Rica. *Journal of Climate*, 9: 2606-2613.
- Waylen, P.R., Quesada, M.E. and Caviedes, C.N., 1996b. Temporal and spatial variability of annual precipitation in Costa Rica and the Southern Oscillation. *International Journal of Climatology*.
- Whitehead, P.G., Barbour, E., Futter, M.N., Sarkar, S., Rodda, H., Caesar, J., Butterfield, D., Jin, L., Sinha, R., Nicholls, R. and Salehin, M., 2015. Impacts of climate change and socio-economic scenarios on flow and water quality of the Ganges, Brahmaputra and Meghna (GBM) river systems: low flow and flood statistics. *Environmental Science: Processes & Impacts*, 17: 1057-1069.
- Wood, A.W., Leung, L.R., Sridhar, V. and Lettenmaier, D.P., 2004. Hydrologic implications of dynamical and statistical approaches to downscaling climate model outputs. *Climatic change*, 62: 189-216.
- Yeh, S.W., Ham, Y.G. and Lee, J.Y., 2012. Changes in the tropical pacific SST trend from CMIP3 to CMIP5 and its implication of ENSO*. *Journal of Climate*, 25: 7764-7771.
- Zhao, T. and Dai, A., 2016. Uncertainties in historical changes and future projections of drought. Part II: model-simulated historical and future drought changes. *Climatic Change*.

Chapter 3: Predictability of Multicategory Seasonal Probabilistic Forecast of Precipitation Conditioned on ENSO Phase

This chapter will be submitted to the Water Resource Research journal

Abstract

High dependence on seasonal precipitation puts emphasis on the need to improve the quality of seasonal forecasts, which in turn enables decision making to avoid potential losses or to gain more benefits in the municipal, agriculture, hydropower generation, and tourism sectors. This study develops a stochastic weather generation model to predict seasonal precipitation by linking a Nonhomogeneous Markov Chain Model that describes the ENSO cycle to a bivariate normal distribution model that represents seasonal precipitation conditioned on ENSO phase. Three verification metrics are suggested to measure the degree of predictability of raw, calibrated, and climatological seasonal rainfall forecasts. The results indicate the potential to narrow the uncertainty of seasonal rainfall forecasts by incorporating ENSO cycle information. Rainfall during the late part of the wet season has a higher degree of predictability than rainfall during the early part of the wet season. In addition, obtaining ENSO cycle information from climate models can also lead to a suitable degree of predictability for subsequent model rainfall in both portions of the wet season. The proposed calibration method improves predictability, which decreases with an increase in lead time for the forecast.

3.1 Introduction

The annual variation in the intensity and duration of seasonal precipitation has significant impacts on the reliability of water, food, and energy supplies. Particularly, most decisions made in the municipal, hydropower generation, agriculture, and tourism industries to avoid or mitigate potential losses are dependent on predicted future changes in the seasonal cycle of precipitation. Interannual variability in weather outcomes is found to be the dominant source of uncertainty associated with regional seasonal precipitation projections across the globe for at least the next decade (Hawkins and Sutton, 2011). Therefore, understanding the influence of internal variability is of great value to decision makers in regulation and planning. El Niño–Southern Oscillation (ENSO) is the main natural source of interannual climate variability observed globally (Trenberth et al., 1998; Meehl et al., 2007; Collins et al. 2010; Hidalgo et al., 2015), and particularly in the tropical Pacific region (Vecchi and Wittenberg, 2010). The ENSO phenomenon is commonly monitored by the periodic change in sea surface temperature anomalies (SSTAs) across the equatorial Pacific Ocean (McCABE and Dettinger, 1999; Ghil and Zaliapin, 2013). A number of studies have found a significant relationship between SSTAs and interannual precipitation variability in Central America (Enfield 1996; Waylen et al. 1996; Enfield and Alfaro 1999; Giannini et al. 2000; Rauscher et al., 2011). The periodicity cycle of the ENSO phenomenon varies from two to seven years (Knutson et al., 1997; Bellenger et al., 2014; Muñoz et al., 2014) and is defined by three phases: a) a warm phase known as El Niño, b) a cold phase known as La Niña, and c) a neither warm nor cold period called neutral.

The failure of most stochastic models to reproduce the observed interannual variability of seasonal precipitation might be due to a failure to incorporate the effect of large-scale climate variables (Katz and Parlange 1998), such as ENSO. Thus, it is essential to verify the potential to narrow uncertainty in seasonal precipitation predictions by incorporating ENSO cycle information. ENSO teleconnection has been incorporated as an attempt to reduce uncertainty and improve streamflow forecasts (Hamlet and Lettenmaier, 1999; Grantz et al., 2005; Regonda et al., 2006; Gobena and Gan, 2006, Sharma et al., 2015), and seasonal precipitation forecasts (Gutzler et al., 2002; Gissila et al., 2004; Zaroug et al., 2014). For instance, Gutzler et al. (2002) found that the ENSO cycle provided more seasonal predictability of winter anomalies of precipitation than the Pacific Decadal Oscillation (PDO) index over western North America. Sharma et al. (2015) also found that an ENSO-conditioned weather generation model provided suitable performance for monthly streamflow forecasting with a three-month lead time, especially for low-flow conditions. ENSO information can also be applied for reducing the risk associated with decision making in the agricultural sector (Letson et al., 2005; Cabrera et al., 2006), and for natural gas purchasing (Changnon et al., 2000). Cabrera et al. (2006) found that predictability of seasonal climate variability with respect to ENSO has the potential to minimize risk by informing necessary changes in planting dates and guiding the purchase of appropriate crop insurance in a farm in Jackson County, Florida.

ENSO climate information can be highly valuable for the process of making operational decisions in water resource systems. Although, the ENSO mechanism is not yet fully understood, a number of statistical and dynamical models have been developed to forecast the ENSO cycle. The former approach can be classified into models which use regression, neural networks, or Markov models

(Flügel and Chang, 1998; Chen and Cane, 2008), while the latter approach ranges from intermediate to fully coupled ocean-atmosphere models (Latif et al., 1994; Barnston et al., 2012). For characterizing predictability in future climate regimes projected by General Climate Models (CGCMs) , we adopt a simpler and less expensive approach that uses the SST field from climate models to construct a Markov chain (MC) model describing the cycle of ENSO phases. This model is embedded into a weather generation (WG) model that forecasts seasonal rainfall rates depending on the ENSO-rainfall teleconnection. The ability of CGCMs to simulate this teleconnection has been verified across the globe (Doherty and Hulme 2002; Joseph and Nigam 2006; Cai et al., 2009; Langenbrunner and Neelin, 2013; King et al., 2015; Dieppois et al., 2015). Hidalgo and Alfaro (2015) developed a number of metrics to evaluate the capability of 48 CGCMs CMIP5 (107 runs) to generate the observed ENSO rainfall teleconnection pattern over Central America as well as other climatic variables. The authors found that some of the runs produce suitable capability to simulate the ENSO-precipitation teleconnections both in the June-July-August (JJA) and September-October-November (SON) seasons and on an annual basis.

In order to demonstrate the objectives and methodology of this study, the northwest region of Costa Rica has been used as a case study. The topographic characteristics of this region influence the evolution of a bimodal seasonal cycle of precipitation (Waylen et al., 1996; Magaña et al., 1999). The region experiences a dry season that lasts for six months and a relative midsummer drought (MSD) episode that interrupts the wet season. In addition, ENSO is one of the major of concern drivers of rainfall and groundwater resources in the northwest Costa Rica (Babcock et al., 2016). It has been related to flooding (Waylen et al., 1996; Waylen and Laporte, 1999) and to fluctuations in monthly and interannual precipitation over Costa Rica (George et al., 1998). Waylen et al.

(1994) found that annual and seasonal precipitation at San Jose in Costa Rica appears to be conditioned on ENSO. Besides that, agricultural production and other activities depend significantly on precipitation during the wet season, which all emphasize the need for high-quality forecasts, especially for the two rainy portions of the wet season. Improving seasonal precipitation forecasts can support make cost-effective decisions. For instance, it helps decision makers decide effective ways to manage tradeoffs between power generation and water supply. It can also be used by stakeholders to improve their decisions, particularly in selection of appropriate crop cultivars and varieties, the purchase of crop insurance, timing of agricultural operations, fertilizer implementation, and livestock management strategies.

This study develops a statistical method to reduce the uncertainty associated with multicategory (dry, wet, and normal) probabilistic seasonal precipitation forecasts at medium temporal range and with different lead times by incorporating ENSO cycle information. Its objectives are a) demonstrating the potential to reduce uncertainty in seasonal precipitation forecasts by incorporating observed ENSO cycle information, and b) evaluating the skill that can be obtained by incorporating simulated ENSO cycle information from climate models. The second objective aims to verify the opportunity for decision makers to use climate models in building future scenarios of potential changes in seasonal precipitation, especially under the influence of global warming. The multicategory probabilistic forecast would make important contributions by providing the likelihood of having dry, wet, and normal rainfall rates, whereas the different lead time analysis would help in determining the optimal lead time.

Three verification metrics are proposed to assist the decision makers (e.g. water managers and farmers) to determine whether or not to rely on the forecast and to estimate its level of predictability over the period of 1996-2015: 1) the ranked probability score skill (RPSS), 2) the root mean square error (RMSE), and 3) a multicategory reliability diagram (MCRD). The relationship between the calibration and verification of the forecast is discussed and the effect of different lead times on the verification is demonstrated. Furthermore, the degree of predictability of the multicategory probabilistic prediction conditioned on ENSO information obtained from selected climate models is compared and evaluated.

The paper is divided into the following sections: section 3.2 presents the data and climate models used; section 3.3 information about models formulation; section 3.4 discusses the results of the predictability measurement by incorporating observed and simulated ENSO cycle information; and section 5 contains conclusions.

3.2 Data and climate models inputs

Observed monthly precipitation data are obtained from the Climatic Research Unit (CRU) TS 3.24 over the domain of (9.5-11 N and 85-86 W) from 1916 to 2015. The monthly precipitation is calculated on high-resolution (0.5x0.5 degree) grids, which are based on information gathered globally from more than 4000 weather stations (Jones and Harris, 2008). Sea surface temperatures (SSTs) for the Nino 3.4 (5S to 5N; 170W to 120W) region are used to monitor the ENSO pattern (Trenberth, 1997). The observed Nino 3.4 SSTs are extracted from a 0.5x0.5 degree grid dataset of the Extended Reconstructed Sea Surface Temperature (ERSST) version 3b of the National Oceanic and Atmospheric Administration (NOAA) (Smith et al, 2008). On the other hand, the

simulated Nino 3.4 SSTs are obtained from a selective sample of CGCMs participating in CMIP5 (Table 4), in which each climate model is represented by the mean of its ensembles. For both observed and simulated Nino 3.4 SSTs, the monthly values from 1916 to 2015 are used to construct SST anomalies with respect to the averaged SSTs of the 1951-1980 period. The reference period is selected to avoid the use of the 1980s, which may result in a negative bias due to unusually strong El Niño events (Pozo-Vázquez et al., 2001, 2005).

A number of indices have been applied in the literature to monitor the ENSO phenomenon. The Oceanic Niño Index (ONI), one of the commonly used indices (Gergis and Fowler, 2005), is used to distinguish between three different ENSO phases. An El Niño event is defined to occur when the three month averages of the SST anomalies are greater than (or equal to) $0.5\text{ }^{\circ}\text{C}$ for five consecutive 3-month periods or more, b) a La Niña event for averages smaller than (or equal to) $-0.5\text{ }^{\circ}\text{C}$ for five consecutive seasons or more and c) a Neutral phase otherwise. ENSO status during the early and late wet season is evaluated independently due to their high dependence on the precipitation (Karnauskas and Busalacchi, 2009) in the studied area. Thus, the ENSO phase in the April-June season represents the early season's ENSO phase, whereas the ENSO phase in the September-November season denotes the late wet season's ENSO phase.

3.3 Materials and Methods

3.3.1 Model training, validation, and testing

The methodology of this study is implemented over three time periods: a training period from 1916 to 1975, a validation period from 1976 to 1995, and a testing period from 1996 to 2015. The

training period (60 years long) is used to: a) determine the best Markov chain model to represent the observed ENSO phase cycle, b) construct a joint distribution model between the proposed theoretical distribution of the early and late wet season precipitation conditioned on each ENSO phase, c) determine 25th and 75th percentiles to classify the amount of seasonal precipitation in the three categories of dry, wet, and normal, and d) compute the long-run probability of each ENSO phase based on a selected ENSO occurrence model. Given that a raw forecast may not always be the best choice due to the chance of having systematic errors, the data for the period from 1976 to 1995, that is called the validating period, are employed to verify the skill of the Distribution-Based Scaling (DBS) method (Yang et al., 2010) in correcting bias in seasonal precipitation forecasts. In this period, a weather generation (WG) model is used to forecast seasonal precipitation at different lead times conditioned on ENSO phases. A set of parameters are estimated by the DBS method over this period, and then are used to calibrate the raw forecasts over the testing period.

Table 4. The selected CMIP5 CGCMs used in the study

Model Name	Model Groups (Country)	Number Ensembles
CNRM-CM5	Centre National de Recherches Meteorologiques and Centre Européen de Recherche et Formation Avancées en Calcul Scientifique (France)	5
HADGEM2-ES	UK Met Office Hadley Centre (UK)	4
MIROC5	University of Tokyo, National Institute for Environmental Studies, and Japan Agency for Marine- Earth Science and Technology (Japan)	1
MPI-ESM-LR	Max Planck Institute for Meteorology (Germany)	3
NorESM1-ME	Norwegian Climate Centre (Norway)	1
GFDL-ESM2G	Geophysical Fluid Dynamics Laboratory	1

Lastly, the testing period (20 years long) is used to judge the predictability and reliability of the multicategory probabilistic raw and calibrated forecast of seasonal precipitation over the period 1996-2015. Three verification measures are proposed to assist decision makers (e.g. water managers and farmers) to determine whether or not to rely on the forecast and to estimate its level of confidence. The verification metrics include the ranked probability score skill (RPSS), the root mean square error (RMSE), and the multicategory reliability diagram (MCRD). Three types of forecast are generated, the raw, calibrated, and climatological forecasts. The climatological forecast is the seasonal precipitation forecast using only the long-run probability of the ENSO phase cycle (i.e., it is not based on the current ENSO information).

3.3.2 ENSO occurrence model

The occurrence of an ENSO phase is modeled as a first-order Non-Homogeneous Markov Chain (NHMC) process. The transition probability between two sequential states embodies the influence of both mechanistic and random factors (e.g. climate change, natural variability) that control any dynamic process such as ENSO. The dynamic evolution of ENSO is represented using three different discrete states $S = \{\text{El Niño, Neutral and La Niña}\}$. To capture the seasonal occurrence of these phases, the model is constructed for both the early and late wet season states.

The NHMC is a stochastic process characterized by a set of states $\{i, j\}$ and their transition probabilities. A single transition matrix $P_{ij}^{n, n+1}$ has elements representing the probability of transiting from state i at season n and to state j at season $n+1$. The transition matrix for season n is a 3×3 matrix with the following properties:

$$\sum_j^S p_{ij}^{n, n+1} = 1, \text{ for each } i \quad (1)$$

$$0 \leq p_{ij}^{n,n+1} \leq 1 \quad (2)$$

The transition probability in the 1st order NHMC implies dependence of the next state on only the present state rather than any, or a sequence of past states:

$$p_{ij}^{n,n+1} = P(X_{n+1} = j | X_n = i) \quad (3)$$

The transition probability of a second order of NHMC $p_{hij}^{n-1,n,n+1}$ represents the probability of moving to state j in season $n + 1$ given state h in season $n - 1$ and state i in season n . The maximum likelihood method (see Appendix 1) is used to estimate the transition probabilities for the two orders of the NHMCs. In order to find the best representation for ENSO occurrence, we compare predictions using a first and second order NHMC, as well as the multinomial model in which ENSO states in sequential seasons are independent, according to the results of both Akaike's information criterion (AIC) (Akaike, 1974) and the Bayesian information criterion (BIC) (Schwarz, 1978) (see Appendix 1 for more information).

3.3.3 Rainfall intensity model

A Gaussian mixture model (Steyn et al., 2016; AlMutairi et al., 2016) is employed to represent the bimodal pattern of seasonal precipitation over northwest Costa Rica, for the rainfall rate as a function of time t , $f(t)$:

$$f(t) = y_o + \sum_{k=1}^{np} \frac{A_k}{\sigma_k \sqrt{2\pi}} \exp\left(-\frac{(t-t_{ck})^2}{2\sigma_k^2}\right) \quad (4)$$

The Gaussian components (Equation 4) are assumed to be superimposed upon a baseline rainfall rate y_o . The parameters for each component k are shown in Figure 2: the area under the curve A_k , the peak location t_{ck} , and the temporal standard deviation σ_k . np denotes the number of

components. These parameters are estimated for each yearly seasonal cycle of precipitation from 1916 to 2015 by the least squares method, which is applied to minimize the square difference between the observed monthly precipitation y_m for month m ($m = 1, 12$) and the Gaussian mixture model prediction $f(t_m)$, where for month m , t_m is assigned the midpoint of the month. The A_{1t} (A_{2t}) is used, in this study, to represent the early (late) wet season precipitation at year t ($t = 1, T$). In order to consider interannual variation in the influence of ENSO on seasonal precipitation, a lognormal probability distribution is fitted to the early and late wet season precipitation conditioned on ENSO phase. Equation 5 shows the cumulative distribution function (CDF) of the lognormal distribution.

$$F(x, \mu, \sigma) = \int_0^x \frac{1}{x \sigma \sqrt{2\pi}} \exp\left(\frac{-(\ln x - \mu)^2}{2\sigma^2}\right) dx \quad (5)$$

where x denotes the amount of seasonal precipitation (that is the area parameter A), and μ and σ are the respective mean and standard deviation of the normal distribution for $\ln x$. These parameters are estimated by fitting the empirical cumulative distribution function (ECDF) of the observations to the lognormal CDF using the maximum likelihood estimation method as an initial guess for random selections in a least-square optimization. The ECDF is given by the Blom plotting position formula $\left(\frac{i-0.375}{N+0.25}\right)$, where i denotes the rank of the given observation in an ascending order and N represents the sample size (Hamed and Rao, 2000).

A bivariate normal (BVN) distribution is used to describe the joint distribution of probability density for the logarithms of the early and late wet season rainfall rates (Yue, 2000; Estrella, 2013). The BVN model is constructed based on the given mean vector and covariance matrix conditioned on ENSO phase. Random generation of bivariate normal variables can be implemented using linear

combinations of two standard BVN column vectors and the given mean vector and covariance matrix. Cholesky decomposition factorization of the covariance matrix is employed to transform a set of uncorrelated variables into variables with the given covariances. For more detail about the BVN, see Appendix 1.

3.3.4 Bias correction method

The Distribution-Based Scaling (DBS) method (Yang et al., 2010) is adopted to bias-correct (adjust) the predicted seasonal precipitation over both the validating and the testing periods. The DBS method has been used to correct the bias in annual precipitation over Europe (Piani et al., 2010) and seasonal precipitation over Sweden (Yang et al., 2010), Finland (Olsson et al., 2015), and Mumbai (Rana et al., 2014). Rana et al. (2014) found that DBS improved the representation of rainfall statistics in Mumbai. Basically, The DBS is a version of a quantile mapping technique that matches observed and simulated frequency distributions, which are assumed to follow a theoretical distribution (e.g. gamma, or lognormal). The gamma distribution is commonly used in the DBS method to correct bias in two partitions of the frequency distributions. Since this study classifies the seasonal precipitation into three categories (dry, normal, wet), DBS is used to match the simulated lognormal density distribution over these three categories to the observation. Thus, the seasonal precipitation distribution is divided into three partitions separated by the 25th and 75th quantiles. For more information about the DBS method, see Appendix 1.

3.3.5 Stochastic weather generation model

A stochastic weather generator (WG) is employed to simulate the time-series of seasonal precipitation over northwest Costa Rica according to the statistical characteristics of the filled

ENSO-dependent bivariate model. The common approach of the WG models relies on dry-wet occurrence and precipitation intensity models in simulations (e.g., Katz 1977; Richardson 1984; Wilks 1989; Wilks, 1998), but it has been found that most studies based on this approach could not fully address the interannual variability of precipitation (Woolhiser et al., 1993; Boughton, 1999; Schoof, 2008), which might be due to large-scale climate variability (Woolhiser, 1992). Therefore, incorporating the influence of interannual variability could be a possible approach to narrow uncertainty in seasonal precipitation forecasts. Woolhiser (1993) examined the effect of ENSO on rainfall in the southwestern United States by using a lagged linear function of the Southern Oscillation Index (SOI) to perturb parameters of a stochastic daily rainfall model. The perturbations of the logits of the dry-dry transition probabilities resulted in statistically significant improvements in the log likelihood function for 23 stations. A study conducted by Grondona et al., (2000) found that conditioning a weather generation model on ENSO phase provide a useful approach to explore ENSO impacts on sectors of interest. Their work tested both ENSO conditional and unconditional weather generation models in simulating the characteristics of rainfall in six meteorological stations over southeastern South America. Both approaches involve a dry-wet days occurrence model represented by a first-order Markov chain and a rainfall intensity model, whereas the parameters of the intensity model in the conditional approach are estimated conditioned on ENSO phase. Clark et al. (2004) used the resampling-type weather generation model to produce sequences of climate variables that are conditioned on the Nino 3.4 index over the contiguous United States. This approach was found to be appropriate for use as input to hydrologic models to produce multiseason forecasts of streamflow.

The models mentioned above, and others available in the literature generally translate ENSO effects by modifying the intensity model of rainfall, while the occurrence model is fixed for dry-wet rainfall cycle. Recently, Wasko et al. (2015) modified a Hierarchical Random Pulse Bartlett Lewis stochastic generation model (HRBLM) to simulate low-frequency continuous rainfall associated with ENSO phases. A first-order Markov chain model was employed to generate the occurrence of ENSO states in a yearly pattern. The HRBLM was able to replicate observed wet spell statistics as well as observed long-term variability. In this study, the proposed stochastic WG model (Figure 10) is applied to predict seasonal precipitation during a specific period (validation or testing) of 20 years duration. The model relies on the ENSO occurrence model (1st order NHMC) constructed based on the ONI of the specific period and the statistics of the three BVN models. Each of the three BVN models is constructed based on all historical records of seasonal rainfall rates occurring in an ENSO phase. For example, all seasonal precipitation data for both ES and LS during an El Niño (La Niña) event are used to construct the El Niño-BVN (La Niña-BVN) model. The neutral-BVN model is constructed based on all historical records of both the ES and LS rainfall rates, unconditioned on any ENSO phase. Sharma et al. (2015) stated that there is a high variability in precipitation during neutral conditions in which a neutral condition preceded by an El Niño condition is different than that of a neutral condition preceded by a La Niña condition.

The WG model simply inputs an observed ENSO phase during the late wet season, and then generates N time-series of rainfall rates for both the early and late wet season at a lead time L . The forecast process is repeated for T time periods ($T = 20$ years over the validating/testing period), in which an observed ENSO phase in the late wet season is re-input at the end of each lead time.

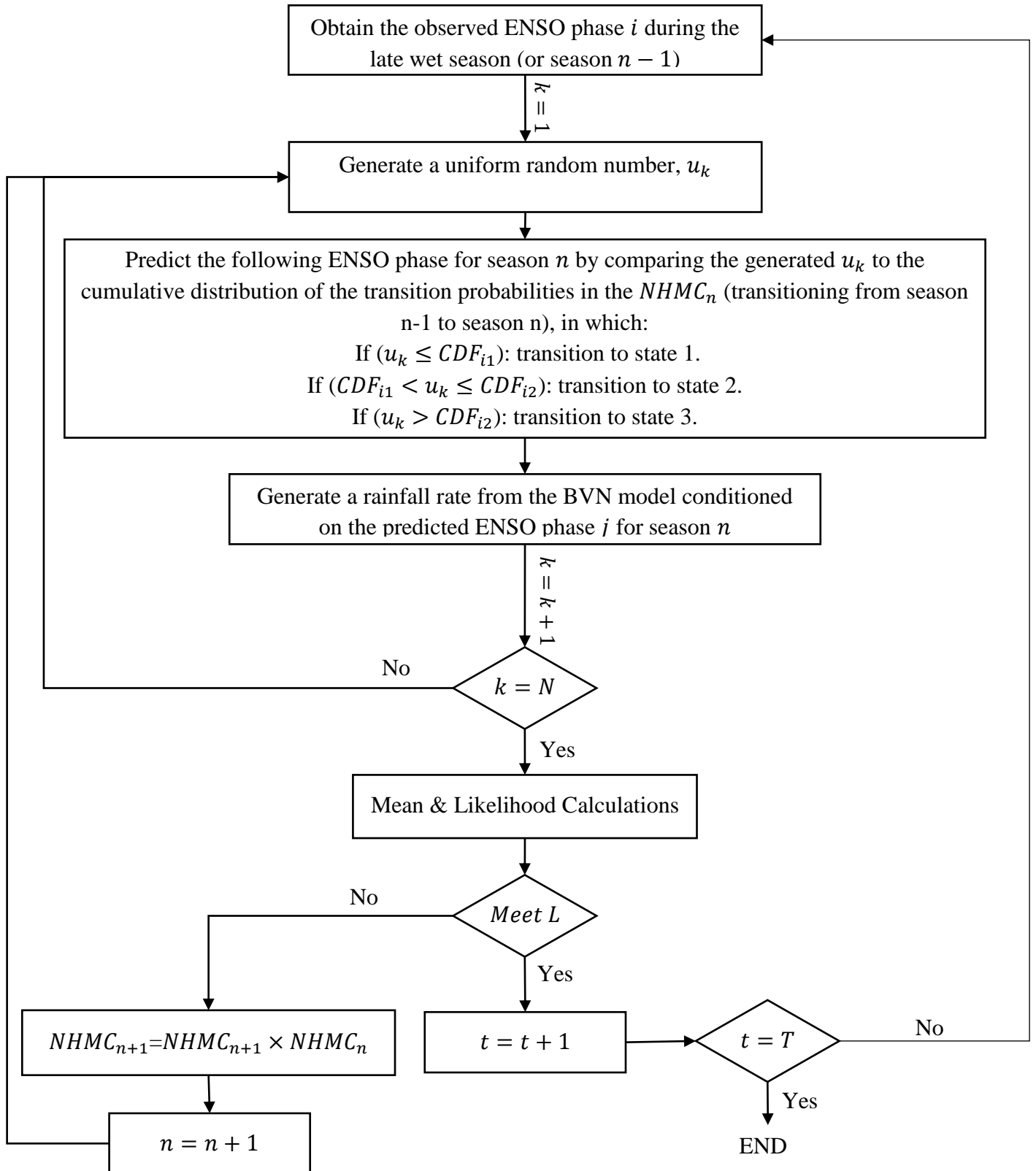


Figure 10. Flowchart of the process taken by the WG to forecast seasonal precipitation with different lead time ($N=1000$; $T=20$ years; $L=1, 2,$ or 3 years)

Three different lead times are demonstrated in this study including lead 1 (one year) forecast (forecasting two seasons ahead), lead 2 forecast (forecasting four seasons ahead), and lead 3 forecast (forecasting six seasons ahead). Although the most used forecast type by the majority of interviewed groups of stakeholders in the northwest Costa Rica is the 3-month/6-month forecasts (Babcock et al., 2016), the study here evaluates the predictability for longer lead times in order to a) determine the limitation and strength of the proposed forecast and b) provide a flexible operational platform that is expected to be of greater benefit to stakeholders than forecasts based on one single lead time. If skillful seasonal precipitation predictions are found for a longer lead time ahead, the capability would give decision-makers more time to modify water management decisions to increase benefits or to decrease unwanted impacts.

3.3.6 Verification metrics

Forecast skill can be measured by skill scores that aim to describe the reduction of the forecast error relative to a reference forecast, which is typically based on less information. As a result, users can rely on the method with the best forecast skills in order to plan for future conditions. For multi-categorical event forecasts that distinguish dry, normal, and wet events, a ranked probability score (RPS) (Epstein, 1969; Wilks, 1995) is used to measure the squared average difference between the cumulative probability distribution of the forecast and that of the observation over a number of categories N_{cat} .

$$RPS_i = \sum_{j=1}^{N_{cat}} (CDF_j^{forecasted} - CDF_j^{observed})^2 \quad (6)$$

$$\overline{RPS} = \frac{1}{T} \sum_{i=1}^T RPS_i \quad (7)$$

where $CDF_{forecast}$ ($CDF_i^{observed}$) represents the cumulative distribution of the forecast (observed) probability for the three assumed categories. To compare the skill of a forecast system to that of the reference forecast, the ranked probability score skill (RPSS) is analyzed. The RPSS has been found to be a proper skill score (Weigel et al., 2007) due to its sensitivity to distance between $CDF_i^{forecasted}$ and $CDF_i^{observed}$ (Wilks, 1995). It measures the forecast error relative to a reference forecast as shown in Equation 8. A climatology forecast is often used as the reference and is based on the long-term probability for observed ENSO phases. An RPSS of 1.0 indicates a perfect forecast, while an RPSS of 0.0 implies the forecast does not add any more skill to the climatology forecast. Negative values of the RPSS are also possible when the forecast method exhibits less skill than the reference forecast.

$$RPSS = 1 - \frac{\overline{RPS}}{\overline{RPS}_{ref}} \quad (8)$$

The RMSE (Equation 9) metric is also used to assess the ability of the forecast system to produce the observed amount of seasonal precipitation over the testing (1996-2015) period. Although this metric is not used to measure the skill of a probabilistic forecast, it is adopted in this study to provide more informative comparisons.

$$RMSE = \sqrt{\frac{\sum_{i=1}^{L_t} (R_{Predicted} - R_{Observed})^2}{L_t}} \quad (9)$$

where i denotes year number and L_t represents the total number of years (20 years in total). The predicted seasonal precipitation $R_{predicted}$ here is just the average prediction in the WG model (see sub-section 3.3.5).

Furthermore, a multicategory reliability diagram (Hamill, 1997) is applied to measure the reliability of the categorical probabilistic forecasts generated by incorporating ENSO information into the seasonal precipitation forecasting. The diagram can be used to a) examine the performance obtained using ENSO information in comparison to the use of climatology (the long-term probability of ENSO phases), b) understand how calibration can improve the reliability, and c) determine the effect of forecast lead time on reliability. A reliability line, averaged over a number of forecast years, is considered perfect when all quantiles of the observation are aligned with the quantiles of the forecast distribution. The diagram has the power to show the type and location of the errors in the forecast probability distribution over all of the predefined quantiles. Thus, when the reliability line is above (below) the diagonal, there is a wet (dry) bias over these quantiles. For how this diagram is calculated, see Appendix 1.

3.4 Results and discussion

3.4.1 Modeling ENSO occurrence

ENSO occurrence is modeled by two different orders of a Nonhomogeneous Markov Chains. The 1st (2nd) order NHMC determines the ENSO probabilistic distribution for a season i conditioned on each ENSO phase during the previous one (two) season(s). The NHMC matrices for the two

orders are shown in Tables 14 and 15 (Appendix 2). The selection for the best occurrence model is based on the result of both the AIC and BIC, which are constructed on the ENSO pattern over the training (1916 -1975) period (shown in Table 5). For more detail about the AIC and BIC, see Appendix 1. In Table 5, the multinomial (equivalent to a zeroth order NHMC) is compared to the 1st and 2nd NHMC models. The 1st order NHMC is found to fit the observed cycle of ENSO phases most successfully with the lowest AIC and BIC (Table 5). This result indicates that the ENSO phase in a season highly depends on the phase during the previous season.

Table 5. The log-likelihood, number of parameters, AIC and BIC for the two orders of the NHMC and the multinomial model that are compared in this study. A lower value of the AIC and BIC indicates a preferred model; the number of parameters is computed (with each order) for two Markov Chains: from early to late wet season and vice versa

Markov Chain	Log-likelihood	Number of Parameters	AIC	BIC
Multinomial Model	-122.7	2	249.5	247.7
1st order NHMC	-97.3	12	218.5	229.2
2nd order NHMC	-89.4	32	251	322.6

The long-run probabilities (basis for the multinomial model) for three ENSO phases are computed according to the 1st order NHMC built on the training (1916-1975) period. They are 0.23, 0.37, and 0.4, for El Niño, Neutral, and La Niña, respectively. It should be noted that the NHMC is constructed for any period by including the LS-ENSO phase (ENSO phase in the late wet season) of a year before in order to not break the relationship between ENSO phase in the late and early wet season. The NHMC for the testing period from 1996 to 2015 is shown in Table 16 (Appendix 2).

Stationarity in this Markov Chain must be maintained in order to ensure that a correct judgement about predictability can be made. Thus, the likelihood ratio test (Anderson and Goodman 1957; Wilks, 1995; Bickenbach and Bode 2003) is applied to the NHMCs over both the validation and testing periods to examine the stationarity (see Appendix 1 for more information). The constructed NHMCs are found to be stationary over the assigned periods as shown in Table 6.

Table 6. The likelihood ratios and associated p-values based on the 1st order NHMC for the validation and testing periods

Markov Chain	Likelihood Ratio	P-value
Validation period	12.1	0.42
Testing period	7.41	0.83

3.4.2 Seasonal precipitation modeling

The early and late wet season rainfall rates over the training period (1916-1975) are fitted to a lognormal distribution conditioned on the ENSO phase (see Figure 20 - Appendix 2). The goodness of fit to the lognormal distribution is tested by the chi-squared test. Table 7 shows the p-values of the chi-squared test (see Appendix 1) used to verify the goodness of fit of these rainfall rates to a lognormal distribution. The p -values for χ^2 tests indicate that the null hypothesis cannot be rejected at a 0.05 level of significance for all the time series conditioned on each of the three ENSO phases. This result of lognormal behavior for both portions of the wet season supports the assumption of adopting the BVN model in joining the rainfall distributions and of using the lognormal distribution in the bias correction (DBS) method.

Table 7. The p-values for χ^2 test for the lognormal distribution goodness of fit

Precipitation	El Niño	Neutral	La Niña
Early wet season	0.77	0.95	0.85
Late wet season	0.84	1.00	0.67

The bivariate normal distribution is constructed according to the good fit of each seasonal rainfall to a lognormal distribution, which indicates that their logarithm follows a normal distribution. Figure 11 shows the probability density function for each of these three joint distributions. From this figure, the fitted joint distribution conditioned on El Niño has the smallest mean with respect to both of the marginal distributions, while these means are larger in the case of conditioning on La Niña. In terms of standard deviation, the joint distribution conditioning on El Niño (La Niña) is shown to have a smaller (larger) standard deviation in the late precipitation than that in the early precipitation, whereas the joint distribution during Neutral shows that the standard deviations in both directions are almost equal, with somewhat higher values for the late wet season.

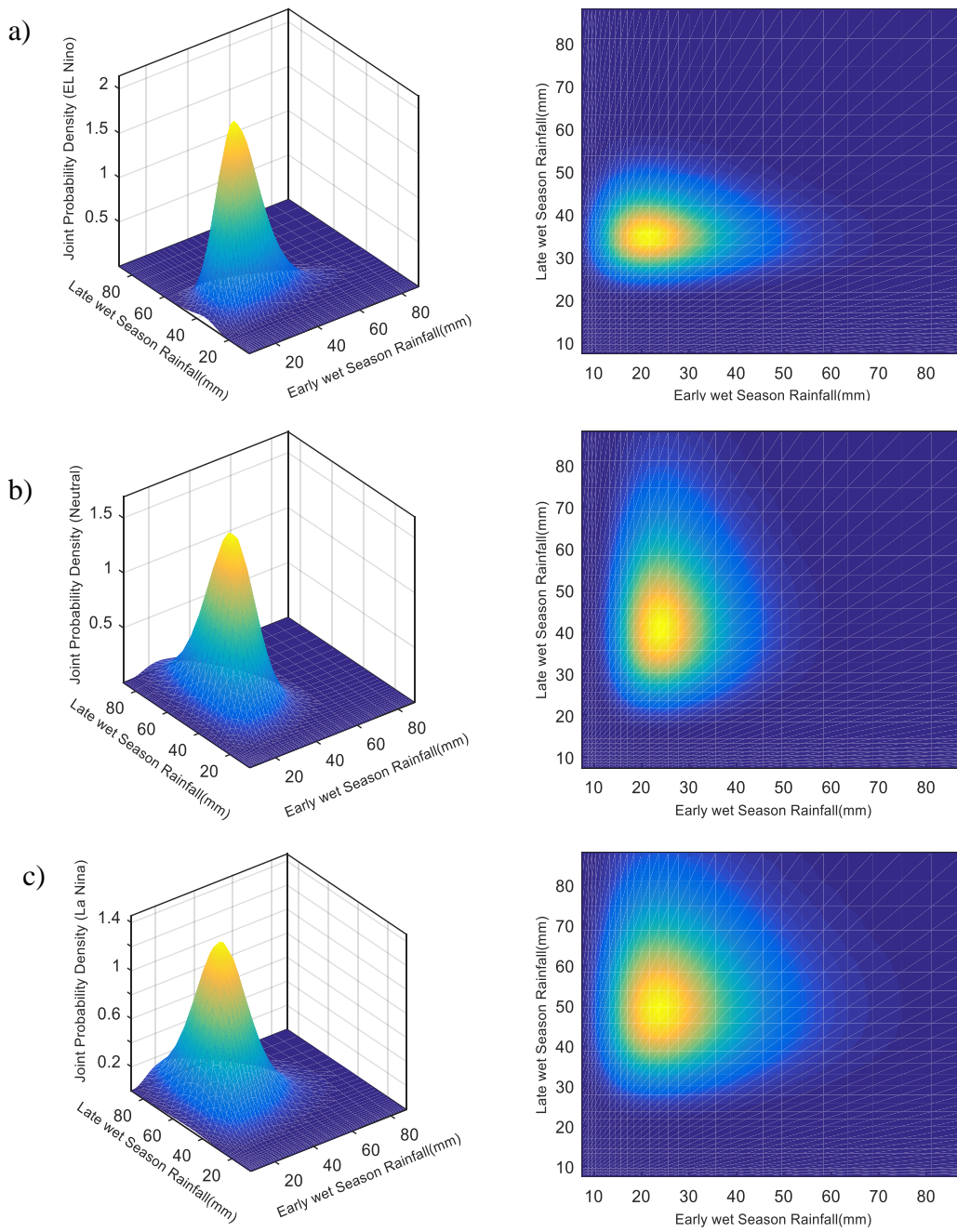


Figure 11. Joint probability density function of the bivariate model conditioned on a) El Niño phase, b) Neutral phase, and c) La Niña phase.

3.4.3 Predictability and calibration

The DBS method is employed to correct systematic bias in the seasonal precipitation forecast, so it is calibrated over the period 1976-1995 and then tested over the period 1996-2015. The method performs well over the calibration period by matching the cumulative distribution function of a forecast system with that of the observation. Over the testing period, the predictability of the probabilistic forecasts is measured by the three verification metrics explained in sub-section 3.3.6. The RPSS values are shown in Figure 12, which presents the measured skill of raw and calibrated forecasts relative to the climatological forecast for the early and late wet season precipitation over the 20 years of the testing (1996-2015) period. It can be seen that all scores in Figure 12 are above zero, which indicates that using the current ENSO information adds more value to the forecast than that obtained by climatology alone. The climatology here means the long-run probability for the three ENSO phases that were constructed based on ENSO pattern during the training period. Although the obtained RPSS values are not very high, obtaining a RPSS above zero could lead to greater benefit for decision makers (forecast users) than that obtained by relying on the climatological forecast system. Furthermore, the RPSS is increased by calibration (using the DBS method). The RPSS of the late wet season precipitation forecast jumps from 0.12 to 0.17, which represents a 42.8 % improvement. On the other hand, the early precipitation forecast is shown to have a lower RPSS, but its percentage of improvement by calibration is much higher (approximately 62%).

To understand the implication of different RPSS values, it is helpful to examine other RPSS values obtained in literature. Tippett et al. (2014) found that a linear regression correction approach

improved the ranked probability skill score (RPSS) values of the December–February (DJF) precipitation forecasts over Costa Rica that are obtained from the National Oceanic and Atmospheric Administration (NOAA) Climate Forecast System version 2 (CFSv2). The resulting RPSS values ranged from -0.1 to 0.1. A study for Ethiopia, Korecha and Sorteberg (2013) found a positive but low predictability for seasonal rainfall forecasts issued by the National Meteorological Agency (NMA), measured by the RPSS values that ranged from 0 to 0.09. As such the RPSS values obtained for seasonal precipitation forecasts in our study (ranging, from 0.08 to 0.17) were comparable to, and in some cases better than, these obtained in other related forecasting applications.

Another verification metric applied in this study is the RMSE (shown in Figure 13), which is measured by mm of rainfall and is computed between the raw, calibrated, and climatological predictions and observation. The calibrated forecasts for both portions of the wet season are shown to have a lower RMSE than that of the raw and climatological forecasts. The early wet season calibrated forecast reduces the RMSE raw and climatological forecasts by 18.7 % and 16 %, respectively. The late wet season calibrated forecast produces a RMSE of about 8.9 mm, which is also lower in comparison to that obtained by other forecast systems. In this study, RMSE test is used not to measure predictability, but to demonstrate the quality of a given forecast. This is because RMSE may mislead the judgment about predictability by showing a low RMSE for the forecasted rainfall rates that are close to the observed rates, but are not in the same category. Therefore, although the RMSE of the late wet season is larger than that of the early wet season, the predictability by incorporating ENSO cycle information into seasonal precipitation forecast is higher in the late than in the early portion of the wet season.

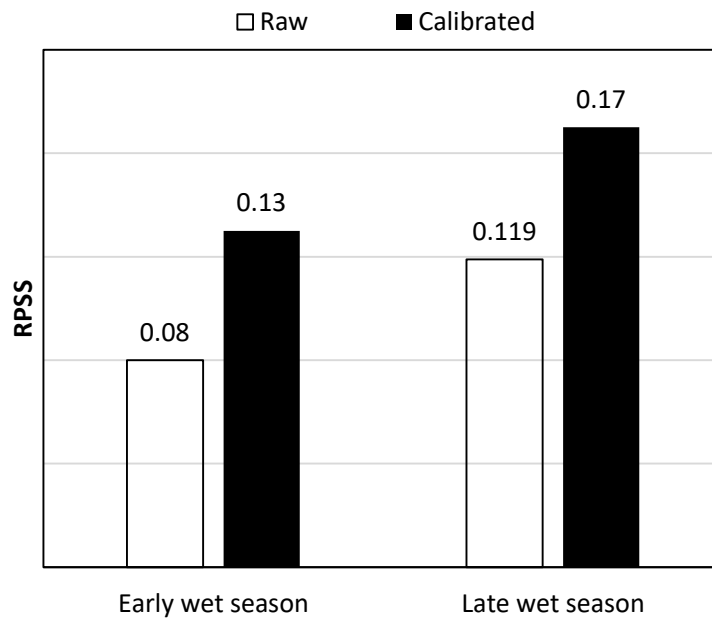


Figure 12. RPSS values of the raw and calibrated rainfall forecasts in the early and late wet seasons relative to the climatological reference.

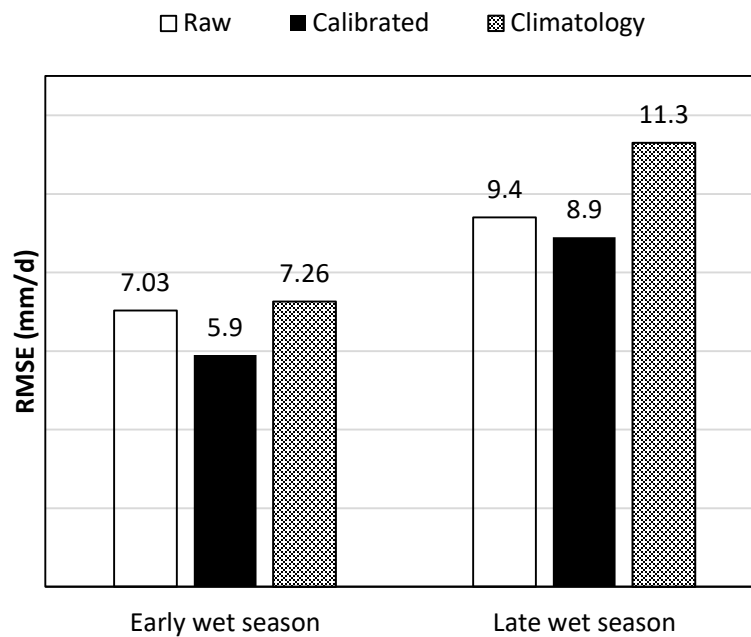


Figure 13. RMSE computed between the raw, calibrated, and climatological rainfall forecasts and observations

Overall, it can be noted that the predictability in the late wet season conditioned on ENSO is higher than that in the early wet season, which can be seen from Figures 12 and 13 (higher RPSS and lower RMSE, respectively). That might be because SST anomalies in the tropical Pacific have a greater impact on the late wet season precipitation than on the early wet season precipitation (Waylen et al., 1998; Rauscher et al., 2008; Hidalgo et al., 2015; Maldonado et al., 2016). However, the early wet season precipitation is still affected by tropical SST anomalies through Atlantic SSTs (Taylor et al. 2002).

The RPSS and RMSE verification metrics may not be sufficient to judge the predictability of the proposed forecast system, thus the multicategory reliability diagram (MCRD) is suggested to be applied as another verification metric. The MCRD indicates the weakness and strength of the forecast distribution, which provides an opportunity for users to improve the seasonal forecast. Figure 14 shows the MCRD drawn for the raw, bias-corrected, and climatological rainfall forecasts for the early and late wet season. It can be seen that relying on the climatological forecast always results in a wet bias over all the quantiles. The reliability line of the raw forecast indicates a wet (dry) bias in the early (late) wet season rainfall forecast. The reliability line of the raw rainfall forecast of the early wet season matches the climatological reliability line for 0.3 and below and for 0.8 and above. The calibration improves the reliability of the rainfall forecast in the early (late) portion of the wet season as shown by moving their reliability lines closer to the 1:1 line, and results in a small wet (dry) bias in the lower quantiles with a dry bias in the upper quantiles.

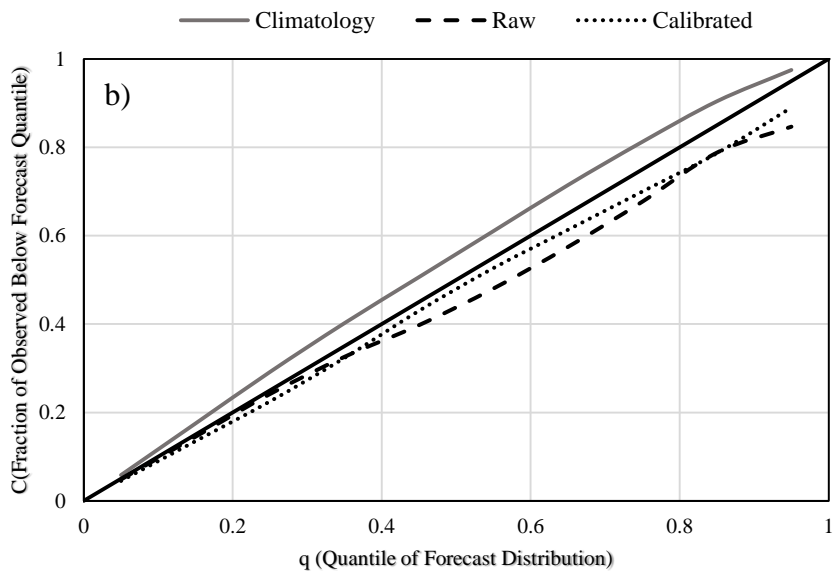
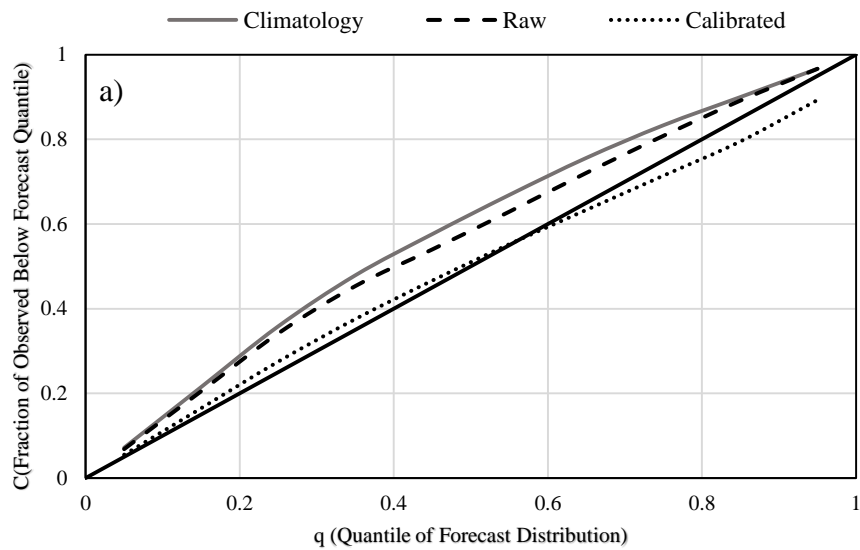


Figure 14. Reliability diagram of the raw, calibrated, and climatology rainfall forecasts in the a) early wet season, and b) late wet season. The perfect reliable system are shown as black solid line and the error bars on the reliability curves are not shown for readability (see Appendix 2).

The reliability line in Figure 14 represents the average reliability (over 20 years), so the confidence in such average reliability at any quantile can be expressed as an error bar at that quantile. Error bars were developed representing the 5th and 95th percentiles of resampled multicategory reliabilities produced via a bootstrap test (1000 runs). In Appendix 2, the difference between the two sides of the error bars is calculated as a readable way to show the degree of confidence at each quantile. Despite the increase in reliability due to calibration, the confidence in the reliability with higher quantiles is reduced as compared to raw and climatological forecasts for both portions of the wet season (shown in Figure 21-Appendix 1).

3.4.4 Predictability and lead times

The objective of this section is to determine the effect of an increase in lead time on the predictability of the calibrated seasonal forecast conditioned on ENSO phase. Table 8 shows the RPSS and RMSE of the calibrated rainfall forecast of the early and late wet season with respect to three different lead times. It should be noted that the RPSS for lead time L is computed relative to the RPSS of the climatological forecast at the same lead time L . With increased lead time, a reduction in the RPSS is shown for both portions of the wet season. The RPSS of the calibrated rainfall forecast in the early (late) wet season is reduced by about 20% (29%) from lead 1 (one year) to lead 2 (two years). The RMSE associated with the calibrated forecasts for the two portions of the wet season increases gradually with the increase in lead time.

Table 8. RPSS and RMSE (mm/d) for the calibrated forecasts of both early and late wet season performed with different lead times (year)

RPSS	Lead 1	Lead 2	Lead 3
Early wet season	0.13	0.10	0.07
Late wet season	0.17	0.12	0.09
RMSE	Lead 1	Lead 2	Lead 3
Early wet season	5.9	6.46	6.76
Late wet season	8.9	9.5	9.84

Similarly, the reliability of the calibrated forecast of both portions of the wet season is reduced with the increase in lead time as shown in Figure 15. For the early wet season, the lead 2 reliability shows a dry-bias-increase in the medium-high quantiles, while the lead 3 reliability indicates a wet-bias-increase in the low-medium quantiles with a dry-bias-increase in the high quantiles. The reliability of the calibrated rainfall forecast in the late wet season results in more dry bias with respect to the increase in lead time. By comparing the reliability lines of both portions of the wet season in Figure 15, the influence of the increase in the lead time appears to be more significant in the early rather than the late portion of the wet season.

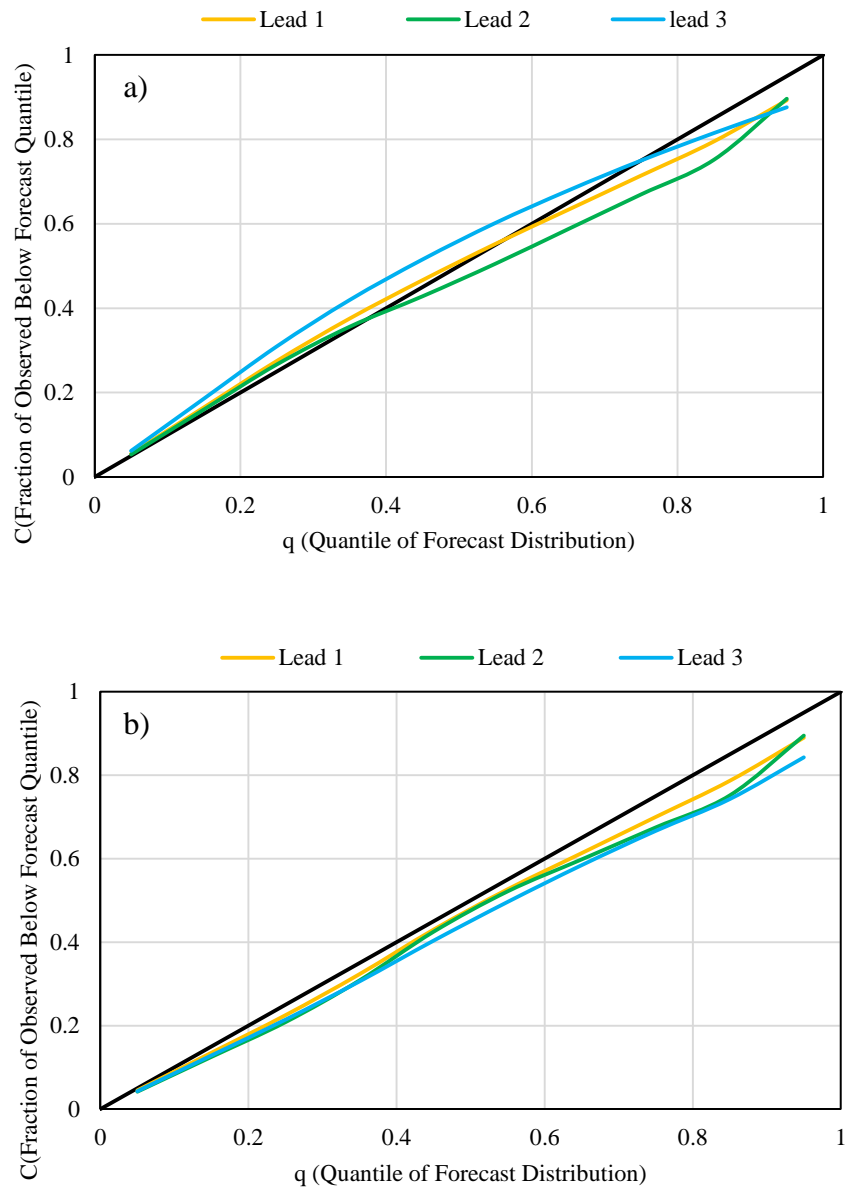


Figure 15. Multicategory reliability diagram for the calibrated rainfall forecast in the a) early wet season and b) late wet season computed with respect to different lead times (year). The perfect reliable system are shown as black solid line.

3.4.5 Predictability for climate model simulations

This section demonstrates the predictability of seasonal precipitation forecasts at a lead time of one year obtained by incorporating ENSO cycle information from a selective sample of six climate models. Table 9 presents the RPSS computed for both the raw and calibrated rainfall forecasts in the early and late wet season. The calibration improves the raw forecast against the climatology as it increases the value of RPSS for both portions of the wet season. The RPSS value for the calibrated rainfall forecast in the early wet season is found to be higher than that in the late wet season by MIROC5 and HadGem2-ES. The CNRM-CM5 produces an RPSS of 0.13 for the calibrated rainfall forecast in the late wet season. GFDL-ESM2G results in a low RPSS of 0.09 in both the early and late wet season. It is noted that the climatological forecast shows better skill than the raw forecast by the NorESM1-ME, since it has a negative RPSS. Overall, the highest predictability is found by incorporating ENSO cycle information in projections with four climate models: MIROC5, CNRM-CM5, HadGem2-ES, and MPI-ESM-LR. These models yield simulated rainfall in which the ENSO-enhanced forecasts exhibit RRPSS values (~0.1-0.15) similar (through somewhat smaller than) to those obtained using the observed rainfall data (~0.1-0.2).

Table 10 displays the RMSE between each of the raw and calibrated rainfall forecasts that are obtained using the SST field from the respective climate models relative to the observations. The RMSE is reduced by calibration in the two portions of the wet season. The NorESM1-ME, GFDL-ESM2G, and MIROC5 all generate a larger RMSE than that obtained by the climatological forecast (7.26 mm) for the raw rainfall forecast in the early wet season.

The calibrated rainfall forecast by the HadGem2-ES produces a RMSE (5.9 mm) equal to that generated by the observed calibrated forecast. The percentage of improvement by calibration in all six models is higher in the early than in the late wet season as shown in Tables 9 and 10.

Table 9. RPSS values for the raw and calibrated forecasts computed based on ENSO information from climate models

CGCM	Early wet season		Late wet season	
	Raw	Calibrated	Raw	Calibrated
MIROC5	0.01	0.13	0.09	0.10
CNRM-CM5	0.02	0.11	0.10	0.13
GFDL-ESM2G	0.03	0.09	0.04	0.09
HadGem2-ES	0.03	0.13	0.09	0.11
MPI-ESM-LR	0.03	0.11	0.08	0.12
NorESM1-ME	-0.02	0.08	0.09	0.11

Figure 22 (23) (Appendix 2) shows the multicategory reliability diagram for the calibrated rainfall forecast in the early (late) wet season at lead 1 according to the six selected climate models. All models determine better reliability than those obtained by climatological forecast in both portions of the wet season. For the calibrated rainfall forecast in the early wet season, five of the selected six models produce a wet (dry) bias in the low (high) quantiles.

Table 10. RMSE (mm/d) computed between both raw and calibrated forecasts and observations

CGCM	Early wet season		Late wet season	
	Raw	Calibrated	Raw	Calibrated
MIROC5	7.27	6.07	9.83	9.6
CNRM-CM5	7.23	6.03	10.06	9.33
GFDL-ESM2G	7.3	6.03	9.6	9.4
HadGem2-ES	6.9	5.9	9.51	9.43
MPI-ESM-LR	7.2	6.24	9.59	9.51
NorESM1-ME	7.4	6.1	10.39	9.93

The exception is for MPI-ESM-LR, which generates a wet bias in the low-medium quantiles. In the case of the calibrated rainfall forecast in the late wet season, all six climate models produce a dry bias over all quantiles. Figure 24 (in Appendix 2) shows that the level of confidence is higher with low quantiles for both portions of the wet season.

3.5 Conclusions

Seasonal fluctuations in precipitation have the potential to impact the effectiveness of water management decisions related to municipal, agriculture, and power generation industries. Since these fluctuations are found to be strongly influenced by large-scale climate variability such as the ENSO phenomenon, this study investigates the potential of incorporating ENSO-rainfall teleconnections to narrow the uncertainty in the seasonal rainfall prediction on the timescale of 1-

20 years (in a categorical form) over northwest Costa Rica as a case study. A statistical method relying on a stochastic weather generation model is constructed to generate a synthetic time-series for each of the early and late wet season rainfall rates. The generation is simply determined according to a prediction for ENSO phase by a Nonhomogeneous Markov Chain (1st order) and a prediction for a rainfall rate based on a bivariate normal distribution conditioned on ENSO phase.

According to three multicategory verification metrics, the results exhibit the degree of predictability that can be obtained by incorporating ENSO cycle information into the multicategory probabilistic forecast of seasonal precipitation. The multi-categorical prediction of the late wet season precipitation shows a higher degree of predictability than that of the early wet season. The reliability of the rainfall forecasts in the early and late wet season is better than that of the climatological forecast. Given the possibility of having systematic errors in seasonal precipitation forecasts, the DBS method is employed to correct systematic bias in the forecast. The DBS method, over the testing period, improves the predictability and reliability associated with the rainfall forecast in the two portions of the wet season. The percentage of improvement by calibration is higher in the early compared to the late wet season. The study also finds that, as expected, the degree of predictability decreases with an increase in the lead time forecast.

In order to pave the road for using ENSO cycle information from CCGMs in seasonal precipitation forecasts, the study investigates their predictability over a historical period (1996-2015) of time. The results indicate that a suitable degree of predictability can be obtained by incorporating the simulated ENSO cycle information from four climate models: MIROC5, CNRM-CM5, HadGem2-ES, and MPI-ESM-LR. These results are obtained by calibrating the raw forecast, whereas the raw

forecast produces low predictability skills. However, the results emphasize the role that could be played by climate models in reducing uncertainty associated with seasonal precipitation forecasts, and in building multiple future scenarios for seasonal precipitations, which would provide great value for planning and managing water and agricultural resources. Given these results, this indicates that there may be potential for similar approaches in other regions as well.

Acknowledgments

We acknowledge the World Climate Research Programme's Working Group on Coupled Modelling, which is responsible for CMIP, and we thank the climate modeling groups (listed in Table 1 of this paper) for producing and making available their model output. For CMIP, the U.S. Department of Energy's Program for Climate Model Diagnosis and Intercomparison provides coordinating support and led development of software infrastructure in partnership with the Global Organization for Earth System Science Portals.

References

- Akaike, H. (1974). A new look at the statistical model identification. *IEEE transactions on automatic control*, 19(6), 716-723.
- AlMutairi, B. S., Grossmann, I., & Small, M. J. (2016). Bimodal Seasonal Rainfall Model for Evaluating of Long-term Climate Model Projections. Manuscript submitted for publication (*International Journal of Climatology*).
- Anderson, T. W., & Goodman, L. A. (1957). Statistical inference about Markov chains. *The Annals of Mathematical Statistics*, 89-110.

- Babcock, M., Wong-Parodi, G., Small, M. J., & Grossmann, I. (2016). Stakeholder perceptions of water systems and hydro-climate information in Guanacaste, Costa Rica. *Earth Perspectives*, 3(1), 1-13.
- Barnston, A. G., Tippett, M. K., L'Heureux, M. L., Li, S., & DeWitt, D. G. (2012). Skill of real-time seasonal ENSO model predictions during 2002–11: Is our capability increasing?. *Bulletin of the American Meteorological Society*, 93(5), 631-651.
- Bellenger, H., Guilyardi, É., Leloup, J., Lengaigne, M., & Vialard, J. (2014). ENSO representation in climate models: from CMIP3 to CMIP5. *Climate Dynamics*, 42(7-8), 1999-2018.
- Bickenbach, F., & Bode, E. (2003). Evaluating the Markov property in studies of economic convergence. *International Regional Science Review*, 26(3), 363-392.
- Boughton, W. C. (1999). A daily rainfall generating model for water yield and flood studies. CRC for Catchment Hydrology.
- Cabrera, V. E., Fraisse, C. W., Letson, D., Podestá, G., & Novak, J. (2006). Impact of climate information on reducing farm risk by optimizing crop insurance strategy. *Trans. Asabe*, 49(4), 1223-1233.
- Cai, W., Sullivan, A., & Cowan, T. (2009). Rainfall teleconnections with Indo-Pacific variability in the WCRP CMIP3 models. *Journal of climate*, 22(19), 5046-5071.
- Changnon, D., Ritsche, M., Elyea, K., Shelton, S., & Schramm, K. (2000). Integrating climate forecasts and natural gas supply information into a natural gas purchasing decision. *Meteorological Applications*, 7(3), 211-216.
- Chen, D., & Cane, M. A. (2008). El Niño prediction and predictability. *Journal of Computational Physics*, 227(7), 3625-3640.
- Clark, M. P., Gangopadhyay, S., Brandon, D., Werner, K., Hay, L., Rajagopalan, B., & Yates, D. (2004). A resampling procedure for generating conditioned daily weather sequences. *Water Resources Research*, 40(4).
- Collins, M., An, S. I., Cai, W., Ganachaud, A., Guilyardi, E., Jin, F. F., ... & Vecchi, G. (2010). The impact of global warming on the tropical Pacific Ocean and El Niño. *Nature Geoscience*, 3(6), 391-397.
- Dieppois, B., Rouault, M., & New, M. (2015). The impact of ENSO on Southern African rainfall in CMIP5 ocean atmosphere coupled climate models. *Climate Dynamics*, 45(9-10), 2425-2442.
- Doherty, R., & Hulme, M. (2002). The relationship between the SOI and extended tropical precipitation in simulations of future climate change. *Geophysical Research Letters*, 29(10).
- Enfield, D. B. (1996). Relationships of inter-American rainfall to tropical Atlantic and Pacific SST variability. *Geophysical research letters*, 23(23), 3305-3308.
- Enfield, D. B., & Alfaro, E. J. (1999). The dependence of Caribbean rainfall on the interaction of the tropical Atlantic and Pacific Oceans. *Journal of Climate*, 12(7), 2093-2103.

- Epstein, E. S. (1969). A scoring system for probability forecasts of ranked categories. *Journal of Applied Meteorology*, 8(6), 985-987.
- Estrella, N., & Menzel, A. (2013). Recent and future climate extremes arising from changes to the bivariate distribution of temperature and precipitation in Bavaria, Germany. *International Journal of Climatology*, 33(7), 1687-1695.
- Flügel, M., & Chang, P. (1998). Does the predictability of ENSO depend on the seasonal cycle?. *Journal of the atmospheric sciences*, 55(21), 3230-3243.
- George, R. K., Waylen, P., & Laporte, S. (1998). Interannual variability of annual streamflow and the Southern Oscillation in Costa Rica. *Hydrological Sciences Journal*, 43(3), 409-424.
- Gergis, J. L., & Fowler, A. M. (2005). Classification of synchronous oceanic and atmospheric El Niño-Southern Oscillation (ENSO) events for palaeoclimate reconstruction. *International Journal of Climatology*, 25(12), 1541-1565.
- Giannini, A., Kushnir, Y. and Cane, M.A., 2000. Interannual variability of Caribbean rainfall, ENSO, and the Atlantic Ocean*. *Journal of Climate*, 13: 297-311.
- Gissila, T., Black, E., Grimes, D. I. F., & Slingo, J. M. (2004). Seasonal forecasting of the Ethiopian summer rains. *International Journal of Climatology*, 24(11), 1345-1358.
- Gobena, A. K., & Gan, T. Y. (2006). Low-frequency variability in Southwestern Canadian stream flow: links with large-scale climate anomalies. *International Journal of Climatology*, 26(13), 1843-1869.
- Grantz, K., Rajagopalan, B., Clark, M., & Zagona, E. (2005). A technique for incorporating large-scale climate information in basin-scale ensemble streamflow forecasts. *Water Resources Research*, 41(10).
- Grondona, M. O., Podestá, G. P., Bidegain, M., Marino, M., & Hordij, H. (2000). A stochastic precipitation generator conditioned on ENSO phase: a case study in southeastern South America. *Journal of Climate*, 13(16), 2973-2986.
- Gutzler, D. S., Kann, D. M., & Thornbrugh, C. (2002). Modulation of ENSO-based long-lead outlooks of southwestern US winter precipitation by the Pacific decadal oscillation. *Weather and Forecasting*, 17(6), 1163-1172.
- Hamill, T. M. (1997). Reliability diagrams for multicategory probabilistic forecasts. *Weather and forecasting*, 12(4), 736-741.
- Hamlet, A. F., & Lettenmaier, D. P. (1999). Columbia River streamflow forecasting based on ENSO and PDO climate signals. *Journal of water resources planning and management*, 125(6), 333-341.
- Harrison, M., & Waylen, P. (2000). A note concerning the proper choice for Markov model order for daily precipitation in the humid tropics: A case study in Costa Rica. *International Journal of Climatology*, 20(14), 1861-1872.
- Hawkins, E., & Sutton, R. (2011). The potential to narrow uncertainty in projections of regional precipitation change. *Climate Dynamics*, 37(1-2), 407-418.

- Hidalgo, H. G., Durán-Quesada, A. M., Amador, J. A., & Alfaro, E. J. (2015). The Caribbean Low-Level Jet, the Inter-Tropical Convergence Zone and Precipitation Patterns in the Intra-Americas Sea: A Proposed Dynamical Mechanism. *Geografiska Annaler: Series A, Physical Geography*, 97(1), 41-59.
- Hidalgo, H.G. and Alfaro, E.J., (2015). Skill of CMIP5 climate models in reproducing 20th century basic climate features in Central America. *International Journal of Climatology*, 35: 3397-3421.
- Jones, P. D., & Harris, I. (2008). Climatic Research Unit (CRU) time-series datasets of variations in climate with variations in other phenomena. NCAS British Atmospheric Data Centre.
- Joseph, R., & Nigam, S. (2006). ENSO evolution and teleconnections in IPCC's twentieth-century climate simulations: Realistic representation?. *Journal of Climate*, 19(17), 4360-4377.
- Karnauskas, K. B., & Busalacchi, A. J. (2009). The role of SST in the east Pacific warm pool in the interannual variability of Central American rainfall. *Journal of Climate*, 22(10), 2605-2623.
- Katz, R. W. (1977). Precipitation as a chain-dependent process. *Journal of Applied Meteorology*, 16(7), 671-676.
- Katz, R. W., & Parlange, M. B. (1998). Overdispersion phenomenon in stochastic modeling of precipitation. *Journal of Climate*, 11(4), 591-601.
- King, A. D., Donat, M. G., Alexander, L. V., & Karoly, D. J. (2015). The ENSO-Australian rainfall teleconnection in reanalysis and CMIP5. *Climate Dynamics*, 44(9-10), 2623-2635.
- Korecha, D., & Sorteberg, A. (2013). Validation of operational seasonal rainfall forecast in Ethiopia. *Water Resources Research*, 49(11), 7681-7697.
- Langenbrunner, B., & Neelin, J. D. (2013). Analyzing ENSO teleconnections in CMIP models as a measure of model fidelity in simulating precipitation. *Journal of Climate*, 26(13), 4431-4446.
- Latif, M., Barnett, T.P., Cane, M.A., Flügel, M., Graham, N.E., Storch, H.V., Xu, J.S. and Zebiak, S.E. (1994). A review of ENSO prediction studies. *Climate Dynamics*, 9(4), 167-179
- Letson, D., Podestá, G. P., Messina, C. D., & Ferreyra, R. A. (2005). The uncertain value of perfect ENSO phase forecasts: stochastic agricultural prices and intra-phase climatic variations. *Climatic Change*, 69(2), 163-196.
- Magaña, V., Amador, J.A. and Medina, S., 1999. The midsummer drought over Mexico and Central America. *Journal of Climate*, 12: 1577-1588.
- Maldonado, T., Alfaro, E., Fallas-López, B. and Alvarado, L., (2013). Seasonal prediction of extreme precipitation events and frequency of rainy days over Costa Rica, Central America, using Canonical Correlation Analysis. *Advances in Geosciences*, 33: 41-52.
- Maldonado, T., Rutgersson, A., Alfaro, E., Amador, J., & Claremar, B. (2016). Interannual variability of the midsummer drought in Central America and the connection with sea surface temperatures. *Advances in Geosciences*, 42, 35-50.

- Meehl, G.A., Stocker, T.F., Collins, W.D., Friedlingstein, P., Gaye, A.T., Gregory, J.M., Kitoh, A., Knutti, R., Murphy, J.M., Noda, A. and Raper, S.C.B. (2007). Global Climate Projections. In 'Climate Change 2007: the Physical Science Basis. Contribution of Working Group I to the Fourth Assessment Report of the Intergovernmental Panel on Climate Change. (Eds S Solomon, D Qin, M Manning, Z Chen, M Marquis, KB Averyt, M Tignor, HL Miller) 747–845.
- Olsson, T., Jakkila, J., Veijalainen, N., Backman, L., Kaurola, J., & Vehviläinen, B. (2015). Impacts of climate change on temperature, precipitation and hydrology in Finland—studies using bias corrected Regional Climate Model data. *Hydrology and Earth System Sciences*, 19(7), 3217-3238.
- Piani, C., Haerter, J. O., & Coppola, E. (2010). Statistical bias correction for daily precipitation in regional climate models over Europe. *Theoretical and Applied Climatology*, 99(1-2), 187-192.
- Pozo-Vázquez, D., Esteban-Parra, M. J., Rodrigo, F. S., & Castro-Díez, Y. (2001). The association between ENSO and winter atmospheric circulation and temperature in the North Atlantic region. *Journal of Climate*, 14(16), 3408-3420.
- Pozo-Vázquez, D., Gámiz-Fortis, S. R., Tovar-Pescador, J., Esteban-Parra, M. J., & Castro-Díez, Y. (2005). El Niño–Southern Oscillation events and associated European winter precipitation anomalies. *International Journal of Climatology*, 25(1), 17-31.
- Rana, A., Foster, K., Bosshard, T., Olsson, J., & Bengtsson, L. (2014). Impact of climate change on rainfall over Mumbai using Distribution-based Scaling of Global Climate Model projections. *Journal of Hydrology: Regional Studies*, 1, 107-128.
- Rao, A. R., & Hamed, K. H. (2000). *Frequency Analysis*.
- Rauscher, S.A., Giorgi, F., Diffenbaugh, N.S. and Seth, A., 2008. Extension and intensification of the Meso-American mid-summer drought in the twenty-first century. *Climate Dynamics*, 31: 551-571.
- Rauscher, S.A., Kucharski, F. and Enfield, D.B., 2011. The role of regional sst warming variations in the drying of meso-america in future climate projections*. *Journal of Climate*, 24: 2003-2016.
- Regonda, S. K., Rajagopalan, B., Clark, M., & Zagana, E. (2006). A multimodel ensemble forecast framework: Application to spring seasonal flows in the Gunnison River Basin. *Water Resources Research*, 42(9).
- Richardson, C. W., & Wright, D. A. (1984). WGEN: A model for generating daily weather variables.
- Schoof, J. T. (2008). Application of the multivariate spectral weather generator to the contiguous United States. *agricultural and forest meteorology*, 148(3), 517-521.
- Schwarz, G. (1978). Estimating the dimension of a model. *The annals of statistics*, 6(2), 461-464.

- Sharma, S., Srivastava, P., Fang, X., & Kalin, L. (2015). Long-Range Hydrologic Forecasting in El Niño Southern Oscillation-Affected Coastal Watersheds: Comparison of Climate Model and Weather Generator Approach. *Journal of Hydrologic Engineering*, 20(12), 06015006.
- Smith, T. M., Reynolds, R. W., Peterson, T. C., & Lawrimore, J. (2008). Improvements to NOAA's historical merged land-ocean surface temperature analysis (1880–2006). *Journal of Climate*, 21(10), 2283-2296.
- Steyn, D., Moisseeva, N., Harari, O., and Welch, W.J., 2016. Temporal and Spatial Variability of Annual Rainfall Patterns in Guanacaste, Costa Rica. FuturAgua internal project report. 17 p.
- Taylor, M. A., Enfield, D. B., & Chen, A. A. (2002). Influence of the tropical Atlantic versus the tropical Pacific on Caribbean rainfall. *Journal of Geophysical Research: Oceans*, 107(C9).
- Tippett, M. K., DelSole, T., & Barnston, A. G. (2014). Reliability of regression-corrected climate forecasts. *Journal of Climate*, 27(9), 3393-3404.
- Trenberth, K. E. (1997). The definition of el nino. *Bulletin of the American Meteorological Society*, 78(12), 2771-2777.
- Trenberth, K. E., Branstator, G. W., Karoly, D., Kumar, A., Lau, N. C., & Ropelewski, C. (1998). Progress during TOGA in understanding and modeling global teleconnections associated with tropical sea surface temperatures. *Journal of Geophysical Research: Oceans*, 103(C7), 14291-14324.
- Vecchi, G. A., & Wittenberg, A. T. (2010). El Niño and our future climate: where do we stand?. *Wiley Interdisciplinary Reviews: Climate Change*, 1(2), 260-270.
- Wasko, C., Pui, A., Sharma, A., Mehrotra, R., & Jeremiah, E. (2015). Representing low-frequency variability in continuous rainfall simulations: A hierarchical random Bartlett Lewis continuous rainfall generation model. *Water Resources Research*, 51(12), 9995-10007.
- Waylen, P. R., Caviedes, C. N., & Quesada, M. E. (1996). Interannual variability of monthly precipitation in Costa Rica. *Journal of Climate*, 9(10), 2606-2613.
- Waylen, P. R., Quesada, M. E., & Caviedes, C. N. (1994). The effects of EL NIÑO-southern oscillation on precipitation in san José, costa rica. *international Journal of Climatology*, 14(5), 559-568.
- Waylen, P., & Laporte, M. S. (1999). Flooding and the El Niño-Southern Oscillation phenomenon along the Pacific coast of Costa Rica. *Hydrological processes*, 13, 2623-2638.
- Waylen, P., Caviedes, C., Poveda, G., Mesa, O., & Quesada, M. (1998, January). Rainfall distribution and regime in Costa Rica and its response to the El Niño-Southern Oscillation. In *Yearbook. Conference of Latin Americanist Geographers* (pp. 75-84). Conference of Latin Americanist Geographers.
- Weigel, A. P., Liniger, M. A., & Appenzeller, C. (2007). The discrete Brier and ranked probability skill scores. *Monthly Weather Review*, 135(1), 118-124.

- Wilks, D. S. (1989). Conditioning stochastic daily precipitation models on total monthly precipitation. *Water Resources Research*, 25(6), 1429-1439.
- Wilks, D. S. (1998). Multisite generalization of a daily stochastic precipitation generation model. *Journal of Hydrology*, 210(1), 178-191.
- Wilks, D. S., 1995: *Statistical Methods in the Atmospheric Sciences*. International Geophysics Series, Vol. 59, Academic Press, 467 pp.
- Woolhiser, D. A. (1992). Modeling daily precipitation—progress and problems. *Statistics in the environmental and Earth sciences*, 5, 71-89.
- Woolhiser, D. A., Keefer, T. O., & Redmond, K. T. (1993). Southern oscillation effects on daily precipitation in the southwestern United States. *Water Resources Research*, 29(4), 1287-1295.
- Yang, W., Andréasson, J., Graham, L.P., Olsson, J., Rosberg, J., and F. Wetterhall (2010) Distribution-based scaling to improve usability of regional climate model projections for hydrological climate change impact studies, *Hydrol. Res.*, 41, 211-229.
- Youden, W. J. (1950). Index for rating diagnostic tests. *Cancer*, 3(1), 32-35.
- Yue, S. (2000). The bivariate lognormal distribution to model a multivariate flood episode. *Hydrological Processes*, 14(14), 2575-2588.
- Zaroug, M. A., Eltahir, E. A., & Giorgi, F. (2014). Droughts and floods over the upper catchment of the Blue Nile and their connections to the timing of El Niño and La Niña events. *Hydrology and Earth System Sciences*, 18(3), 1239-1249.

Chapter 4: The Relative Value of Seasonal Drought-event Forecasts Conditioned on ENSO Phase for Water Management Decisions

This chapter will be submitted to the Environment Systems and Decisions journal

Abstract

Predicting seasonal drought events in advance provides the opportunity to make proper decisions in a range of applications. Stress has been put on decision-makers by the uncertainty in seasonal rainfall forecasts, which is commonly associated with the variable cycle of the El Niño Southern Oscillation (ENSO). Methods that incorporate ENSO information into the process of seasonal rainfall prediction have shown the potential to narrow this uncertainty. However, the usefulness of forecasts to the process of making decisions cannot be guaranteed by forecast quality. This study investigates to what extent seasonal drought-event forecasts can be utilized in the process of making decisions. Two statistical measures are applied including the Relative Operating Characteristic (ROC) and the value of information in a cost-loss decision model. The ROC measures the ability of a forecast to predict dry vs. non-dry events, while the decision model estimates the relative value that provides an indication of the economic benefit provided by a proposed forecast system relative to the perfect system. The findings indicate that: a) the proposed calibration method improves both of the discrimination ability and relative value of the raw forecasts, b) an increase in lead time results in a reduction in the usefulness of the forecasts, c) the lead time of one year provides the potential for suitable benefits to the decision-making process, d) improvements in the relative value could be obtained by enhancing the ability of discrimination, e) the drought-event forecast in the late part of the wet season results in a higher potential benefit

to the decision-making process than that in the early part of the wet season, f) the positivity in the relative value never remains for the whole range of cost-loss ratio, which implies usefulness for certain cases only. Overall, incorporating ENSO information into seasonal rainfall forecasting would be beneficial to the decision-making process.

4.1 Introduction

Interest in reducing uncertainty in the prediction of drought event occurrence has grown due to the increased stress arising from climate change, population growth, and agricultural and industrial expansions across a large region of the globe. Improper mitigation strategies in handling drought events are frequently related to inaccurate seasonal rainfall forecasts that led to inappropriate decisions. In a developing nation like Costa Rica, inappropriate decisions in handling drought events may lead to blackouts and interruptions in the hydropower supply, deterioration of water supply for drinking and sanitation, harvest failure, and losses in lucrative tourism. In addition, they may affect the effectiveness of decisions made in agricultural business related to the selection of appropriate crop cultivars and varieties, the purchase of crop insurance, the timing of agricultural operations, fertilizer implementation, and livestock management strategies. Due to limitations in the existing statistical and dynamical prediction models (Krzysztofowicz, 2001; Gneiting, et al., 2007), or to the difficulty in addressing the irregular interannual variability of seasonal rainfall (Katz and Parlange 1998; DeChant and Moradkhani, 2014), uncertainties can be reduced but not completely eliminated. A question arising, then, is how to cope with remaining uncertainty-in particular to what extent seasonal dry-event forecasts can be utilized in the process of making decisions.

An analysis of the value of drought event forecasts should be of particular interest to decision-makers in northwest Costa Rica given that recent studies project reduced rainfall and intensified of extreme weather conditions over Central America in a climate change scenario (Rauscher et al., 2008; Anderson et al., 2008; Neelin et al., 2006; Maldonado et al., 2013; Karmalkar et al., 2013). Rauscher et al. (2008) projected a reduction in summer precipitation over Central America by 25% in the twenty-first century, with the greatest reduction experienced in June and July. Pascale et al. (2015) estimated an increase in the annual number of dry days over South and Central America of up to 1 month by the end of the twenty-first century. Hidalgo et al. (2013) identified a reduction in the runoff over Central America of 10% to 30% through employing downscaled runs from 30 General Circulation Models.

Typically, dry event forecasts could be communicated to a user either in a deterministic or probabilistic form. The latter form is more preferable in making decisions (Krzysztofowicz, 2001; Madadgar et al., 2014; Demargne et al., 2014) since it provides likelihood of having dry and non-dry events that assist decision makers in considering a range of possible outcomes. Hence, evaluating the ability of a probabilistic forecast system to discriminate between dry and non-dry events occurrence would be critical to maintain reliable and sustainable services with a range of sectors. A discrimination-based graphical verification called Relative Operating Characteristic (ROC) has been applied in psychology (Swets, 1973), clinical diagnosis (Swets and Pickett, 1982), and in weather forecast quality (Mason, 1982). The ROC curve measures discrimination ability in a forecast system for the purpose of decision making. Trambauer et al. (2015) employed the ROC method in measuring the discrimination ability of three proposed forecast scenarios to distinguish between the occurrence and non-occurrence of seasonal hydrological drought in the Limpopo

River basin, southern Africa. Lloyd-Hughes et al. (2013) investigated the reliability of the Met Office Hadley Centre Unified Model (HadGEM1) in predicting the occurrence of observed drought events by adopting the ROC method.

The seasonal cycle of precipitation over northwest Costa Rica has a bimodal pattern (Waylen et al., 1996; Magaña et al., 1999) that consists of dry and wet seasons lasting six months each (Hastenrath, 1967). The bimodality pattern appears in the wet season, in which an early and late wet season is separated by a midsummer drought. The strength of bimodality in the seasonal cycle is found to be related to the interchangeable phases of El Niño Southern Oscillation (ENSO) (Waylen et al., 1996; Rauscher et al., 2011). Three phases of the ENSO cycle have been recognized: a) a warm phase known as El Niño, b) a cold phase known as La Niña, and c) a neither warm nor cold episode called neutral. There is a tendency of having dry (wet) events during El Niño (La Niña) years (Waylen et al., 1996). Waylen et al. (1994) found that annual and seasonal precipitation at San Jose in Costa Rica appears to be conditioned on ENSO. Incorporating ENSO cycle information into prediction processes has been applied worldwide as an attempt to narrow uncertainty in streamflow predictions (Hamlet and Lettenmaier, 1999; Grantz et al., 2005; Regonda et al., 2006; Gobena and Gan, 2006, Sharma et al., 2015), in seasonal rainfall predictions (Gutzler et al., 2002; Gissila et al., 2004; Zaroug et al., 2014), in reducing the risk associated with decision making in the agricultural sector (Letson et al., 2005; Cabrera et al., 2006) and in natural gas purchasing (Changnon et al., 2000). Hamlet and Lettenmaier (1999) pointed out an increase in lead time and forecast specificity over climatology by incorporating ENSO and the Pacific Decadal Oscillation (PDO) into Columbia River streamflow forecasts. Gutzler et al. (2002) found that the ENSO cycle provided more seasonal predictability of winter precipitation anomalies than that of

the PDO index over western North America. As it can be indicated from Chapter 3, an increase in the degree of predictability of seasonal rainfall forecast over northwest Costa Rica by incorporating ENSO information. Cabrera et al. (2006) found that the predictability of seasonal climate variability with respect to ENSO has the potential to minimize farm risk by informing farmers of necessary changes in planting dates and guiding their purchasing of appropriate crop insurance.

The usefulness of a forecast system to the process of making decisions cannot be guaranteed by forecast quality (Palmer et al., 2000; Hartmann et al. 2002; Cabrera et al., 2009). In fact, drought event forecasts used in decision making often involve economic purposes, which are interpreted either by gaining or losing. To determine how beneficial a forecast system is, the expected returns must be better in comparison to the use of any other systems. A cost-loss decision model (Murphy 1977; Katz and Murphy 1997; Richardson 2000) has been employed to assess the usefulness of a forecast system to the decision making process. The model determines a value called “economic or relative value” *RV* that provides an indication for the amount of saving relative to the perfect forecast scenario. Richardson (2000) examined the relative economic value of the European Centre for Medium Range Weather Forecast (ECMWF) ensemble prediction system. Palmer et al. (2000) discussed the relationship between the skill and value of seasonal ensemble forecasts in a probabilistic framework. Jones et al. (2011) evaluated the relationship between Madden-Julian Oscillation (MJO) and the relative value of a deterministic forecast of extreme precipitation over the contiguous United States. In addition, the relationship between the quality and relative value of a weather forecast system has been studied (Murphy and Ehrendorfer 1987; Richardson 2001). Chang et al. (2015) suggested that the *RV* of a forecast system can be increased only by improving its discrimination ability.

This study addresses the quality of seasonal drought-event forecasts in the context of making decisions over northwest Costa Rica. The study applies a forecast system developed by AlMutairi et al. (2017) (in-preparation - see Chapter 3), which is constructed based on a stochastic weather generation (WG) model that forecasts the likelihood of drought-event occurrences during both the early and late wet season. The model relies on the teleconnection relationship between ENSO and seasonal rainfall cycle, thus it links a joint distribution of seasonal rainfall in the two portions of the wet season conditioned on ENSO phase with an ENSO occurrence model represented by a (1st order) Nonhomogeneous Markov Chain. The raw forecasts of the proposed model are calibrated using the Distribution-Based Scaling (DBS) method (Yang et al., 2010). Climatological forecasts are generated by conditioning the proposed model on the long-run probability of the ENSO cycle rather than today's ENSO cycle. For 20 years of data from 1996 to 2015, a Relative Operating Characteristic (ROC) curve is drawn to measure the ability of the raw, calibrated, and climatological forecast scenarios to discriminate between the two alternative outcomes of a drought-event. Then, a cost-loss decision model is constructed for all possible cutoff points with respect to the cost-loss ratios (0-1). The relationship between the resulting skills-based decision making and lead time is also investigated. Overall, the analysis of this paper aims to determine whether or not incorporating ENSO into seasonal rainfall forecasts would be beneficial to the process of making decisions over northwest Costa Rica.

In this chapter, section 4.2 presents information about the data used; section 4.3 explains model construction and the used verification metrics; section 4.4 shows the results on the usefulness of drought-event prediction by incorporating ENSO cycle information for decision making; and section 5 presents conclusions.

4.2 Data used

Observed monthly precipitation data is obtained from the Climatic Research Unit (CRU) TS 3.24 (Jones and Harris, 2008) over the domain (9.5-11 N and 85-86 W) from 1916 to 2015. These monthly precipitation data are fitted to a Mixture Gaussian model (Steyn et al., 2016; AlMutairi et al., 2016) and then the outputs parameters utilized in the study. Sea surface temperatures (SSTs) for the Nino 3.4 (5S to 5N; 170W to 120W) region are used to monitor the ENSO pattern (Trenberth, 1997). Observed Nino 3.4 SSTs are extracted from a (0.5x0.5 degree) grid dataset of the Extended Reconstructed Sea Surface Temperature (ERSST) version 3b of the National Oceanic and Atmospheric Administration (NOAA) (Smith et al, 2008). Monthly SST values from 1916 to 2015 are used to construct SST anomalies with respect to the averaged SSTs of the 1951-1980 period. The reference period is selected to avoid the use of the 1980s, which may result in a negative bias due to strong El Niño events (Pozo-Vázquez et al., 2001, 2005).

The Oceanic Nino Index (ONI) is used to distinguish between three different ENSO phases. An El Niño event is defined to occur when the three month averages are greater than (or equal to) $0.5\text{ }^{\circ}\text{C}$ for five consecutive seasons or more, b) a La Niña event for averages smaller than (or equal to) $-0.5\text{ }^{\circ}\text{C}$ for five consecutive seasons or more and a Neutral phase otherwise. ENSO status during the early and late wet season is evaluated independently. Thus, the ENSO phase in the April-June season represents the early season`s ENSO phase, whereas the ENSO phase in the September-November season denotes the late wet season`s ENSO phase.

4.3 Materials and Methods

4.3.1 Model construction

The study uses a methodology developed by AlMutairi et al. (2017) (in-preparation - see Chapter 3). A Bivariate Normal (BVN) Distribution was constructed as a joint distribution of normal density functions for the logarithm of the early and late wet season rainfalls. To address the influence of the interannual variability, the BVN model was conditioned on each ENSO phase over a training period from 1916 to 1975. The ENSO cycle is represented by three different discrete states $S = \{\text{El Niño, Neutral and La Niña}\}$, where the transition probability between these states is determined from a first-order Non-Homogeneous Markov Chain (NHMC), which was found as the best representation for the ENSO cycle (see Chapter 3). In the 1st order NHMC, The transition probability implies dependence of the next state on only the present state rather than any, or a sequence of, past states:

$$p_{ij}^{n,n+1} = P(X_{n+1} = j | X_n = i) \quad (1)$$

The maximum likelihood method is used to estimate the transition probabilities as follows:

$$p_{ij}^{n,n+1} = P(X_{n+1} = j | X_n = i) = \frac{N_{ij}^{n,n+1}}{N_i^n} \quad (2)$$

where $N_{ij}^{n,n+1}$ is the total number of times being in state i at season n and transitioning to state j at season $n+1$; N_i^n is the total number of times being in state i at season n .

The bimodal pattern of seasonal precipitation, as a function of time, is represented by a Gaussian mixture model (Steyn et al., 2016; AlMutairi et al., 2016). Seven parameters of the Gaussian

mixture model are estimated for each yearly seasonal cycle of precipitation from 1916 to 2015 by the least squares method, which is applied to minimize the square difference between the observed monthly precipitation and the Gaussian mixture model prediction. The parameter that is demonstrating the area under the first (second) peak is used, in this study, to represent the early (late) wet season precipitation. These two parameters conditioned on ENSO phase showed to follow a lognormal distribution (see Chapter 3). The dry-event occurrence was defined as the 25th percentiles to the lognormal distribution of each of the rainfall of the two portions of the wet season. The Bivariate Normal (BVN) Distribution is employed to describe the joint distribution of normal density functions for the logarithm of these two parameters conditioned on ENSO phase. The logarithm is used to transform the lognormal behavior of seasonal rainfall to normal, while the exponential is also used to transform the BVN output to the seasonal rainfall form. For more detail about BVN construction and random generation, see Appendix 1.

This proposed stochastic weather generation (WG) model (Figure 10) is employed to predict the future occurrence of dry events in the early and late wet season over the time period from 1996 to 2015. The model has been adopted as it demonstrates the potential to narrow uncertainty in seasonal rainfall forecasts over northwest Costa Rica (AlMutairi et al., 2017 (in-preparation – see Chapter 3)). Given that incorporating ENSO into the process of seasonal rainfall forecast cannot completely remove uncertainty, this study develops a statistical approach that allows decision makers to determine to what extent the forecasts can still be utilized in making decisions as an approach to cope with the remaining uncertainty. The WG model consists of an ENSO occurrence model (1st order NHMC) and three BVN models. Each of the three BVN models maps the joint distribution of rainfall occurring in the early and late wet season conditioned on ENSO phase. The

exception is only for the BVN model conditioned on neutral phase, where, in fact, it is unconditioned on any ENSO phase. It has been found that rainfall during the neutral phase has a high rate of variability in which a rainfall preceded by an El Niño phase is different than that preceded by a La Niña phase (Sharma et al., 2015). The Distribution-Based Scaling (DBS) method (Yang et al., 2010) is used to correct the bias of seasonal rainfall predictions of the WG model (For more information about the DBS method, see Appendix 1).

The suggested WG model inputs an observed ENSO phase in the late wet season, and then generates N time-series of the seasonal rainfall in the early and late wet season for a lead time L . The forecast process is repeated for T time, in which the observed ENSO phase is re-input at the end of each lead time. When $L = 1$ (lead 1), the model forecasts one wet season of two portions (early and late). Similarly, lead 2 (3) simply means to forecast 2 (3) wet seasons (each with two portions). Babcock et al. (2016) found that most members of an interviewed groups of stakeholders in northwest Costa Rica use 3- 6-months forecasts, which represents lead 1 forecast in this study. However, this study investigates the extent that the proposed forecast system can benefit the decision making processes with different lead times. In other words, if benefits can be observed by using the proposed forecasts with a longer lead time ahead, it would provide decisions makers with enough time to modify decision in a way to increase benefits or to decrease unwanted impacts.

4.3.2 Relative operating characteristic (ROC)

The occurrence and nonoccurrence of an adverse event (e.g. dry event) can be summarized by a 2x2 contingency table (Table 11). The contingency table represents a two-dimensional discrete joint distribution between forecasts and observations that consists of four outcomes: Hit, Miss, False-alarm, and Correct-negative. Each cell of this table gives a count of the respective outcome over a medium range time frame. A perfect forecast scenario thus would have zero count in both the Miss and False-alarm outcomes. Based on the contingency table, the Hit (*HR*) and False-alarm (*FR*) rates can be computed for a given adverse event as follows:

$$\text{Hit rate} = \frac{\text{Hit}}{\text{Hit} + \text{Miss}} \quad (3)$$

$$\text{False-alarm rate} = \frac{\text{False-alarm}}{\text{False-alarm} + \text{Correct-negative}} \quad (4)$$

Table 11. Contingency table of an adverse event forecast performance over a set of cases during a range of time frames

		Event forecast	
		Yes	No
Event observed	Yes	Hit	Miss
	No	False Alarm	Correct Negative

In a probabilistic forecast system, a forecasted probability of an event to occur can be unclear (ambiguous) to decision makers. Thus, the probabilistic system can be transformed into a deterministic system through defining a cutoff point (threshold probability) θ , in which an event is predicted to occur if its probability forecast is greater than the defined cutoff point. By giving θ values from 0 to 1, both the Hit and False-alarm rates can be defined as $HR = HR(\theta)$ and $FR = FR(\theta)$.

The relative operating characteristic (ROC) (Swets, 1973; Mason, 1982) is adopted in this study to assess the ability of a forecast system to separate dry from non-dry events in the early and late wet season. The ROC curve is given by $HR(\theta)$ versus $FR(\theta)$, so that a trade-off relationship is presented such that if the Hit rate increases, the False-alarm rate decreases. In fact, the Hit (False-alarm) rate indicates the probability of a warning that was provided correctly (incorrectly). Hence, a score value of interest is the area under the ROC curve (AUC), which gives an indication of the ability of a forecast system to discriminate (Murphy, 1993) between the alternative outcomes. A perfect forecast scenario would have an AUC equal to 1, while a no-skill forecast system, for which $HR = FR$, would have an AUC equal to 0.5. The no-skill forecast system can be seen if the ROC curve lies on the diagonal line, which means that the given forecast system does not provide any useful information regarding dry-event occurrence. If the ROC curve lies below the diagonal line, the given forecast system would have a negative skill.

There are two methods to estimate the AUC (ROC score): a) a non-parametric approach by constructing a trapezoid under the curve as an approximation of the area, and b) a parametric approach that fits a smooth curve line to the data points. The trapezoidal approach may result in

underestimation of the ROC area (Hanley and McNeil, 1982). One of the most appropriate approaches adopted in meteorological verification practice is the bi-normal method (Mason, 1982; Swets, 1986). Its accuracy has been empirically validated in many different fields (Swets, 1986). However, when verification samples are small, specifically when the number of occurrences of the event is small, the trapezoidal rule is a suitable alternative to compute the area. Thus, the trapezoidal rule has been adopted in this study to measure the AUC.

In this study, the ROC metric is adopted to assess the ability of the three proposed forecast scenarios (raw, calibrated, and climatology) over 20 years of the period (1996-2015) to distinguish between the occurrence and nonoccurrence of dry-events in the early and late wet season. In addition, the influence of different lead time forecast on the ability of discrimination in the best forecast scenario is addressed.

4.3.3 Relative (Economic) value

Given uncertainty inherent in forecasts, decision makers need a method to reduce the possible loss associated with a decision that could be made. A cost-loss decision-analytic model (Murphy 1977; Katz and Murphy 1997; Richardson 2000) can be applied to compare between different forecast systems in order to determine the best available system that reduces losses and maximizes benefits associated with a given decision. Taking preventive measures (actions) depending on a given forecast system will incur a Cost C , irrespective of whether or not an adverse event (dry-event) occurs. However, if the dry-event occurs, a Loss L will be incurred in the absence of preventative

measures. Table 12 shows four possible combinations of decisions and dry-event outcomes given in the decision model.

Table 12. Expense matrix for the four combinations of decisions and dry-event occurrence

	Action taken	No action taken
Event occurs	C^*	L^*
Event does not occur	C	0

* *Some amount of loss might be added due to unexpected damages.*

In fact, decision makers have the choice to either use a forecast system or not. When they do not rely on a forecast system to make a decision, such a case is called (in this study) a “no-forecast” scenario. Therefore, the Cost-loss decision model would be applied to compare the performance of four forecast scenarios (options): raw, calibrated, climatology, and no-forecast. Figure 16 shows a decision tree that simplifies the output strategies that can be made according to these forecast scenarios. Consider a potential forecast user who decides to not rely on any forecast system. The strategy that could then be taken would be to either always, or never protect. Always taking a protective action will always incur C , whereas never taking a protective action will incur L when a dry-event occurs. The expected (average) expense of the no-forecast scenario $E_{no-fcst}$ thus would either equal C or L multiplied by the observed relative frequency O_{rf} of the dry-event. As a result, the optimal strategy that can be made by this scenario (option) is given by:

$$E_{no-fcst} = \min[O_{rf} \times L, C] \quad (5)$$

The expected expense of a forecast system E_{f-fcst} over a number of forecasts (20 years) can be expressed by both the Hit rate HR and False-alarm rate FR of the given forecast system, and the observed relative frequency of the dry-event O_{rf} (shown in Equation 6).

$$E_{f-fcst} = FR \times C \times (1 - O_{rf}) - HR \times O_{rf} \times (L - C) + O_{rf} \times L \quad (6)$$

This equation is employed to determine the expected expense associated with the use of each of the three forecast systems: raw, calibrated, climatology. A perfect operation strategy can be produced if a preventive action is only taken when a dry-event occurs. Thus, the expected expense of a perfect forecast E_{p-fcst} can be expressed as follows:

$$E_{p-fcst} = O_{rf} \times C \quad (7)$$

Given imperfect in forecasts, users will either take action or not based on an available forecast, so having an expected expense that is lower than that of the no-forecast scenario would be a better choice for decision makers (Zhu, 2002). For generalizing the Cost-loss decision model, all the expected expense are expressed per unit loss, so that a cost-loss ratio $\frac{C}{L}$ is generated. Thus,

Equation 6 is written as:

$$E_{f-fcst} = FR(\theta) \times C \times (1 - O_{rf}) - HR(\theta) \times O_{rf} \times (L - C) + O_{rf} \times L \quad (8)$$

The potential relative (economic) value RV is provided by the Cost-loss decision model with respect to a cost/loss ratio of the user's interest. Since this study does not interpret this value into dollar amounts (see e.g. Palmer et al., 2000; Räisänen and Palmer, 2001; Jones and Morse, 2010;

Jones et al., 2011; Griesser and Spillman, 2016), it would be called a relative value instead of an economic value.

The RV can be obtained as a relative fraction of the difference in expected expenses generated by both a given forecast and no-forecast scenarios to that generated by both the perfect forecast no-forecast scenarios as shown in Equation 9. In other words, RV determines the amount of savings earned by adopting a given forecast scenario relative to the maximum saving obtained by the perfect forecast scenario with respect to the case of no-forecast.

$$RV = \frac{E_{no-fcst} - E_{f-fcst}}{E_{no-fcst} - E_{p-fcst}} \quad (9)$$

The RV can also be expressed by the Hit rate HR , False-alarm rate FR , observed relative frequency of the dry-event O_{rf} , and cost-loss ratio $\frac{C}{L}$. Given that each of the HR and FR is a function of the cutoff point θ as shown in the subsection 4.3.2, the RV is a function of both the cost-loss ratio $\frac{C}{L}$ and the cutoff point θ as expressed as follows:

$$RV\left(\frac{C}{L}, \theta\right) = \frac{\min\left(\frac{C}{L}, O_{rf}\right) - FR(\theta)\left(\frac{C}{L}\right)(1 - O_{rf}) + HR(\theta)O_{rf}\left(1 - \left(\frac{C}{L}\right)\right) - O_{rf}}{\min\left(\frac{C}{L}, O_{rf}\right) - O_{rf}\left(\frac{C}{L}\right)} \quad (10)$$

Since the dry-event forecast information is expressed in a probabilistic form, decision makers need an optimal cutoff point θ to determine how high a dry event forecast probability should be in order to process an action in preparation for a dry event. In this study, the optimal θ_{opt} for each forecast scenario is determined by maximizing RV as shown in Equation 11. Since $\frac{C}{L}$ varies between 0

and 1, θ_{opt} could be simply found as $\max RV(\theta)$. A random walk search is developed by selecting random values for θ from 0 to 1 with respect to the full range of $\frac{C}{L}$.

$$\theta_{opt} \cong \max RV\left(\frac{C}{L}, \theta\right) \quad (11)$$

The horizontal axis in an RV plot represents the cost-loss ratio ranging from 0 to 1, whereas the y-axis is the respective relative value. It should be noted that the cost associated with any decision is assumed to never exceed losses so that the cost-loss ratio is only defined between 0 and 1.

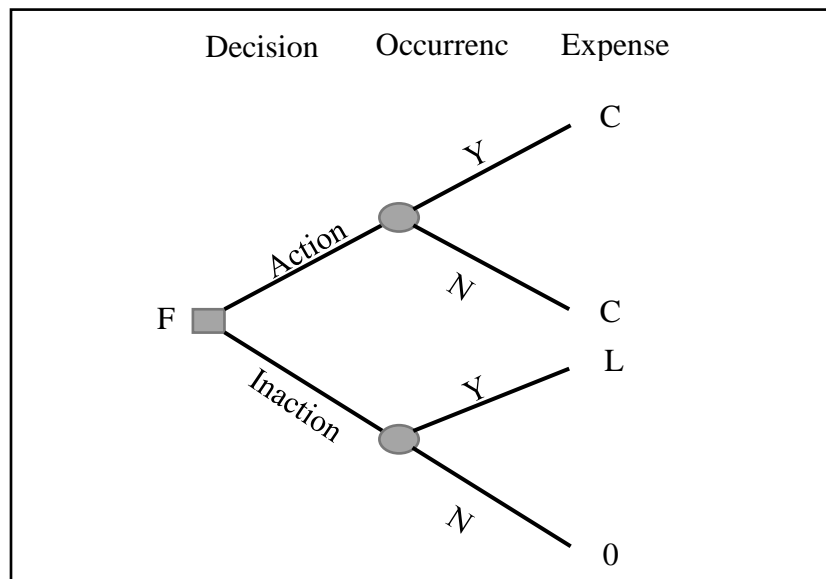


Figure 16. Decision tree demonstrating strategies associated with the use of a forecast scenario F. Decision: Action or Inaction; Dry-event occurrence: Y (yes) or N (no); Expense: C (cost), L (loss), or 0 (nothing).

The cost-loss ratios provide a platform for tradeoffs which helps decision makers to determine whether or not to take an action. For example, if decision makers find that the estimated cost associated with a given action is larger than the estimated loss when no action is taken, they would prefer to not take the given action. A RV of 1.0 indicates that the forecast is perfect while a no-forecast scenario has a value of 0. Thus, a beneficial forecast should be close to 1.0, while a negative RV indicates the given forecast system is costly as compared to the no-forecast scenario. Overall, the purpose of the Cost-loss decision model can be summarized as: a) determining the optimal cutoff point associated with the RV_{max} for each forecast system, and b) comparing the maximum relative value RV_{max} generated by all the proposed forecast systems in order to find the best system that is associated with the lowest expense over a number of cases (Palmer et al., 2000) that occur over the time period 1996 to 2015.

4.4 Results and discussion

4.4.1 Effect of calibration

The ROC test is not sensitive to bias in any given forecast system (Trambauer et al., 2015), but it measures the ability of the forecast to discriminate between two alternative outcomes (occur or non-occur). As mentioned in the subsection 4.3.2, forecast quality can be interpreted by considering the area under the ROC curve (AUR). The ROC curve for dry-event forecasts based on the raw, calibrated, and climatological forecast scenarios in both early (A_1) and late (A_2) wet season constructed over the period (1996-2015) are shown in Figure 17. Dry-event forecasts in the

early wet season based on the climatology are shown to have an AUC = 0.5, which indicates no-skill.

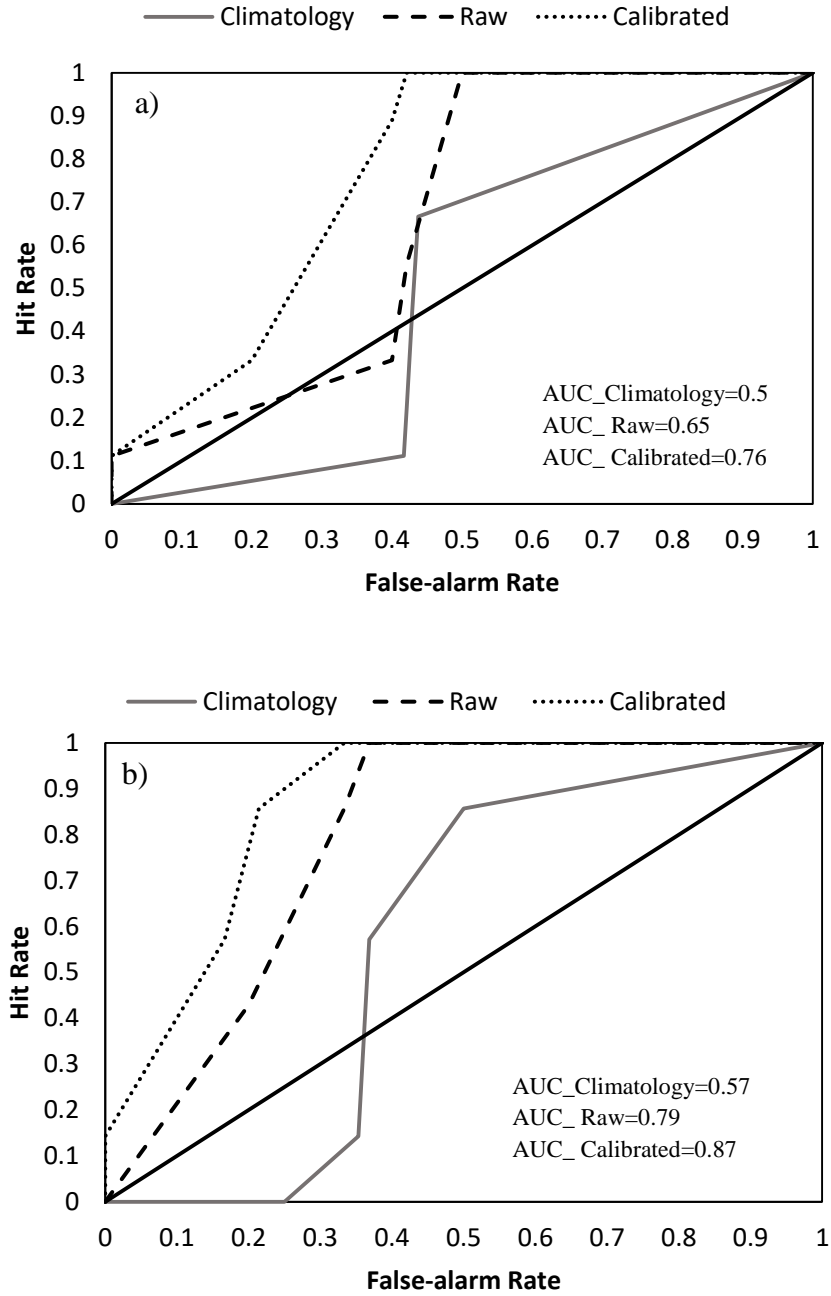


Figure 17. ROC curve generated based on the raw calibrated, climatology dry-event forecast in the a) early, and b) late wet season over the 1996-2015 period

However, the climatological forecast scenario shows little improvement in the skill ($AUC = 0.57$) to distinguish between dry and non-dry events in the LS. Overall, it can be noted that a dry-event forecast in the late wet season produces a higher AUC than that in the early wet season according to all three forecast scenarios as shown in Figure 17. This indicates greater ability in predicting dry events in the late rather than in the early wet season by conditioning on ENSO information. The calibration method (DBS) enhances the distinguishing ability between dry and not-dry events in both portions of the wet season through increasing the AUC. The AUC of the calibrated dry-event forecast increases in the early (late) wet season by approximately 17 % (10 %) as compared to the raw forecast. The results show that calibration is most effective in the early wet season.

Given the ROC curve and the resultant tradeoff between the HR and FR , the optimal cutoff point θ can be estimated to help decide whether a dry event is predicted to occur or not. In fact, the optimal cutoff point is a choice of forecast users (e.g. stakeholders) based on the given tradeoff relationship. For example, picking a high θ would result in a high HR with a high FR , which means that there is a lower chance of missing dry events, but a high number of false dry events. The most common approach used to estimate the optimal cutoff point from the ROC is Youden's index (Youden, 1950). This index aims to maximize the vertical distance between the equality line (diagonal line) and a point on the ROC curve. In fact, this approach maximizes the difference between the Hit rate HR and false-alarm rate FR such that $Max d = HR - FR$. Another approach to determine the optimal threshold is to minimize the distance between a point on the curve and the upper left corner point. This point is just the (1, 1) point, which by concept is the best cutoff point that could be selected. However, the optimal cutoff point, in this study, is determined by considering the relative value associated with decisions that might be taken according to the

selected cutoff point. As such, the optimal cutoff point of a forecast system is the point that results in the maximum relative value. A Monte Carlo optimization model is applied to search for the optimal cutoff point lying in a range of points from 0 to 1 with respect to the full range of cost/loss ratios (0-1). Then, a cutoff point θ that is associated with the maximum RV is considered the optimal θ for the corresponding forecast system.

It is clear that relying on the ROC alone cannot ensure selecting the cutoff point associated with the maximum economic benefit (relative value). As shown in Table 13, the optimal cutoff points are not always close to the upper left corner point (1, 1) of the ROC curve. For predictions of dry-events in the early wet season, the optimal θ of the raw forecast is associated with a HR (FR) that is larger (smaller) than that of the calibrated forecast. Specifically, the HR (FR) of the raw forecast is approximately 17% (40%) above (below) the calibrated forecast. In the case of dry-event forecasts in the late wet season, the calibrated forecast is found to have the largest (smallest) HR (FR) among all three of the forecast scenarios. It should also be noted that the climatological forecast has the smallest HR and the largest FR with forecasting dry events in the two partitions of the wet season.

The relative values of the probabilistic dry-event forecast in both partitions of the wet season are drawn in Figure 18 for the three proposed forecast scenarios. These values are shown according to the corresponding optimal θ shown in Table 13. The calibration, as shown in this figure, improves the relative value of the dry-event forecast in the early and late wet season. For example, the relative value of the calibrated forecast is higher than that of the raw forecast by 79% (156%) in the early (late) wet season. The lower percentage of improvement in the early wet season compared

to the late wet season could be due to the lower HR in the calibrated forecast as shown in Table 13.

Table 13. Optimal cutoff points and associated Hit and false-alarm rates for the raw, calibrated, and climatology forecasts of dry events in the early and late wet season.

Early wet season	Cutoff Point (θ)	Hit rate	False-alarm rate
Climatology	0.28	0.43	0.45
Raw	0.35	0.57	0.42
Calibrated	0.33	0.47	0.25
Late wet season	Cutoff Point	Hit rate	False-alarm rate
Climatology	0.23	0.35	0.36
Raw	0.31	0.52	0.23
Calibrated	0.37	0.86	0.22

The relative values of both the raw and calibrated dry-event forecasts are larger than that of the climatological forecast in both portions of the wet season, which indicates the skill that can be obtained by incorporating the current ENSO information in seasonal precipitation forecasts. In fact, the skill of the climatological forecast is close to that of the no-forecast scenario for which $RV = 0$.

In addition, it can be seen that the relative values of the three forecast scenarios (raw, calibrated, and climatology) are found to be larger in the late than in the early portion of the wet season, which

emphasizes the degree of predictability that can be gained by incorporating ENSO information, particularly in forecasting rainfall in the late wet season.

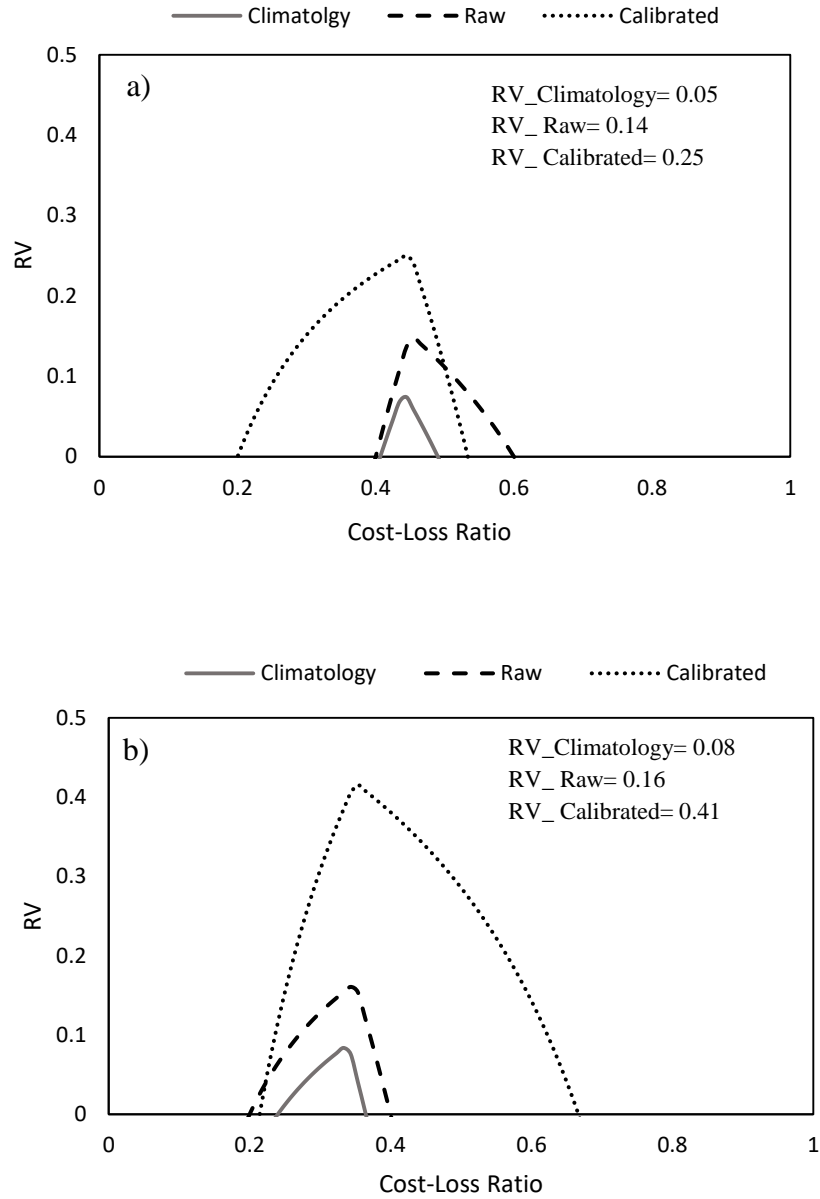


Figure 18. Relative value of the raw, calibrated and climatological dry-event forecasts in the a) early and b) late wet season according to the use of optimal cutoff points (Table 13)

This might be because ENSO has a greater effect on precipitation during the late portion than that of the early portion of the wet season. The greater effect during the late wet season has been attributed to the relationship between ENSO and the Caribbean Low Level Jet (CLLJ) (Waylen et al., 1998; Amador and Magana, 1999; Wang, 2007; Rauscher et al., 2008; Hidalgo et al., 2015; Maldonado et al., 2016). A warm ENSO event is found to be associated with a strengthening of the CLLJ, which induces drying from July through October. Warm events are also associated with a southward displacement of the eastern Pacific Intertropical Convergence Zone (ITZC) (Waylen et al. 1996; Rauscher et al., 2011; Hidalgo et al., 2015).

The positive relative values occur when the expected expense of a given dry-event forecast system is below that obtained by the no-forecast scenario. The calibration, as shown in Figure 19, performs well in reducing the expected expenses associated with dry-event forecasts in both portions of the wet season, especially in the early portion. It also increases the number of situations where the forecast can be beneficial to the process of making decisions by enlarging the cost-loss ratio range associated with a positive RV . The calibrated dry-event forecast scenario remains valuable for the cost-loss ratio range of 0.2-0.52 (0.2-0.67) in the early (late) wet season. Beyond this range, the given forecast should be ignored because it could result in a large loss or cost. When $C/L < 0.2$, the no-forecast scenario would be preferable. Decisions makers, in this scenario, have to either always or never take action, so that it would be beneficial to take action because the potential loss is approximately five times larger than the expected cost in both portions of the wet season. When approaching a cost-loss ratio of 1, accepting loss is a possible choice (Griesser and Spillman, 2016) since taking an action or not will not make a difference.

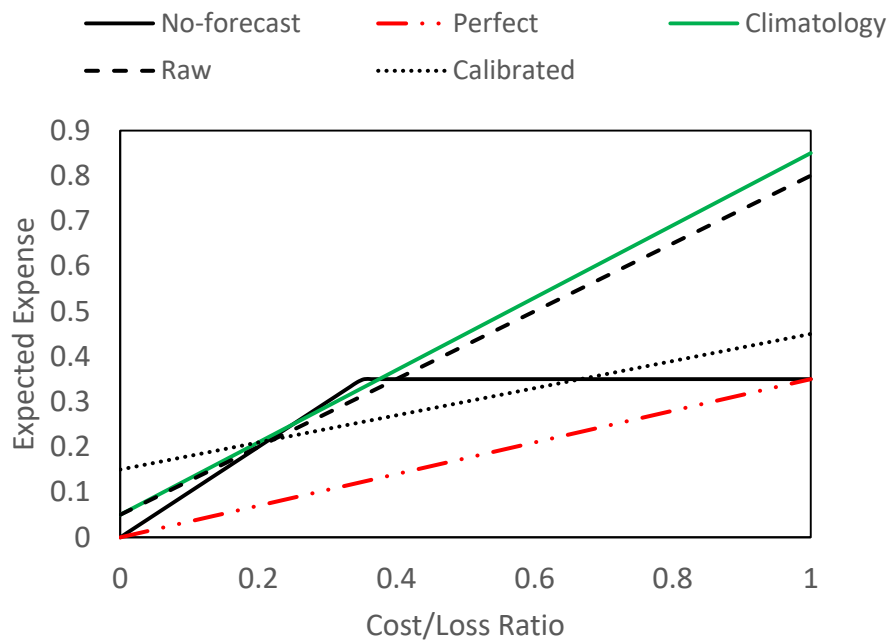
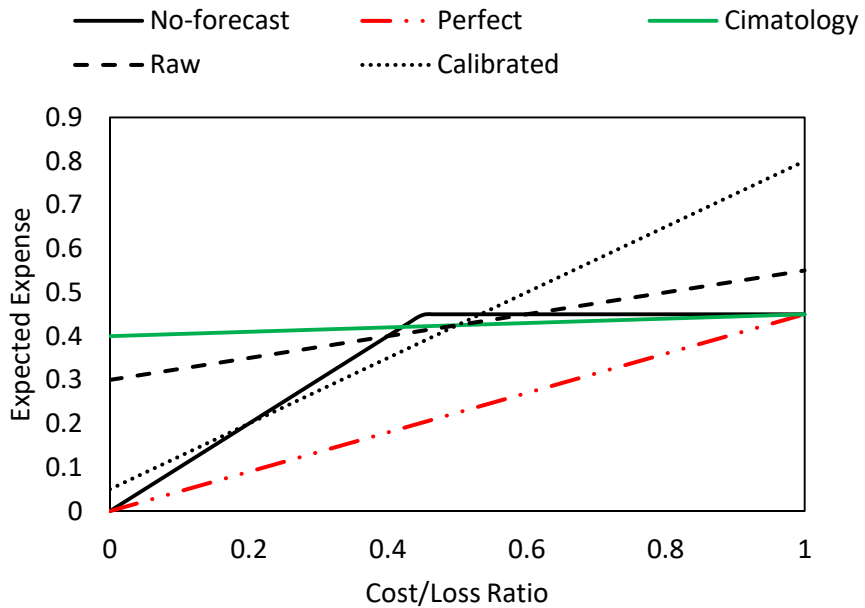


Figure 19. Expected expense generated by forecasting dry events in both the a) early, and b) late wet season based on the raw, calibrated, climatology, perfect (dash gray), and no-forecast (dark black) scenarios.

Overall, to benefit from the RV analysis, decisions should be made based on: a) accurate knowledge about the situation, especially the loss and cost estimations, and b) correct selection for the appropriate forecast system.

4.4.2 Effect of lead times

This subsection analyzes the influence of lead time forecast on the discrimination ability and relative value of the calibrated forecast scenario in the two partitions of the wet season. Figure 25 (Appendix 3) shows the ROC curve of dry-event forecast (calibrated) in the early and late wet season with respect to different lead times. It can be seen that the AUC decreases with lead time increases. For example, the AUC of the calibrated forecast for a dry event in the early (late) wet season drops from 0.76 (0.87) at a lead time of 1 year (lead 1) to 0.52 (0.63) at a lead time of 3 years (lead 3). For lead 3, a dry-event forecast in the early portion of the wet season produces an AUC of 0.52, which means that almost half of the observed dry-events were not predicted.

Similarly, an increase in lead time results in a reduction in the relative value obtained at the selected optimal cutoff points (Table 13) as shown in Figure 26 (Appendix 3). The *RV* of a dry-event forecast in the early (late) wet season reduces to 0.04 (0.2) at lead 2, which is associated with a reduction of about 84% (51%). At lead 3, a dry-event forecast in the early wet season results in a negative $RV = -0.05$, which implies that using the given forecast information will not be beneficial to the decision making.

4.5 Conclusions

Drought events can cause major negative impacts on ecosystems and socioeconomic systems, especially if ineffective mitigation decisions have been made. There is a need for predicting the occurrence of drought events accurately at significant lead times in order to provide decision-makers with a greater opportunity to improve the resilience of systems that rely on the water-food-energy nexus. The proposed methodology in the work of (AlMutairi et al., 2017) (see Chapter 3) was found to have the potential to narrow the uncertainty in seasonal rainfall forecasts over northwest Costa Rica. However, an increase in predictability does not guarantee higher benefits to decision making processes. This study thus investigates to what extent the proposed forecasts might be utilized in the process of making decisions.

The raw forecast shows a higher AUC than that of the climatological dry-event forecast in both the early and late wet season, which implies a higher ability to separate dry and non-dry events. The climatological forecast has an AUC =0.5 for a dry-event forecast in the early wet season, which indicates that no skill can be obtained from forecasts based solely on climatology. The calibration method enhances the discrimination ability associated with the raw forecast scenario for both portions of the wet season. In spite of a larger percentage of improvement in the discrimination ability in the early wet season, the measurable ability in discrimination is found to be higher in the late wet season than in the early wet season. Additionally, the discrimination ability of all three forecast scenarios, as expected, is reduced with increased lead time. The results show a relationship between the ability of discrimination and the relative value. Hence, as long as

the ability of discrimination of a forecast improves, the contribution to decision making processes as measured by a relative value is enhanced.

The optimal cutoff point for each of the three forecast scenarios is assumed to be associated with the corresponding maximum relative value. Therefore, the optimal cutoff point for any of the three forecast scenarios does not always have the best hit or false-alarm rate. The climatological forecast has an optimal cutoff point that is found to correspond to the smallest hit rate and the largest false-alarm rate in the two portions of the wet season. Due to the reported effect of ENSO on the late season rainfall, the study indicates that the positive relative value of dry-event forecasts in the late wet season is higher than in the early wet season for all three forecast scenarios.

Although the maximum relative values obtained by all proposed forecast scenarios are positive, the positivity never remains for the whole range of the cost-loss ratio. This indicates that these forecast scenarios would be a useful tool for decision-makers at certain cases only. By calibration, the usefulness of the forecast appears only if the cost-loss ratio is between 0.2 and 0.52 (0.2 and 0.67) in the early (late) wet season. When C/L is less than the lower value, the decision makers should take preventative action no matter what the forecast is. When C/L is greater than the upper value, accepting loss is a possible choice since taking an action or not will not make a difference. The findings also show that the relative value reduces as long as the lead time increases, which implies that a forecast with a lead time of one year could be most beneficial to the process of making decisions.

References

- AlMutairi, B. S., Grossmann, I., & Small, M. J. (2016). Bimodal Seasonal Rainfall Model for Evaluating of Long-term Climate Model Projections. Manuscript submitted for publication (International Journal of Climatology).
- AlMutairi, B. S., Small, M. J., & Grossmann, I. (2017). Predictability of Multicategory Seasonal Probabilistic Forecast of Precipitation Conditioned on ENSO Phase. Unpublished manuscript.
- Amador, J. A., & Magana, V. (1999, January). Dynamics of the low level jet over the Caribbean Sea. In Preprints, Third Conference on Hurricanes and Tropical Meteorology.
- Anderson, E.R., Cherrington, E.A., Tremblay-Boyer, L., Flores, A.I. and Sempris, E., 2008. Identifying critical areas for conservation: Biodiversity and climate change in Central America, Mexico, and the Dominican Republic. *Biodiversity*, 9: 89-99.
- Babcock, M., Wong-Parodi, G., Small, M. J., & Grossmann, I. (2016). Stakeholder perceptions of water systems and hydro-climate information in Guanacaste, Costa Rica. *Earth Perspectives*, 3(1), 1-13.
- Cabrera, V. E., Fraisse, C. W., Letson, D., Podestá, G., & Novak, J. (2006). Impact of climate information on reducing farm risk by optimizing crop insurance strategy. *Trans. Asabe*, 49(4), 1223-1233.
- Cabrera, V. E., Solís, D., Baigorria, G. A., & Letson, D. (2009). Managing climate variability in agricultural analysis. *Ocean Circulation and El Niño: New Research*. Gainesville-Florida: Nova Science Publishers, 163-179.
- Chang, H. L., Yang, S. C., Yuan, H., Lin, P. L., & Liou, Y. C. (2015). Analysis of the Relative Operating Characteristic and Economic Value Using the LAPS Ensemble Prediction System in Taiwan. *Monthly Weather Review*, 143(5), 1833-1848.
- Changnon, D., Ritsche, M., Elyea, K., Shelton, S., & Schramm, K. (2000). Integrating climate forecasts and natural gas supply information into a natural gas purchasing decision. *Meteorological Applications*, 7(3), 211-216.
- DeChant, C. M., & Moradkhani, H. (2014). Toward a reliable prediction of seasonal forecast uncertainty: Addressing model and initial condition uncertainty with ensemble data assimilation and sequential Bayesian combination. *Journal of Hydrology*, 519, 2967-2977.
- Demargne, J., Wu, L., Regonda, S.K., Brown, J.D., Lee, H., He, M., Seo, D.J., Hartman, R., Herr, H.D., Fresch, M. and Schaake, J., (2014). The science of NOAA's operational hydrologic ensemble forecast service. *Bulletin of the American Meteorological Society*, 95(1), pp.79-98.
- Giannini, A., Kushnir, Y. and Cane, M.A., 2000. Interannual variability of Caribbean rainfall, ENSO, and the Atlantic Ocean*. *Journal of Climate*, 13: 297-311.

- Gissila, T., Black, E., Grimes, D. I. F., & Slingo, J. M. (2004). Seasonal forecasting of the Ethiopian summer rains. *International Journal of Climatology*, 24(11), 1345-1358.
- Gneiting, T., Balabdaoui, F., & Raftery, A. E. (2007). Probabilistic forecasts, calibration and sharpness. *Journal of the Royal Statistical Society: Series B (Statistical Methodology)*, 69(2), 243-268.
- Gobena, A. K., & Gan, T. Y. (2006). Low-frequency variability in Southwestern Canadian stream flow: links with large-scale climate anomalies. *International Journal of Climatology*, 26(13), 1843-1869.
- Grantz, K., Rajagopalan, B., Clark, M., & Zagona, E. (2005). A technique for incorporating large-scale climate information in basin-scale ensemble streamflow forecasts. *Water Resources Research*, 41(10).
- Griesser, A. G., & Spillman, C. M. (2016). Assessing the Skill and Value of Seasonal Thermal Stress Forecasts for Coral Bleaching Risk in the Western Pacific. *Journal of Applied Meteorology and Climatology*, 55(7), 1565-1578.
- Gutzler, D. S., Kann, D. M., & Thornbrugh, C. (2002). Modulation of ENSO-based long-lead outlooks of southwestern US winter precipitation by the Pacific decadal oscillation. *Weather and Forecasting*, 17(6), 1163-1172.
- Hamlet, A. F., & Lettenmaier, D. P. (1999). Columbia River streamflow forecasting based on ENSO and PDO climate signals. *Journal of water resources planning and management*, 125(6), 333-341.
- Hanley, J. A., & McNeil, B. J. (1982). The meaning and use of the area under a receiver operating characteristic (ROC) curve. *Radiology*, 143(1), 29-36.
- Hartmann, H. C., Pagano, T. C., Sorooshian, S., & Bales, R. (2002). Confidence builders: Evaluating seasonal climate forecasts from user perspectives. *Bulletin of the American Meteorological Society*, 83(5), 683-698.
- Hastenrath, S., 1976. Variations in low-latitude circulation and extreme climatic events in the tropical Americas. *Journal of the Atmospheric Sciences*, 33: 202-215.
- Hastenrath, S.L., 1967. Rainfall distribution and regime in Central America. *Archiv für Meteorologie, Geophysik und Bioklimatologie, Serie B*, 15: 201-241.
- Hidalgo, H. G., Amador, J. A., Alfaro, E. J., & Quesada, B. (2013). Hydrological climate change projections for Central America. *Journal of Hydrology*, 495, 94-112.
- Hidalgo, H. G., Durán-Quesada, A. M., Amador, J. A., & Alfaro, E. J. (2015). The Caribbean Low-Level Jet, the Inter-Tropical Convergence Zone and Precipitation Patterns in the Intra-Americas Sea: A Proposed Dynamical Mechanism. *Geografiska Annaler: Series A, Physical Geography*, 97(1), 41-59.
- Jones, A. E., & Morse, A. P. (2010). Application and validation of a seasonal ensemble prediction system using a dynamic malaria model. *Journal of Climate*, 23(15), 4202-4215.

- Jones, C., Carvalho, L. M., Gottschalck, J., & Higgins, W. (2011). The Madden–Julian oscillation and the relative value of deterministic forecasts of extreme precipitation in the contiguous United States. *Journal of Climate*, 24(10), 2421-2428.
- Jones, P. D., & Harris, I. (2008). Climatic Research Unit (CRU) time-series datasets of variations in climate with variations in other phenomena. NCAS British Atmospheric Data Centre.
- Karmalkar, A.V., Taylor, M.A., Campbell, J., Stephenson, T., New, M., Centella, A., Benzanilla, A. and Charlery, J., 2013. A review of observed and projected changes in climate for the islands in the Caribbean. *Atmósfera*, 26: 283-309.
- Katz, R. W., & Murphy, A. H. (1997). Forecast value: prototype decision-making models. *Economic value of weather and climate forecasts*, 183-217.
- Katz, R. W., & Parlange, M. B. (1998). Overdispersion phenomenon in stochastic modeling of precipitation. *Journal of Climate*, 11(4), 591-601.
- Krzysztofowicz, R. (2001). The case for probabilistic forecasting in hydrology. *Journal of hydrology*, 249(1), 2-9.
- Letson, D., Podestá, G. P., Messina, C. D., & Ferreyra, R. A. (2005). The uncertain value of perfect ENSO phase forecasts: stochastic agricultural prices and intra-phase climatic variations. *Climatic Change*, 69(2), 163-196.
- Lloyd-Hughes, B., Shaffrey, L. C., Vidale, P. L., & Arnell, N. W. (2013). An evaluation of the spatiotemporal structure of large-scale European drought within the HiGEM climate model. *International Journal of Climatology*, 33(8), 2024-2035.
- Madadgar, S., Moradkhani, H., & Garen, D. (2014). Towards improved post-processing of hydrologic forecast ensembles. *Hydrological Processes*, 28(1), 104-122.
- Magaña, V., Amador, J.A. and Medina, S., 1999. The midsummer drought over Mexico and Central America. *Journal of Climate*, 12: 1577-1588.
- Maldonado, T., Alfaro, E., Fallas-López, B. and Alvarado, L., 2013. Seasonal prediction of extreme precipitation events and frequency of rainy days over Costa Rica, Central America, using Canonical Correlation Analysis. *Advances in Geosciences*, 33: 41-52.
- Mason, I. (1982). A model for assessment of weather forecasts. *Aust. Meteor. Mag*, 30(4), 291-303.
- Murphy, A. H. (1977). The value of climatological, categorical and probabilistic forecasts in the cost-loss ratio situation. *Monthly Weather Review*, 105(7), 803-816.
- Murphy, A. H., & Ehrendorfer, M. (1987). On the relationship between the accuracy and value of forecasts in the cost–loss ratio situation. *Weather and Forecasting*, 2(3), 243-251.
- Murphy, E. J., & Horrocks, L. A. (1993). Composition of the phospholipids and their fatty acids in the ROC-1 oligodendroglial cell line. *Lipids*, 28(1), 67-71.
- Neelin, J.D., Münnich, M., Su, H., Meyerson, J.E. and Holloway, C.E., 2006. Tropical drying trends in global warming models and observations. *Proceedings of the National Academy of Sciences*, 103: 6110-6115.

- Palmer, T. N., Branković, Č., & Richardson, D. S. (2000). A probability and decision-model analysis of PROVOST seasonal multi-model ensemble integrations. *Quarterly Journal of the Royal Meteorological Society*, 126(567), 2013-2033.
- Pascale, S., Lucarini, V., Feng, X., Porporato, A. and ul Hasson, S., 2015. Projected changes of rainfall seasonality and dry spells in a high greenhouse gas emissions scenario. *Climate Dynamics*, 46: 1331-1350.
- Pozo-Vázquez, D., Esteban-Parra, M. J., Rodrigo, F. S., & Castro-Díez, Y. (2001). The association between ENSO and winter atmospheric circulation and temperature in the North Atlantic region. *Journal of Climate*, 14(16), 3408-3420.
- Pozo-Vázquez, D., Gámiz-Fortis, S. R., Tovar-Pescador, J., Esteban-Parra, M. J., & Castro-Díez, Y. (2005). El Niño–Southern Oscillation events and associated European winter precipitation anomalies. *International Journal of Climatology*, 25(1), 17-31.
- Räisänen, J., & Palmer, T. N. (2001). A probability and decision-model analysis of a multimodel ensemble of climate change simulations. *Journal of Climate*, 14(15), 3212-3226.
- Rauscher, S.A., Giorgi, F., Diffenbaugh, N.S. and Seth, A., 2008. Extension and intensification of the Meso-American mid-summer drought in the twenty-first century. *Climate Dynamics*, 31: 551-571.
- Rauscher, S.A., Kucharski, F. and Enfield, D.B., 2011. The role of regional sst warming variations in the drying of meso-america in future climate projections*. *Journal of Climate*, 24: 2003-2016.
- Regonda, S. K., Rajagopalan, B., Clark, M., & Zagona, E. (2006). A multimodel ensemble forecast framework: Application to spring seasonal flows in the Gunnison River Basin. *Water Resources Research*, 42(9).
- Richardson, D. S. (2000). Applications of cost-loss models. In *Proc. Seventh ECMWF Workshop on Meteorological Operational Systems* (pp. 209-213).
- Richardson, D. S. (2001). Measures of skill and value of ensemble prediction systems, their interrelationship and the effect of ensemble size. *Quarterly Journal of the Royal Meteorological Society*, 127(577), 2473-2489.
- Sharma, S., Srivastava, P., Fang, X., & Kalin, L. (2015). Long-Range Hydrologic Forecasting in El Niño Southern Oscillation-Affected Coastal Watersheds: Comparison of Climate Model and Weather Generator Approach. *Journal of Hydrologic Engineering*, 20(12), 06015006.
- Smith, T. M., Reynolds, R. W., Peterson, T. C., & Lawrimore, J. (2008). Improvements to NOAA's historical merged land–ocean surface temperature analysis (1880–2006). *Journal of Climate*, 21(10), 2283-2296.
- Steyn, D., Moisseeva, N., Harari, O., and Welch, W.J., 2016. Temporal and Spatial Variability of Annual Rainfall Patterns in Guanacaste, Costa Rica. *FuturAgua internal project report*. 17 p.
- Swets, J. A. (1973). The relative operating characteristic in psychology. *Science*, 182(4116), 990-1000.

- Swets, J. A. (1986). Form of empirical ROCs in discrimination and diagnostic tasks: Implications for theory and measurement of performance. *Psychological bulletin*, 99(2), 181.
- Swets, J. A. and Pickett, R. M. (1982). *Evaluation of Diagnostic Systems: Methods from Signal Detection theory*, Academic Press, New York.
- Trambauer, P., Werner, M., Winsemius, H. C., Maskey, S., Dutra, E., & Uhlenbrook, S. (2015). Hydrological drought forecasting and skill assessment for the Limpopo River basin, southern Africa. *Hydrology and Earth System Sciences*, 19(4), 1695-1711.
- Trenberth, K. E. (1997). The definition of el nino. *Bulletin of the American Meteorological Society*, 78(12), 2771-2777.
- Vecchi, G. A., & Wittenberg, A. T. (2010). El Niño and our future climate: where do we stand?. *Wiley Interdisciplinary Reviews: Climate Change*, 1(2), 260-270.
- Wang, C. (2007). Variability of the Caribbean low-level jet and its relations to climate. *Climate dynamics*, 29(4), 411-422.
- Waylen, P. R., Caviedes, C. N., & Quesada, M. E. (1996). Interannual variability of monthly precipitation in Costa Rica. *Journal of Climate*, 9(10), 2606-2613.
- Waylen, P. R., Quesada, M. E., & Caviedes, C. N. (1994). The effects of EL NIÑO-southern oscillation on precipitation in san José, costa rica. *international Journal of Climatology*, 14(5), 559-568.
- Waylen, P., & Laporte, M. S. (1999). Flooding and the El Niño-Southern Oscillation phenomenon along the Pacific coast of Costa Rica. *Hydrological processes*, 13, 2623-2638.
- Yang, W., Andréasson, J., Graham, L.P., Olsson, J., Rosberg, J., and F. Wetterhall (2010) Distribution-based scaling to improve usability of regional climate model projections for hydrological climate change impact studies, *Hydrol. Res.*, 41, 211-229.
- Youden, W. J. (1950). Index for rating diagnostic tests. *Cancer*, 3(1), 32-35.
- Yue, S. (2000). The bivariate lognormal distribution to model a multivariate flood episode. *Hydrological Processes*, 14(14), 2575-2588.
- Zaroug, M. A., Eltahir, E. A., & Giorgi, F. (2014). Droughts and floods over the upper catchment of the Blue Nile and their connections to the timing of El Niño and La Niña events. *Hydrology and Earth System Sciences*, 18(3), 1239-1249.
- Zhu, Y., Toth, Z., Wobus, R., Richardson, D., & Mylne, K. (2002). The economic value of ensemble-based weather forecasts. *Bulletin of the American Meteorological Society*, 83(1), 73-83.

Chapter 5: Conclusion

Future changes in the seasonal cycle of precipitation have the potential to cause major impacts on ecosystems, socioeconomic systems, and water management decisions. Thus, there is a need for predicting changes in precipitation, in particular for developing countries, due to climate change. Objectives of this study are demonstrated for northwest Costa Rica, which is an example of a developing country where distinctive patterns of dry and wet seasons exert a strong influence on water management decisions and economic activities. A statistical method relying on a Gaussian Mixture (GM) model is developed (see Chapter 2) to better characterize climate models projections and evaluate their performance. The rainfall projections are found to be uncertain in both sign and magnitude, especially for the early and late wet season. However, the proposed method provides a) suitable skills in characterizing uncertainty associated with climate model projections, b) more information can be obtained from the seasonal cycle of precipitation, and c) the possibility of performing detailed comparison tests among climate models over a set of simulations and projections.

The region's climate is found to be strongly influenced by large-scale climate variability, in particular the El Niño Southern Oscillation (ENSO) phenomenon. Therefore, this study also (see Chapter 3) investigates to what extent incorporating ENSO-rainfall teleconnection would assist to narrow the uncertainty in the seasonal precipitation predictions (in a categorical form) over a timescale of 20 years. A stochastic weather generation model is constructed to simulate a synthetic time-series for each of the early and late wet season rainfall rates. The generation is based on an ENSO occurrence model represented by a Nonhomogeneous Markov Chain (1st order) and a

precipitation intensity model specified by a bivariate normal distribution conditioned on ENSO phase. By using three multicategory verification metrics, the results exhibit that a degree of predictability and reliability can be obtained by incorporating ENSO information into the multicategory probabilistic forecast of seasonal precipitation. The multi-categorical predictions of the late wet season precipitation (i.e., dry, normal, and wet) shows a higher degree of predictability than that of the early wet season. The study also finds that almost the same degree of predictability can be obtained by incorporating the simulated ENSO information from four coupled AOGCMs: MIROC5, CNRM-CM5, HadGem2-ES, and MPI-ESM-LR in forecasting seasonal precipitation over northwest Costa Rica. This emphasizes the role that could be played by coupled climate models in reducing uncertainty associated with seasonal precipitation forecasts on timescales up to 20 years, and in building multiple future scenarios for seasonal precipitations, which would provide great value for planning and managing of water resource-based systems.

Like many portions of developing countries where climate variability exerts stress on the available water resources, early anticipation for drought events-in particular during a well-known rainy season would reduce the operational stress involved in water allocation processes. Two verification metrics (see Chapter 4) are applied, in which the ROC test is used to measure the ability of the drought-event forecast system to distinguish between the two alternative outcomes and a cost-loss decision model is adopted to determine the relative value of the forecast system. The optimal cutoff point is determined by developing a Monte-Carlo search for the point associated with the maximum relative value. The study shows that a) a positive relative value is obtained by all three of the forecast systems (raw, calibrated, and climatological), which indicates possible benefits can be gained by incorporating ENSO information in forecasting seasonal precipitation, b) both the

discrimination ability and the relative value for the three drought event forecast systems in the late wet season are higher than that in the early wet season, c) improvement in the relative value could be obtained by enhancing the discrimination ability, and d) the largest relative value is obtained by the calibrated forecast, which is found to be valuable only if the cost-loss ratio is between 0.2 (0.2) and 0.52 (0.67) in the early (late) wet season. Beyond this range, the given forecast system is not recommended since it may result in a large loss or increased costs. The results indicate that ENSO information can be useful to anticipate dry-event occurrences in the two portions of the wet season.

Given the possibility of having systematic errors in seasonal precipitation forecasts, the DBS method is employed to correct any systematic bias in them. The method is validated over the period 1976-1995 and then is tested over the period 1996-2015. The method performs well over the validating period by matching the cumulative distribution function of a forecast system with that of the observation. The calibration method, over the testing period, improves the predictability and reliability associated with the probabilistic categorical seasonal precipitation forecast. The discrimination ability and relative value for the drought-event forecast in the two portions of the wet season are also enhanced by calibration. Regardless of skills found with the calibration forecast in the late wet season, the percentage of improvement in skills by calibration is higher in the early wet season.

Flexibility in making any operational decision relies on having an accurate forecast system with different lead times. This study thus investigates the effect of three lead times on the predictability of seasonal precipitation forecast (calibrated), and on the ability of discrimination and relative

value of the calibrated drought-event forecast in the early and late wet season. This kind of investigations aims to determine the limitation and strength of the proposed forecast systems and provide a flexible operational platform of greater value to decision-makers rather than one single lead time. It has been indicated that the increase in lead time results in a reduction in the skills of the forecast systems. Overall, the study suggests that the lead time of one year could reflect suitable benefits to the decision-making process related to water-management in the early and late wet season.

Appendix 1: Detailed information about the methods used to construct the multicategory seasonal probabilistic forecast model of precipitation

1 ENSO occurrence model

1.1 Transition probability estimating

The maximum likelihood method is used to estimate the transition probabilities for the two orders of the NHMCs as follows:

$$p_{ij}^{n,n+1} = P(X_{n+1} = j | X_n = i) = \frac{N_{ij}^{n,n+1}}{N_i^n} \quad (A1)$$

$$p_{hij}^{n-1,n,n+1} = P(X_{n+1} = j | X_n = i, X_{n-1} = h) = \frac{N_{hij}^{n-1,n,n+1}}{N_{hi}^{n-1,n}} \quad (A2)$$

where $N_{ij}^{n,n+1}$ is the total number of times being in state i at season n and transitioning to state j at season $n+1$; N_i^n is the total number of times being in state i at season n .

1.2 ENSO occurrence model selection

The best representation for ENSO occurrence is selected according to the results of both Akaike's information criterion (AIC) and the Bayesian information criterion (BIC). The criteria are computed using the following equations for the m^{th} order NHMC model:

$$AIC = 2 S^m (S - 1) - 2 \ln L \quad (A3)$$

$$BIC = S^m \ln q - 2 \ln L \quad (A4)$$

$$L = \begin{cases} \sum_{i=1}^S \sum_{j=1}^S N_{ij} \ln(p_{ij}) & 1^{st} \text{ order NHMC} \\ \sum_{h=1}^S \sum_{i=1}^S \sum_{j=1}^S N_{hij} \ln(p_{hij}) & 2^{nd} \text{ order NHMC} \end{cases} \quad (\text{A5})$$

where L is the log-likelihood function for the transition matrix and q is the total number of observations. The best model is the one which has the minimum value of either the AIC or BIC, or both. The first-order model has $S^2 - S = 6$ parameters, while the second-order model has $S^2 (S - 1) = 18$ parameters.

1.3 Markov Chain Stationary test

The stationary property of the preferable Markov Chain model is tested through applying the log-likelihood ratio (LR) test. The main objective of this test is to verify whether the assumption of constant transition probabilities over time is correct. The pattern of ENSO phases over a given period of time (e.g. validation or testing periods) thus is divided into T different equal length subintervals. Then, the probability of a given ENSO phase (e.g. in the 1st order NHMC) transiting from state i at season n and to state j at season $n+1$ estimated for each of the T subintervals are statistically tested to be equal to that estimated for the full period. Therefore, the null hypothesis H_o of this test can be written as $p_{ij}^{n,n+1}(t) = p_{ij}^{n,n+1}$, where $t = (1, \dots, T)$. The LR test statistic (Equation A6) is found to follow a chi-square distribution under the null hypothesis with a degree of freedom $df = (T - 1)S(S - 1)$, given that S is the total number of states.

$$LR = 2 \sum_{t=1}^T \sum_{i=1}^S \sum_{j=1}^S f_{ij,t} [\ln(p_{ij}^{n,n+1}(t)) - \ln(p_{ij}^{n,n+1})] \quad (\text{A6})$$

where $f_{ij,t}$ denotes the number of times ENSO transitions from state i at season n and to state j at season $n+1$ with a transition probability $p_{ij,t}$ over period t . The LR test uses $\alpha = 0.05$ as a level of significance in which a p –value below 0.05 represents a rejection of the null hypothesis.

2 Rainfall intensity model

2.1 Lognormal distribution and goodness of fit

It should be noted that the mean m and variance v of the lognormal distribution can be obtained through Equation A7 and A8.

$$m = \exp\left(\mu + \frac{\sigma^2}{2}\right) \quad (\text{A7})$$

$$v = \exp(2\mu + \sigma^2) (\exp(\sigma^2) - 1) \quad (\text{A8})$$

In addition, the goodness of fit is measured by a chi-squared test, which is a statistical hypothesis test used to determine whether there is a significant difference between the expected frequencies based on the fitted CDF and the observed frequencies in c bins ($c = 5$) (Equation AB1.9). Chi-square χ^2 has $c - k - 1$ degrees of freedom, where k is the number of estimated parameters.

$$\chi^2 = \sum_{i=1}^c \frac{(O_i - E_i)^2}{E_i} \quad (\text{A9})$$

Therefore, the hypothesis that the two datasets are from the same distribution is rejected if a p –value is below the level of significance α .

2.2 Bivariate Normal (BVN) Distribution construction

To construct a BVN distribution, u_1 and u_2 are assumed to follow a bivariate normal distribution $\mathcal{N}(\mu_{BVN}, \Sigma_{BVN})$, where μ_{BVN} is a vector of the means, and Σ_{BVN} is the covariance matrix.

$$\mu_{BVN} = \begin{bmatrix} \mu_1 \\ \mu_2 \end{bmatrix} \quad (\text{A10})$$

$$\Sigma_{BVN} = \begin{bmatrix} \sigma_1^2 & \rho \sigma_1 \sigma_2 \\ \rho \sigma_1 \sigma_2 & \sigma_2^2 \end{bmatrix} \quad (\text{A11})$$

The probability density function for the bivariate normal distribution for $U = \begin{bmatrix} u_1 \\ u_2 \end{bmatrix}$ can be written as:

$$f_U(U) = \frac{1}{2\pi |\Sigma_{BVN}|^{1/2}} e^{-\frac{1}{2} (U - \mu_{BVN})^T \Sigma^{-1} (U - \mu_{BVN})} \quad (\text{A12})$$

$$\Sigma_{BVN}^{-1} = \frac{1}{(1 - \rho^2)} \begin{bmatrix} \frac{1}{\sigma_1^2} & \frac{-\rho}{\sigma_1 \sigma_2} \\ \frac{-\rho}{\sigma_1 \sigma_2} & \frac{1}{\sigma_2^2} \end{bmatrix} \quad (\text{A13})$$

$$|\Sigma_{BVN}| = \sigma_1^2 \sigma_2^2 (1 - \rho^2) \quad (\text{A14})$$

Random bivariate normal variables can be generated as linear combinations of two standard BVN column vectors $Z_{BVN} \sim \mathcal{N}(0, I)$, where I is the identity matrix. The set of the generations is computed for a given mean vector and covariance matrix. Cholesky decomposition factorization of the covariance matrix is employed to transform a set of uncorrelated variables into variables with the given covariances. The Cholesky decomposition for the positive definite covariance

matrix is defined such that $\Sigma_{BVN} = LL^T$, where L is the lower triangular elements. Then a set of the generated random variables U_R can be computed as:

$$U_R = Chol(\Sigma_{BVN}) Z_{BVN} + \mu_{BVN} \quad (A15)$$

The parameters μ and σ obtained for seasonal precipitation with respect to each ENSO phase are used to obtain both the μ_{BVN} and Σ_{BVN} required to construct the BVN model as: a) μ_1 (μ_2) in the vector μ_{BVN} is assumed to be the estimated mean parameter μ for the individual ES (LS) precipitation conditioned on a given ENSO phase and b) Σ_{BVN} is computed between ten-thousand randomly generated normal variables for ES and LS precipitation along with their estimated parameters (μ and σ) with respect to the given ENSO phase.

3 Distribution-Based Scaling (DBS) method

DBS is a version of quantile mapping technique that matches observed and simulated frequency distributions, which are assumed to follow a theoretical distribution (e.g. gamma, or lognormal). The gamma distribution is commonly used in the DBS method to correct bias in two partitions of the frequency distributions. Since this study classifies the seasonal precipitation into three categories (dry, normal, wet), DBS is used to match the simulated lognormal density distribution over these three categories to the observation. Thus, the seasonal precipitation distribution is divided into three partitions separated by the 25th and 75th quantiles. As a results, three sets of parameters ($\mu_{lw}, \sigma_{lw}; \mu_{im}, \sigma_{im}; \mu_{hh}, \sigma_{hh}$) are estimated for each of the observed and simulated

precipitation amounts over the validating (1976-1995) period. The observed three parameter sets are then applied to correct the seasonal precipitation over the testing period (1996-2015) according to the following equations:

$$P_{DBS} = F^{-1} \left(\mu_{obs, lw}, \sigma_{obs, lw}, F(P, \mu_{sim, lw}, \sigma_{sim, lw}) \right) \text{ if } P \leq 25^{\text{th}} \text{ quantile value} \quad (\text{A16})$$

$$P_{DBS} = F^{-1} \left(\mu_{obs, im}, \sigma_{obs, im}, F(P, \mu_{sim, im}, \sigma_{sim, im}) \right) \text{ if } 25^{\text{th}} < P < 75^{\text{th}} \text{ quantile value} \quad (\text{A17})$$

$$P_{DBS} = F^{-1} \left(\mu_{obs, hh}, \sigma_{obs, hh}, F(P, \mu_{sim, hh}, \sigma_{sim, hh}) \right) \text{ if } P \geq 75^{\text{th}} \text{ quantile value} \quad (\text{A18})$$

where *obs* denotes the parameters estimated from observation and *sim* denotes parameters estimated from the simulated seasonal precipitation over the testing period. F^{-1} represents the inverse lognormal distribution.

4 Multicategory reliability diagram

A multicategory reliability diagram is applied to measure the reliability of the categorical probabilistic forecasts generated by incorporating ENSO information into the seasonal precipitation forecasting. Hence, the diagram is constructed for three mutually exclusive categories J ($j = 1, \dots, J$) (dry, normal, and wet) as follows: for each i th forecast year ($i = 1, \dots, N$), there is a probability forecast vector y_{ij} , where N is the total number of forecasted years and J is the total number of forecasted categories.

- A) The probability for each category j in the y_{ij} vector is rounded to the nearest 10% and a vector q is defined to represent the preset quantiles at the middle of each 10% increment of the forecast (q is $1 \times Q$, where Q is the tenth quantile)

B) The vector y_i is converted into a vector z_i that represents the forecast category number at each quantile (z_i is $1 \times Q$).

C) The reliability C_q for each given quantile is the probability that the observed category o_i is less than the forecast category z_{iq} at the given quantile q , averaged over all N forecasts [such that $C_q = \text{avg}_N (P(o_i < z_{iq}))$].

D) The probability for each i th forecast year can be computed as follows :

$$P(o_i < z_{iq}) \begin{cases} = 0 & \text{if } o_i > z_{iq} \\ = \frac{q - q_{\min}}{q_{\max} - q_{\min}} & \text{if } o_i = z_{iq} \\ = 1 & \text{if } o_i < z_{iq} \end{cases}$$

E) The diagram is constructed by plotting C_q versus q ; and error bars are generated by bootstrapping (1000 resampling).

Appendix 2: Supporting Materials for Chapter 3: Predictability of Multicategory Seasonal Probabilistic Forecast of Precipitation Conditioned on ENSO Phase

Table 14. The 1st order Nonhomogeneous Markov Chain for training period 1916-1975

Early wet season	El Niño	Neutral	La Niña
El Niño	0.38	0.46	0.15
Neutral	0.08	0.79	0.13
La Niña	0.14	0.55	0.32
Late wet season	El Niño	Neutral	La Niña
El Niño	0.70	0.10	0.20
Neutral	0.16	0.54	0.30
La Niña	0	0.25	0.75

Table 15. The 2nd order Nonhomogeneous Markov Chain for training period 1916-1975

Early wet season	El Niño	Neutral	La Niña
El Niño - El Niño	0.29	0.57	0.14
El Niño - Neutral	0.00	1.00	0.00
El Niño - La Niña	0.00	1.00	0.00
Neutral - El Niño	0.50	0.33	0.17
Neutral - Neutral	0.10	0.80	0.10
Neutral - La Niña	0.09	0.45	0.45
La Niña - El Niño	0.33	0.33	0.33
La Niña - Neutral	0.00	0.67	0.33
La Niña - La Niña	0.22	0.56	0.22
Late wet season	El Niño	Neutral	La Niña
El Niño - El Niño	0.40	0.20	0.40
El Niño - Neutral	0.00	0.50	0.50
El Niño - La Niña	0.00	0.00	1.00
Neutral - El Niño	1.00	0.00	0.00
Neutral - Neutral	0.16	0.53	0.32
Neutral - La Niña	0.00	0.00	1.00
La Niña - El Niño	1.00	0.00	0.00
La Niña - Neutral	0.25	0.58	0.17
La Niña - La Niña	0.00	0.43	0.57

Table 16. The 1st order Non-homogeneous Markov Chain for the testing (1996-2015) period

Early wet season	El Niño	Neutral	La Niña
El Niño	0.57	0.43	0
Neutral	0.33	0.67	0
La Niña	0	0.75	0.25
Late wet season	El Niño	Neutral	La Niña
El Niño	0.71	0.14	0.14
Neutral	0.25	0.58	0.17
La Niña	0	0	1.00

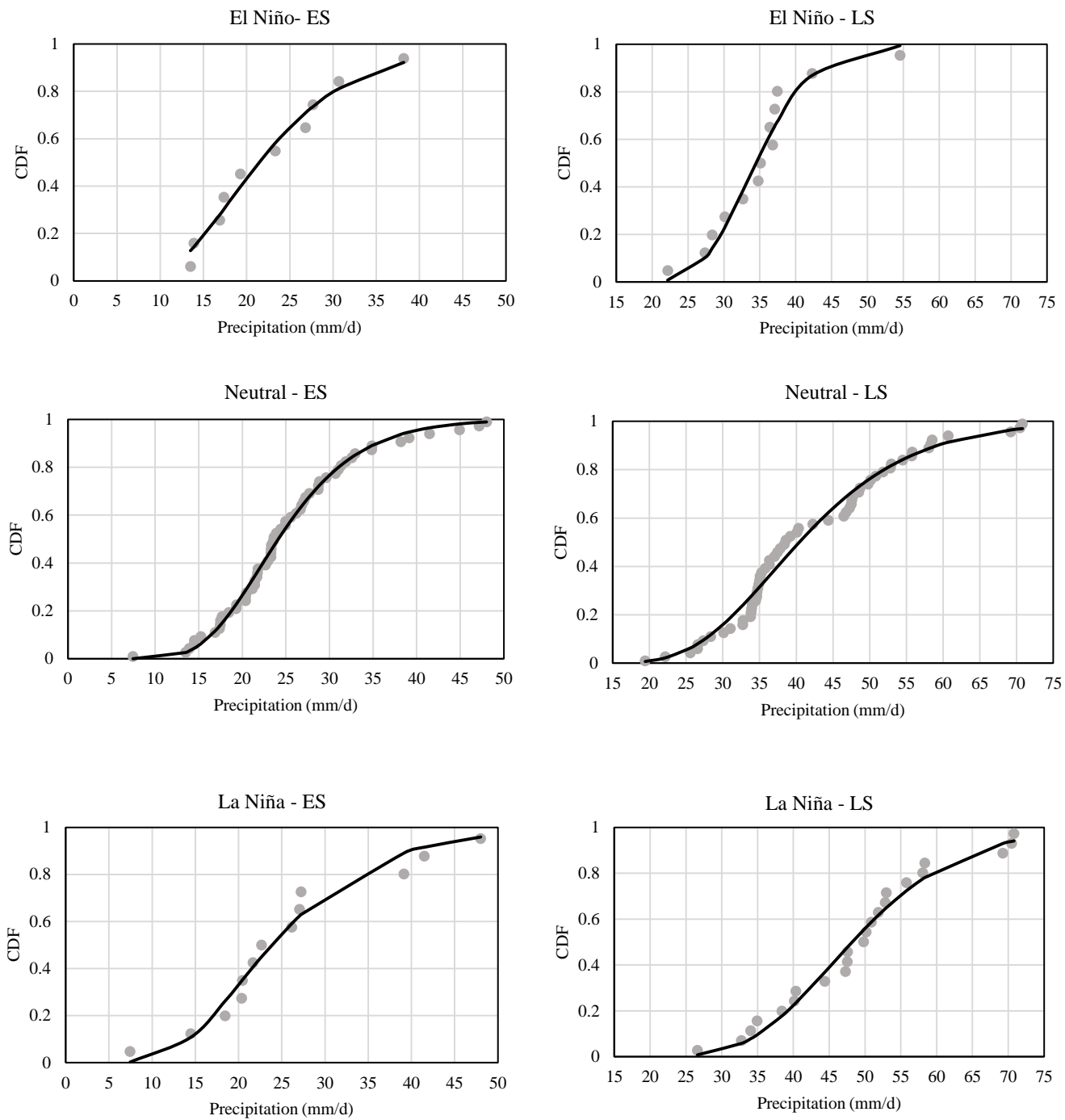
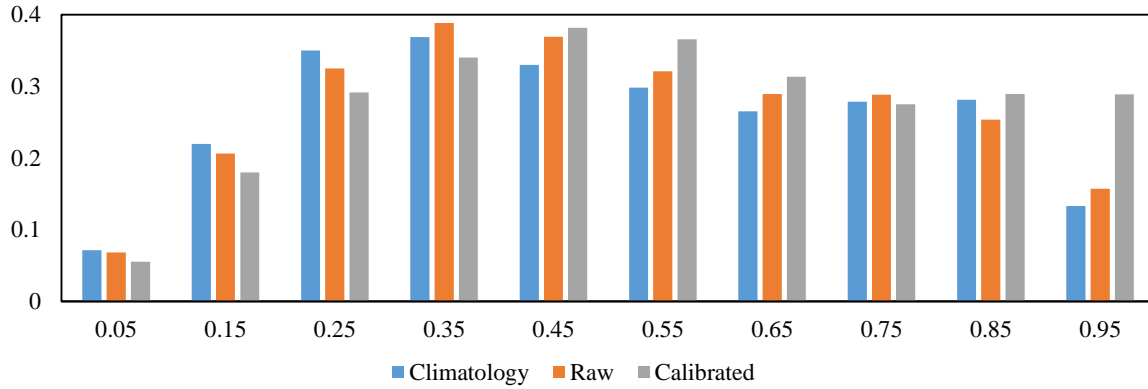


Figure 20. Cumulative distribution functions (CDF) for both the observations and fitted lognormal distributions

Difference in Error Bars in the MCRD (a)



Difference in Error Bars in the MCRD (b)

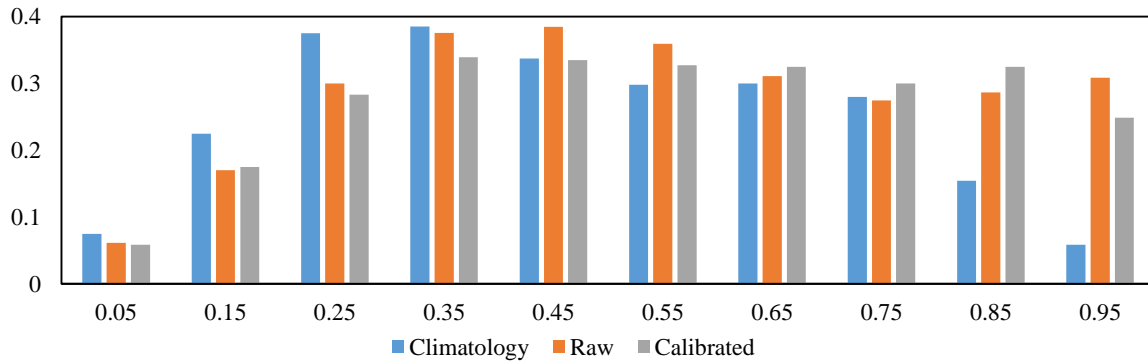


Figure 21. Difference between error bars in the MCRD generated by the raw, calibrated, climatological forecast for dry events in the a) early and b) late portion of the wet season.

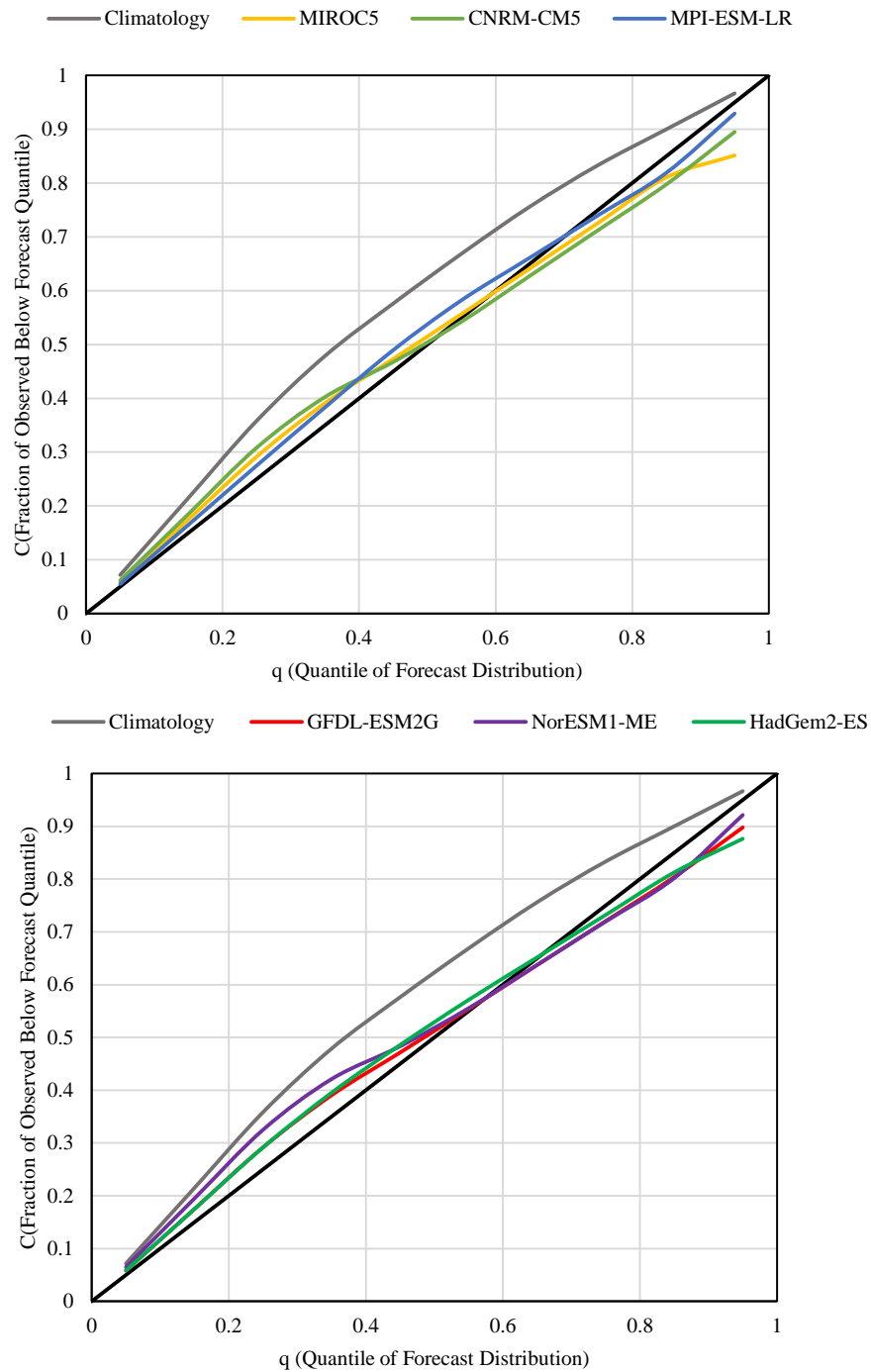


Figure 22. Multcategory reliability diagram for the calibrated rainfall forecast in the early wet season driven by the output of six climate models (separated into two plots for readability)

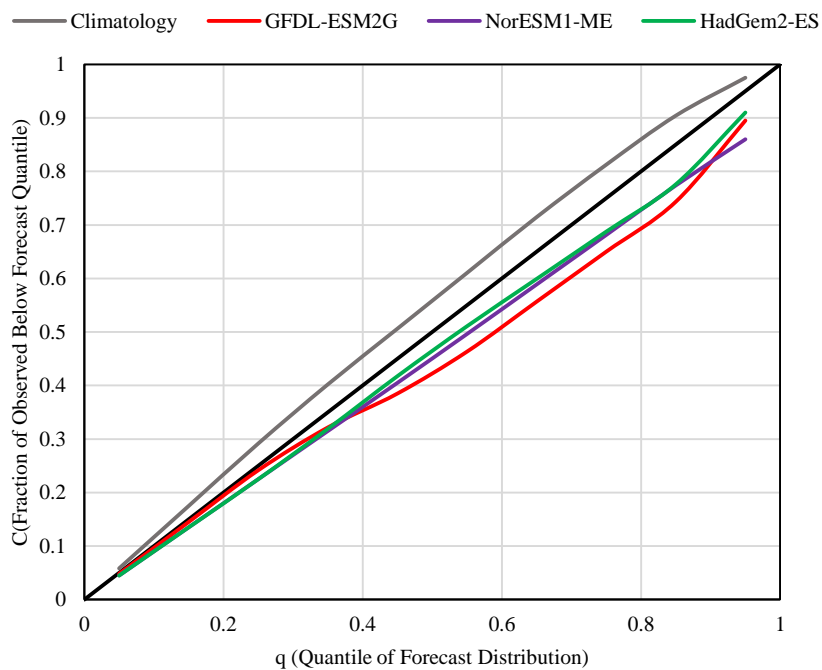
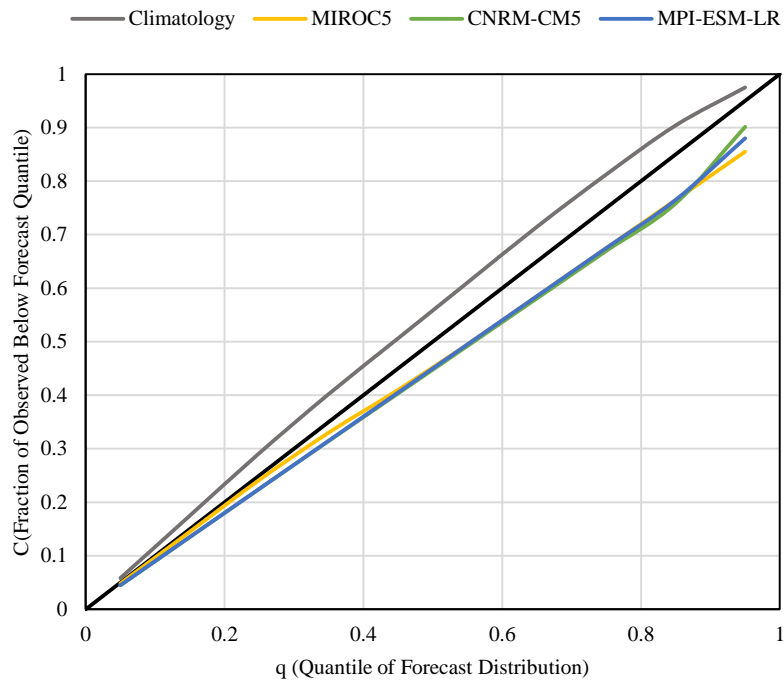
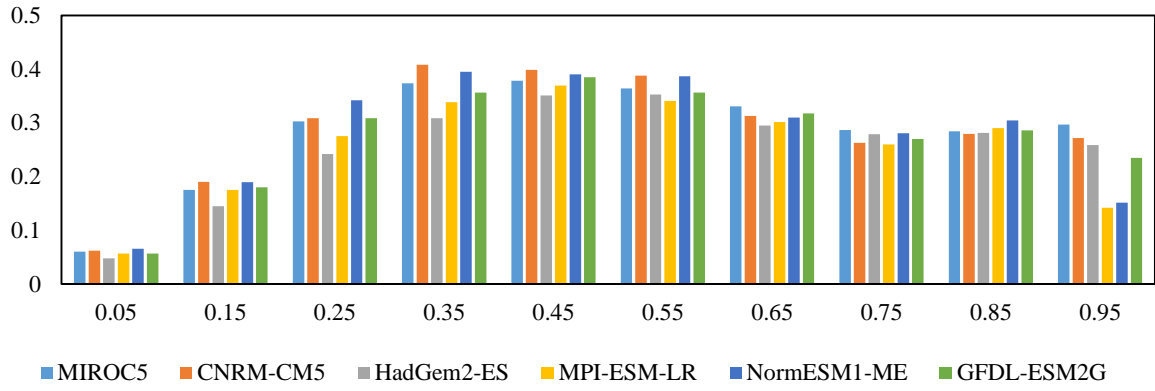


Figure 23. Multicategory reliability diagram for the calibrated rainfall forecast in the late wet season driven by the output of six climate models (separated into two plots for readability)

Difference between Error Bars in the MCRD (a)



Difference between Error Bars in the MCRD (b)

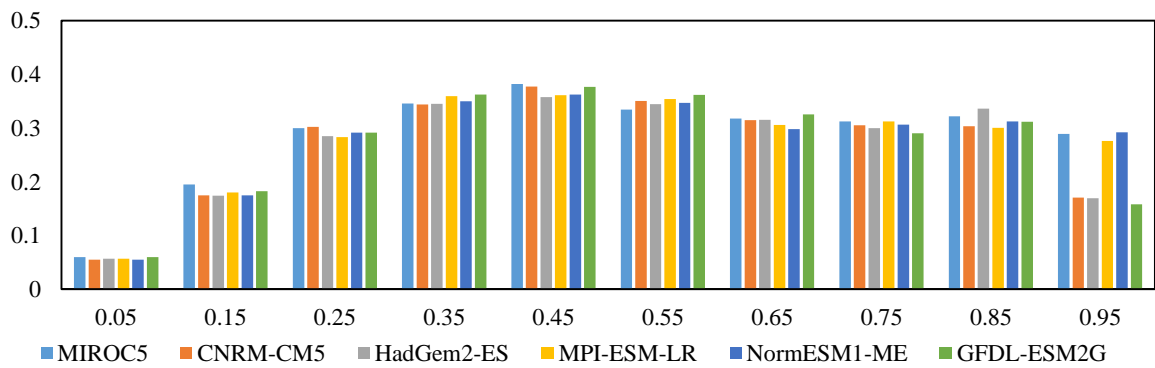


Figure 24. Difference between error bars in the MCRD generated by the calibrated forecast- based ENSO information obtained from climate model in the a) early and b) late portion of the wet season.

Appendix 3: Supporting Materials for Chapter 4: The Relative Value of Seasonal Drought-event Forecasts Conditioned on ENSO Phase for Water Management Decisions

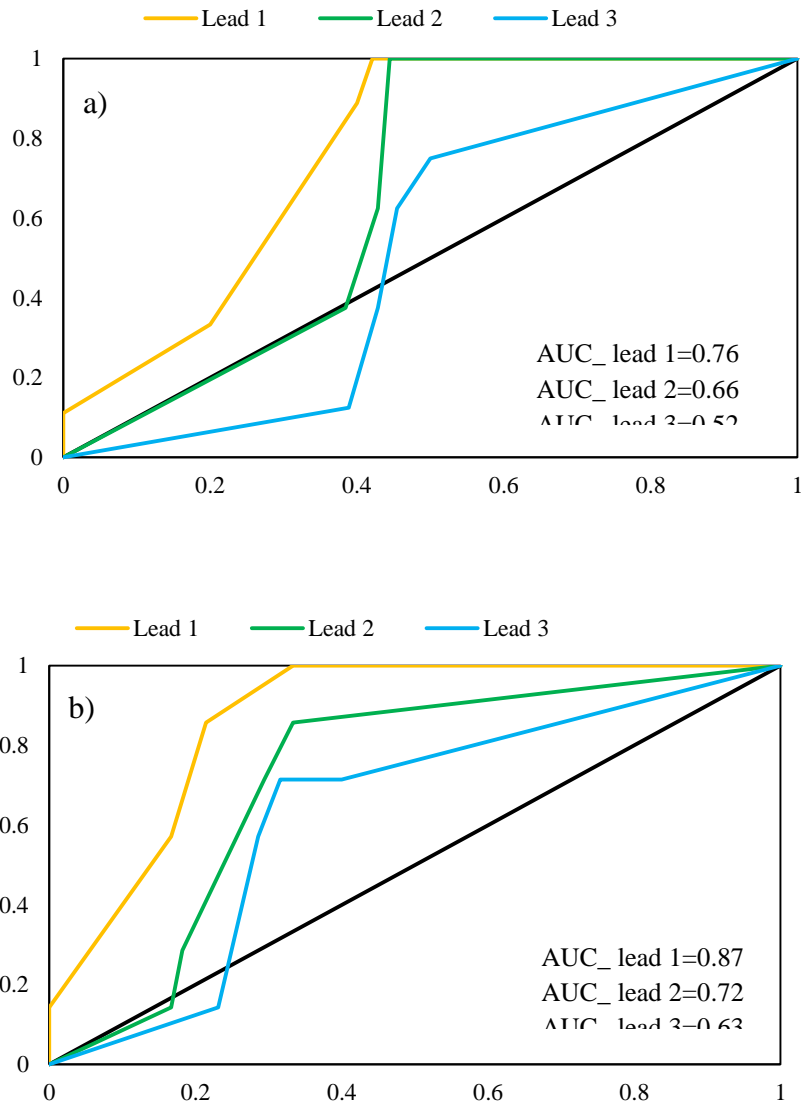


Figure 25. ROC curves of the calibrated forecast of dry events in both the a) early and b) late wet season with respect to three different lead times

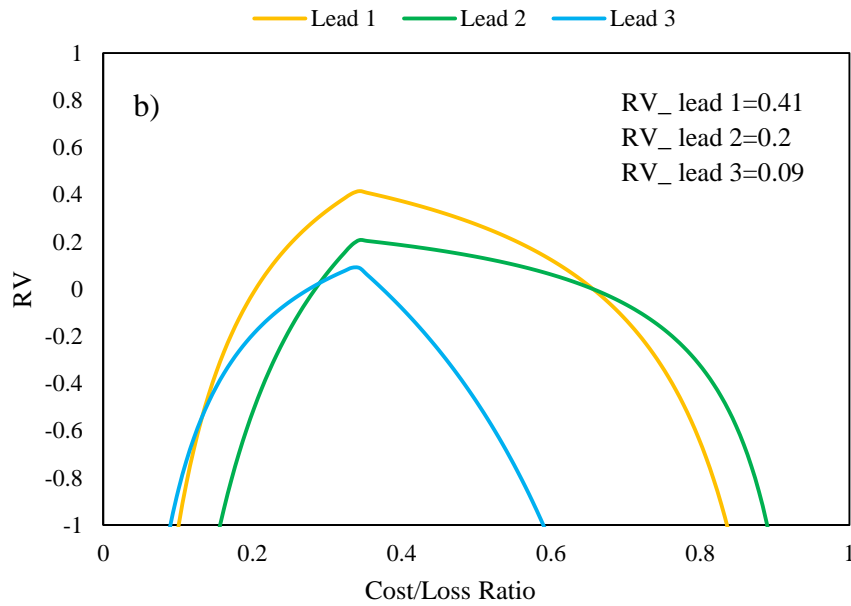
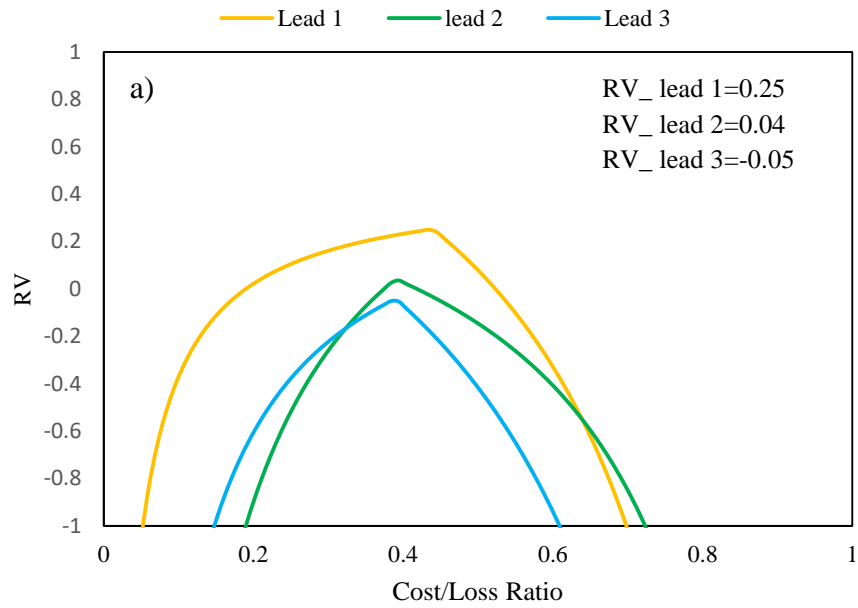


Figure 26. Relative value obtained by optimal cutoff points of the calibrated forecast of dry events in both the a) early and b) late wet season with respect to different lead times